CHAPTER 4: CHARACTERISTICS OF OPTICAL FIBRES MADE BY HCVD

The HCVD process has been employed to manufacture multimode and monomode fibres for optical communications purposes, and also to manufacture specialised monomode fibres for use as transducers in instrumentation. Obviously the characteristics of interest depend largely upon the fibre's application, and it is illogical to present an all-encompassing description of the fibre properties and the characterisation techniques. Hence in this chapter the principal characteristics of the HCVD fibres are reported in relation to the type of fibre and its application.

4.1 Multimode Fibres

4.1.1 Fibre Geometry

Factors such as core diameter, core ellipticity, core/cladding concentricity and overall fibre diameter have a direct influence upon the performance of a fibre within an optical communications system; for example, jointing losses within a concatenated link will be affected by differences in core size and ellipticity. Experience with phosphosilicate fibres[1] had shown that great care was required in the preform collapsing process if core circularity was to be maintained, and that, in general, core ellipticity was inevitable, particularly when high doping levels were employed. However, by adopting the ternary P_2O_5-GeO_2-SiO_2 system for the core glass, a significant improvement in core circularity has been obtained.

Figure 4.1a shows the cross-section of a graded-index fibre having a borosilicate cladding and a graded phospho-germanosilicate core. The core diameter is 63 μm, and as can be verified from the figure, the core ellipticity is immeasurably small. The borosilicate cladding layer has a radial thickness of 4 μm and is distinguishable as the dark annular ring surrounding the core. The silica supporting structure can be resolved as the outer annular ring of intermediate brightness, and has an overall diameter of 125 μm.

Though the borosilicate cladding contributes to the numerical aperture of the fibre, its prime function is to act as a buffer layer which reduces the diffusion into the core glass of impurities such as hydroxyl ions from the silica support tube. The configuration present in this fibre was adopted as the "standard" for the graded-index multimode fibres produced at Southampton. By employing the high-deposition-rate CVD described in Chapter 2, it has been possible to routinely produce high-quality preforms which yield long lengths of fibre having substantially uniform geometrical characteristics along their length. Thus, for the fibre shown in the figure, the core diameter differed by less than 1.5 μm at the ends of the 5.1 km length.

The versatility of the HCVD process allows the core size to be tailored at will simply by varying parameters such as the number of deposition layers and the glass deposition rate. Thus large-core fibres can be manufactured for use in systems where large-area, low-radiance LED sources are to be employed. As an illustration, figure 4.16 shows the cross-section of a fibre having a 75 μm core diameter in a 125 μm overall diameter; again the excellent degree of core circularity is self-evident.

4.1.2 Numerical Aperture (NA)

In multimode fibres the numerical aperture is an important parameter which plays a vital part in determining the bandwidth and guidance properties. In a step-index fibre the pulse dispersion varies with $(NA)^2$, whilst in an optimised graded-index fibre the minimum pulse broadening varies as $(NA)^4$; thus in both cases, increasing the numerical aperture reduces the bandwidth of the fibres. On the other hand, the coupling efficiency varies with $(NA)^2$, and microbending losses have been found to have a $(NA)^{-4.3}$ dependence [2]. Hence, the selection of the numerical aperture involves a trade-off between bandwidth, launching efficiency, and guidance properties.

The phosphogermanosilicate glass system enables the numerical aperture of a borosilicate-clad fibre to be as high as 0.3 without introducing excessive stress or ellipticity into the core. However, a value of 0.23 was adopted for the NA of the standard graded-index fibres because it was found to provide excellent guidance characteristics without serious degradation of bandwidth or intrinsic attenuation. Thus, the two fibres shown in figure 4.1 possessed numerical apertures of 0.23 and 0.22 respectively at the output of a short length of fibre. Over fibre lengths in excess of one kilometre an equilibrium power distribution is attained and a steady-state NA of approximately 0.2 is generally found.

4.1.3 Attenuation Characteristics

The performance of an optical fibre system is often determined by the attenuation characteristics of the fibres within the link. Using both the phosphosilicate and phosphogermanosilicate glass systems, it has been possible to achieve very low attenuation levels in graded-index fibres. The spectral attenuation characteristics of fibres having different core/cladding configurations have been measured using the so-called 'cut-back method'. In all measurements the fibres were fully excited by imaging a large-size, high-NA spot onto the launch end-face of the fibre under test; a cut-back length of 2 metres was typically employed.

4.1.3.1 Phosphosilicate Fibres

Figure 4.2 shows the spectral attenuation properties of two graded-index fibres having binary phosphosilicate glass cores. In one fibre the cladding was formed by the silica support tube, whilst in the second fibre a borosilicate cladding had been deposited prior to the core; in each case the loss was measured in lengths in excess of 1km. Both fibres exhibit very low losses over a broad spectral range from below 0.7 μm to beyond 1 μm. In the silica-clad fibre the attenuation in the 0.5 μm region was comparable with that of pure silica, showing that the addition of phosphorus pentoxide to silica does not substantially affect the absorption and scattering losses.

Apart from the hydroxyl absorption peak at 0.95 μm the attenuation is less than 4 dB/km over the range 0.75 μm to 1.1 μm. In the borosilicate-clad fibre, the attenuation rises sharply at short wavelengths due to a drawing-induced absorption centre in the borosilicate glass. Nevertheless over the 0.8 μm to 0.9 μm region, in which 'first-generation' optical fibre systems are operating, the loss of the borosilicate-clad fibre is less than 3.5 dB/km. It should be noted that these results were obtained in fibres drawn without diameter monitoring and control, and that further reduction of the attenuation levels is certainly possible; using the method which will be described in section 4.1.3.2, the waveguide losses of the silica-clad and borosilicate-clad fibres are estimated to be 1 dB/km and 1.3 dB/km respectively.

Indeed, by paying meticulous attention to the purification of starting materials, and by minimising the waveguide losses, Horiguchi and Osanai [3] were able to achieve a minimum loss of 0.47 dB/km at 1.2 μm in a borosilicate-clad, phosphosilicate-core step-index fibre, with an attenuation of less than 1 dB/km over the range 0.9 μm to 1.4 μm. This result is still the lowest loss reported in the 0.9 μm region, and shows that, whilst phosphosilicate glass has limitations in regard to its physical characteristics, it offers the ability to achieve ultra-low loss in fibres where the need for a high NA is of secondary importance (e.g. in monomode fibres - see Section 4.2.3).

4.1.3.2 Phospho - germanosilicate Fibres

Figure 4.3 shows the spectral attenuation characteristics of a typical graded-index fibre having a phospho-germanosilicate core in a borosilicate cladding. Comparison with the results for phosphosilicate fibres (figure 4.2) reveals that the attenuation of the ternary fibre is substantially higher at shorter wavelengths, but that the losses of the two types are similar in the 1 μm region.

To understand the causes of the differences between the two types of fibre, it is useful to review the loss mechanisms which give rise to the attenuation within an optical fibre. At any wavelength in the near-infrared region, the attenuation can be considered to be the sum of the following components[4]:-

1/ Intrinsic absorption arising from the ultraviolet (UV) and infrared (IR) absorption tails.

2/ Rayleigh scattering loss due to microscopic variations of density and refractive index within the glass. The index deviations are caused by concentration fluctuations which are frozen into the glass at its fictive temperature. The Rayleigh scattering loss is inversely proportional to (wavelength)^4 and extends over the full spectral range, the loss decreasing with increasing wavelength.

3/ Absorption due to colour centres in the glass, created by rupturing of Si-O, P-O, Ge-O and B-O bonds during drawing, and in some cases by incomplete oxidation of the core dopant during deposition.

4/ Absorption due to impurities such as transition metal ions and hydroxyl ions within the glass.

5/ Waveguide losses due to factors such as diameter variations, core ellipticity, NA variations and other imperfections along the length of the fibre.

Inada[5] has reported a simple and convenient method for isolating the various loss components within a fibre. The total attenuation for a silica-based fibre can be expressed as:-

$$A(\lambda) = \frac{A}{\lambda^4} + B + C_1 \exp\left(\frac{C_2}{\lambda}\right) + D_1 \exp\left(\frac{D_2}{\lambda}\right) + E(\lambda) \qquad (4.1)$$

where $A(\lambda)$ = total attenuation

A = Rayleigh scattering coefficient

B = waveguide loss

$C_1 \exp\left(\frac{C_2}{\lambda}\right)$ = UV absorption loss

$D_1 \exp\left(\frac{D_2}{\lambda}\right)$ = IR absorption loss

$E(\lambda)$ = absorption loss due to impurities and colour centres.

The attenuation can thus be regarded as the sum of the absorption and Rayleigh scattering losses at the various wavelengths, plus the wavelength-independent waveguide loss. Thus, by plotting the spectral attenuation data as a function of $(\text{wavelength})^{-4}$, the Rayleigh scattering component will be manifested as a straight line of gradient A.

Furthermore, by extrapolating the line to infinite wavelength (i.e. $\lambda^{-4} = 0$), the intersection with the ordinate directly yields the wavelength-independent component of the attenuation.

Hence, figure 4.4 shows the data of figure 4.3 plotted on a $(\text{wavelength})^{-4}$ scale. Also shown is the spectral loss of the phosphosilicate fibre developed by Horiguchi. Both sets of data obey the λ^{-4} relationship over much of the measurement range. For the P_2O_5-GeO_2-SiO_2 fibre the waveguide losses amount to approximately 0.8 dB/km, whilst the phosphosilicate fibre exhibits less than 0.2 dB/km excess loss. The other striking feature of the curves is that the Rayleigh scattering is considerably higher in the ternary glass system; at 0.85 μm the scattering losses are approximately 2.5 dB/km and 1.5 dB/km for the phosphogermanosilicate and phosphosilicate fibres respectively. It follows that at 0.85 μm a loss penalty of about 1 dB/km must be tolerated if the ternary system is used in preference to the phosphosilicate glass.

Referring to the loss curve for the P_2O_5-GeO_2-SiO_2 fibre, it can be seen that there are two regions where the total attenuation curve departs appreciably from the line denoting the sum of Rayleigh scattering and waveguide losses. Firstly at the short wavelength end, there is a progressive increase of excess loss with decreasing wavelength, and secondly at 0.95 μm where a narrow absorption band contributes an excess loss of about 1dB/km:-

1/ The increased loss at wavelengths below 0.8 μm is associated with the combined effects of intrinsic absorption due to the tail of the UV absorption bands, and an additional absorption loss due to the presence of colour centres in the core and cladding glasses[6]. The colour centres are formed during the fibre drawing and deposition processes, and can be minimised by correct selection of the processing conditions.

The formation of colour centres during fibre drawing has been found to be particularly sensitive to the fibre drawing temperature. For example, figure 4.5a shows the influence of drawing temperatures of 1950°C and 2150°C upon the attenuation of two lengths of graded-index fibre drawn from the same preform. In the fibre drawn at lower temperature the loss rises sharply below 0.8 μm, and at 0.7 μm is 2.5 dB/km above that of the fibre drawn at 2150°C. It is thought that the higher drawing temperature has a dual effect in minimising the excess loss: firstly, the lower viscosity of the glass at the drawing temperature will lead to a reduction in the number of oxygen bonds which are ruptured, and secondly, the increased molecular mobility and the longer time period between the fibre being formed and the glass reaching its fictive temperature will allow some annealing of any absorption centres which have been formed.

This annealing effect was observed at an early stage in the development of phosphogermano-silicate fibres, when the short-wavelength attenuation was found to decrease significantly in fibres subjected to a short heat treatment at 700°C, as is shown by the attenuation results plotted in figure 4.5b.

2/ The narrow absorption band centred at 0.95 μm is due to the presence of hydroxyl ions within the core glass, and contributes an additional loss of about 1 dB/km in the fibre of figure 4.4. The fundamental stretching vibration of the OH radical in silica glass occurs at 2.73 μm and leads to first and second overtone bands at 1.39 μm and 0.95 μm respectively[7]; additional combination bands occur at 0.87 μm and 1.25 μm. The hydroxyl contamination of the core glass arises from three sources, namely diffusion of OH ions from the silica subtrate tube, oxidation of hydrogen-containing species in the deposition reactant gases, and oxidation of hydrogen-containing species in the closure zone during preform collapse. It is possible to correlate the height of the respective OH absorption peaks with the OH content of the glass[7]; hence, the 1 dB/km peak at 0.95 μm corresponds to an OH level of about 1 part per million (ppm) within the core glass. Using the deposition and collapse conditions given in Chapter 2 the height of the OH peak at 0.95 μm generally does not exceed 2 dB/km, and in some cases is barely discernable. The cause of this apparently random variation from fibre to fibre has not been conclusively established, but factors such as the OH-content of the substrate tube, the preform collapsing temperature and duration of collapse have a marked effect upon the diffusion of hydroxyl ions from the substrate tube into the deposited glass during the collapse. In addition, the presence of hydrogen-containing species in the carrier gases greatly affects the hydroxyl content of the deposited glass (as will be illustrated in section 4.1.3.4).

4.1.3.3 Reduction of Waveguide Losses due to Fibre Diameter Variations

The addition of feedback control of fibre diameter during drawing, and the elimination of major diameter variations due to preform surface contamination have enabled uniform fibres to be drawn in long lengths. The reduction in fibre diameter variations has been accompanied by a reduction of the waveguide losses in the graded-index fibres. Figure 4.6 shows the spectral attenuation characteristics of a length of fibre VD280, which had less than $\pm$ 1 μm diameter deviation along its entire length. Extrapolating the linear fit of the λ^{-4} attenuation plot to infinite wavelength reveals that the waveguide loss amounts to only 0.2 dB/km. Accordingly, at 0.85 μm the total attenuation is only 2.8 dB/km of which 2.5 dB/km is attributable to Rayleigh scattering loss.

Other noteworthy features of the attenuation characteristics of this fibre are the remarkably low hydroxyl absorption at 0.95 μm and the reduced level of excess loss at wavelengths below 0.8 μm. Thus, apart from the 0.2 dB/km waveguide loss, the total attenuation lies very near to the intrinsic limit for the P_2O_5-GeO_2-SiO_2 glass which constitutes the core of the fibre. To achieve any significant reduction of the total attenuation it would therefore be necessary to either reduce the germania content of the glass (thereby reducing both the Rayleigh scattering loss and numerical aperture) or to shift the wavelength of operation to beyond 1 μm where the benefit of low Rayleigh scattering loss can be realised without compromising the numerical aperture.

4.1.3.4 Long-wavelength Attenuation Characteristics

The Rayleigh scattering loss imposes a limit on the minimum attenuation that can be achieved in the 0.8 μm to 0.9 μm region. Payne and Gambling[8] demonstrated that considerable benefit could be gained by increasing the wavelength of operation to the 1.3 μm region, where the Rayleigh scattering and UV absorption losses are greatly reduced.

Furthermore, it was shown that the material dispersion in silica-based fibres fell to zero near 1.3 μm, and that by operating at this wavelength a significant improvement in bandwidth could be obtained, particularly in LED-based systems.

At wavelengths above 1.2 μm, the total loss in silica-based fibres is dominated by impurity absorption and absorption due to the infrared tails of the glass components[9]. Care must be exercised in the selection of dopant materials and dopant concentrations to ensure that excessive IR absorption losses do not occur. The long-wavelength attenuation characteristics of the graded-index P_2O_5-GeO_2-SiO_2 fibres have been investigated to assess the fibres' suitability for long wavelength operation.

Figure 4.7 shows the spectral attenuation of a 3.03 km length of fibre over the wavelength range 0.7 μm to 1.7 μm; the results were obtained with the fibre being fully excited. The fibre was manufactured to the 'standard' specificiation and had a numerical aperture of 0.21, a core diameter of 61 μm and an overall diameter of 125 μm. The potential benefit of operating at 1.3 μm is clearly evident, as the loss falls to a minimum of 0.8 dB/km at 1.2 μm and is only 0.9 dB/km at 1.3 μm. Apart from the OH absorption peak at 1.39 μm, the attenuation is less than 2dB/km over a broad transmission window from 1.0 μm to 1.7 μm. The OH overtone bands at 1.39 μm and 0.95 μm contribute additional losses of 12 dB/km and 0.3 dB/km respectively, corresponding to a hydroxyl content of less than 0.5 ppm in the core glass. There is no evidence of absorption due to transition metal impurities, and, using the "λ^{-4} method" the waveguide losses are found to be approximately 0.3 dB/km.

In spite of the fact that the addition of phosphorus pentoxide to silica introduces an absorption band in the 8 μm region[9], and accordingly shifts the infrared absorption edge to shorter wavelengths, the loss at 1.55 μm is only 1 dB/km. In fact, lower losses can be attained at this wavelength in P_2O_5-GeO_2-SiO_2 fibres having very low hydroxyl levels.

Edahiro et al[10] deduced that the loss in the 1.6 μm region was affected by the first overtone of the 3.05 μm absorption band of OH radicals trapped at phosphorus sites. By reducing the OH level in the ternary core glass, losses as low as 0.3 dB/km were obtained at 1.55 μm. Although the present study has not involved direct measures to minimise the 1.39 μm absorption peak, in some fibres the excess loss has been as low as 4 dB/km at 1.39 μm, and the fibres have exhibited less than 1.5 dB/km attenuation at 1.75 μm.

The detrimental effect of the OH content upon the loss at 1.6 μm has been observed in fibres having an abnormally high hydroxyl level. By using low-grade oxygen as the carrier gas during the deposition process, 1.39 μm OH-peaks in excess of 40 dB/km were obtained in P_2O_5-GeO_2-SiO_2 and GeO_2-SiO_2 graded-index fibres. Examination of the spectral loss curves of two such fibres, figure 4.7, reveals that at 1.6 μm the attenuation of the fibre containing phosphorus pentoxide was 9 dB/km above that of the germanosilicate fibre; in spite of the high OH content, the latter fibre exhibited only 1dB/km attenuation at 1.6 μm. However, both fibres possess similar properties in the 0.7 μm to 1.5 μm region, and it should be noted that the tailing of the OH peaks at 1.25 μm and 1.39 μm lead to a marked increase of attenuation at 1.3 μm. It can thus be concluded that the graded-index phosphogermano-silicate fibres are well suited to operation in the 1.3 μm and 1.55 μm regions provided that care is taken to maintain the hydroxyl content of the core glass below the 1 ppm level. Furthermore, the elimination of the phosphorus pentoxide from the glass reduces the OH-absorption loss at 1.6 μm, but a similar effect does not occur at 1.3 μm; hence even in GeO_2-SiO_2 fibres a residual OH content of less than 1 ppm is desirable if the full potential of the fibres is to be realised.

4.1.4 Refractive Index Profiles in Graded-index Fibres

By grading the core refractive index profile in multimode fibres according to a power law relationship the group velocity differences between modes can effectively be equalised, and a bandwidth improvement of up to three orders of magnitude can be obtained over the equivalent step-index fibre[11]. However, slight departures of the profile from the ideal power law can produce a sharp reduction in bandwidth; accurate profile control is thus essential if high-quality fibres are to be reproducibly manufactured. Measurement and analysis of the refractive index profiles in HCVD graded-index fibres has been undertaken using the near-field scanning technique, developed at Southampton University by Dr. F.M.E. Sladen.

To attain high bandwidth fibres, the refractive index profile in the preform is tailored layer by layer during the deposition in a step-wise approximation to the desired power-law profile; it is assumed that little or no diffusion of the dopant species occurs during the fibre drawing operation and that the fibre thus has a profile identical to that of the preform. The limitations to the profile control are, firstly, the accuracy of the index control in the individual deposition layers, and, secondly the perturbation of the profile due to the outdiffusion of dopant from the innermost core layers during collapse. In this latter respect the P_2O_5-GeO_2-SiO_2 fibres have proved far superior to the binary P_2O_5-SiO_2 fibres.

Figure 4.9 shows the refractive index profile of a borosilicate clad, phosphosilicate core graded-index fibre having an NA of 0.18. The high volatility of the P_2O_5 dopant at the collapsing temperature has led to excessive outdiffusion of the dopant even though a dopant-rich atmosphere had been created in the collapse zone. Thus the profile exhibits a characteristic depletion at the core centre, and the actual index profile is severely perturbed from the intended parabolic profile.

In the P_2O_5-GeO_2-SiO_2 system, the P_2O_5 doping levels are generally very low and although dopant evaporation does occur during the collapse it can be compensated by creating a germania-rich atmosphere in the closure zone. Figure 4.10 shows the refractive index profiles of three fibres in which varying degrees of GeO_2 compensation were employed during collapse. Fibre A was made without compensation and it can be seen that the characteristic index depletion falls to the index of silica at the core centre; it should be noted however that the width of the depleted zone is much narrower than is found in phosphosilicate fibres. The loss of P_2O_5 and GeO_2 were obviously overcompensated in fibre B, and a considerable index 'pip' has resulted on the core axis. The presence of such a perturbation in the profile effectively creates a'core within the core' and can lead to a reduction in bandwidth due to the reduced propagation velocities of the modes supported by the perturbed region. In fibre C the dopant depletion has been well compensated and the refractive index profile deviates only marginally from the intended profile. Thus, as a matter of course, the collapsing process for P_2O_5-GeO_2-SiO_2 graded-index fibres is controlled in a manner similar to that employed for fibre C, and in general only slight perturbations of the index profile occur on the core axis.

A second and most important factor which influences the fibre bandwidth is the accuracy with which the actual index profile approximates the desired power law profile. One way of assessing this is to fit the measured profile to the power law relationship and to compare the measured power law exponent with the desired exponent. Figure 4.11 shows the refractive index profile measured in a short length of the graded index fibre VD230; the refractive index profile was derived by applying leaky-mode correction factors to the near-field intensity distribution measured at the output of a 35 cm length of the fibre. The fibre was designed to have an optimal bandwidth in the 0.85 μm region, and had been manufactured to have $\alpha = 2.05$ in the power law relationship characterising the profile:-

$$n(r) = n_1 \left[1 - 2\Delta \left(\frac{r}{a}\right)^{\alpha} \right]^{1/2} \qquad (4.2)$$

The measured index profile is seen to be smoothly varying over much of the core, with the last three deposition layers being resolvable near the core axis; the dopant depletion on the core axis has not been entirely compensated and there is some asymmetry in the profile. Nevertheless, it can be seen that the actual profile is in reasonable agreement with the intended profile. It should be noted, however, that at $^{r}/a \sim 0.5$ the actual profile crosses the power law curve, and that at $^{r}/a > 0.5$ it lies below the desired curve. In effect this means that the profile might be more accurately described by a double alpha profile with $\alpha < 2.05$ for $0.5 \leqslant {}^{r}/a \leqslant 1$ and $\alpha > 2.05$ for $0 < {}^{r}/a < 0.5$

The ambiguity of fitting a measured index profile to a single alpha exponent was overcome by Dr. M.J. Adams who used a perturbation theory to calculate the modal transit times from the measured index profile, and then to equate the predicted pulse-broadening to that calculated for an ideal α-profile exhibiting the same pulse broadening. Using this procedure it is thus possible to determine an equivalent alpha value which, although it may not be an accurate fit to the measured profile, will accurately describe the bandwidth characteristics of the fibre. Hence, in figure 4.12 the near-field intensity distribution and refractive index profile are shown for another graded-index P_2O_5-GeO_2-SiO_2 fibre. In this case the dopant depletion has been almost perfectly compensated during collapse, and the symmetry of the profile is excellent. It can be seen that the equivalent alpha value derived for the refractive index profile lies very near the desired value of 2.05. The same technique was also employed to fit the near-field data, and it is interesting to note the error that would be introduced in alpha if the index profile were assumed to follow the near-field profile rather than the corrected near-field.

4.1.5 Bandwidth Measurements on Graded-index Fibres

Although a knowledge of the refractive index profile is a useful indicator of the bandwidth potential of a multimode fibre, it must be realised that theoretical calculations of pulse broadening from profile data cannot take into account extraneous factors such as mode coupling, differential mode attenuation and profile variations with length, and that meaningful bandwidth data can only be obtained by direct measurements upon the fibre itself. Bandwidth measurements have been made on the phospho-germanosilicate graded-index fibres by measuring the temporal broadening of short pulses propagating through the fibre under test. By deconvolving the pulse waveform at the input to the fibre from that at the output it is possible to obtain the impulse response of the fibre; by transferring the time domain data into the frequency domain the amplitude/frequency response can be determined.

The pulse dispersion measurement is performed using a pulsed GaAlAs laser operating at about 0.85 μm as the light source. The subnanosecond pulses from the laser are launched into the test fibre using 1:1 imaging optics and x-y-z manipulators to image the laser's emitting stripe onto the fibre core. Light emerging from the far end of the fibre is similarly imaged onto the active area of a high-speed silicon avalanche photodiode. As the laser repetition rate is only 10 kHz, a time delay generator is used to compensate for the delay time of the propagating pulse before triggering a sampling oscilloscope on which the photodetector output is displayed. The measurement proceeds by measuring the output pulse waveform from the length of fibre under test and then measuring the "input" pulse waveform from a 1 metre length of fibre; in this way the risetimes of the laser, photodetector and oscilloscope are common to both measurements, and are therefore cancelled out when the input and output pulse waveforms are deconvolved.

The pulse waveforms may be recorded by making a photographic record of the oscilloscope display, or by using a computer-controlled data acquisition system to read the waveform from the oscilloscope into computer memory. The computer-based system also enables signal averaging of the waveforms and fast Fourier transformation (FFT) into the frequency domain.

Figure 4.13 shows the pulse broadening measured in a 3 km length of the fibre VD230 whose refractive index profile was given in figure 4.11. The dual trace of input and output pulse waveforms was obtained by multiplexing the triggering of the sampling oscilloscope. The input pulse waveform is the narrower pulse of 650 ps full width half-maximum (fwhm) pulsewidth. At the output of the 3 km length the pulsewidth has broadened to 1.3 ns fwhm due to the combined effects of intermodal dispersion and material dispersion. Thus, assuming that the two pulse shapes are Gaussian, the impulse response of the fibre can be deconvolved using the relationship[12]:-

$$S_o^2 = S_I^2 + S_f^2 \qquad (4.3)$$

where S_o = Output pulse width

S_I = Input pulse width

S_f = Pulse response of the fibre itself.

The pulse broadening at 50% height is found to be only 1.1 ns over 3 km; when the 2 nm linewidth of the laser is considered and the material dispersion effects are deconvolved, the pulse dispersion reduces to 1.0 ns over the full length. The degree of mode mixing in this fibre was very low as the output pulse shape from the 3 km length was found to be sensitive to launching conditions at the input end. Assuming therefore that the pulse broadening varies linearly with length, the remarkably low pulse dispersion of 0.33 ns/km is obtained. This is more than two orders of magnitude lower than the pulse dispersion expected in a step-index fibre of the same numerical aperture, and represents an equivalent analogue bandwidth of the order of 1.3 GHz.km.

It should be noted that this figure is probably optimistic because the output pulse waveform from the fibre exhibits "tailing" of the rising and falling edges: taking the pulsewidths at 10% pulse height gives 1 ns/km pulse broadening at the 10% level which corresponds to a 3 dB optical bandwidth of about 1.2 GHz.km[13]. Whichever figure is employed the bandwidth is found to be well in excess of 1 GHz.km.

Using a dye-laser/parametric-oscillator combination to provide a tunable wavelength source, Mr. A.H. Hartog was able to measure the pulse dispersion of this fibre over a broad wavelength range from 0.75 μm to 1.35 μm[14]. The measured pulse dispersion (fwhm values) is plotted as a function of wavelength in figure 4.14. At 0.85 μm the dispersion of 0.32 ns/km agrees with the result obtained using the semiconductor laser source. Interesting features of the tunable wavelength measurements are, firstly, the fact that the pulse dispersion is low over a broad wavelength range, and, secondly, that the results do not exhibit a narrow wavelength band where the pulse dispersion falls to an ultra-low value, as is usually observed in alpha-profile fibres at the wavelength where the profile is near optimal[11]. Thus, the pulse dispersion has a broad minimum of approximately 0.3 ns/km over the 0.75 μm to 0.9 μm range, and at 1.3 μm the dispersion is still well below 1 ns/km.

The fact that the dispersion is a minimum in the 0.85 μm region agrees well with the prediction from the alpha value fitted to the refractive index profile. Moreover the wideband performance over a broad spectral range empirically endorses the observation that the refractive index profile of this fibre might be more accurately described by a double-alpha profile[15]. The significance of this effect is that the minimum pulse dispersion of 0.3 ns/km is higher than would be expected in an ideal alpha profile (< 0.1 ns/km), but the reduced bandwidth arising due to a shift from the optimal wavelength is not as high as with an ideal alpha profile.

4.1.6 Repeatability Studies

To assess the repeatability of the techniques for the manufacture of P_2O_5-GeO_2-SiO_2 graded-index fibres, twenty "standard" HCVD preforms were produced under nominally identical deposition conditions. The preforms were subsequently drawn into 125 μm diameter fibre which was in-line coated with a soft primary coating of silicone rubber (see Chapter 5). More than 65 km of fibre was drawn, giving a mean yield of >3.25 km of fibre per preform. Measurements of the geometrical and optical characteristics of each fibre were made to gain an impression of the performance distribution which could be expected in a fibre production environment.

Transverse cross-sections through each of the twenty fibres are shown in figure 4.15. The fibres were intended to have a 63 μm core in a 125 μm overall diameter with a borosilicate cladding thickness of about 4 μm. The striking feature about the cross-sections is the remarkable degree of circular symmetry exhibited by the majority of fibres; in only two fibres did the core ellipticity exceed 5%, and in the remainder it was generally less than 2%. Core diameter measurements revealed that more than 80% of the fibres had core diameters within the range 63 ± 4 μm and the extreme values of the population were 57 μm and 70 μm. Core diameter variations were thought to have resulted from two effects: Firstly, no account was taken of the wall thickness variations of the silica substrate tubes, and differences in cross-sectional area from tube to tube would lead to variations in the core:fibre diameter ratio. Secondly, differences in the temperature and duration of the preform collapsing process would lead to variations in the volume of silica evaporated from the surface of the preform, thereby changing the core aspect ratio.

Spectral attenuation measurements were performed on each length of fibre, and the envelope of the results is given in figure 4.16. The remarkable feature of the results was that in almost every case the shape of the attenuation characteristic was the same but the base-line level of the curve was shifted from fibre to fibre.

This indicates that the greatest variability lies in the wavelength independent losses associated with diameter fluctuations, core size variations, scatter centres etc. At 0.85 μm the minimum and maximum attenuation levels were 2.6 dB/km and 4.2 dB/km respectively, and the mean level was 3.7 dB/km for the full sample population. As many of the fibres were drawn without diameter monitoring and feedback control, it is felt that the large spread in attenuation results from waveguide losses due to diameter noise, and that the distribution of results would be considerably reduced if the exercise were repeated on fibres drawn under diameter control. (This is endorsed by recent experience with fibres drawn with controlled diameters where the attenuation at 0.85 μm has always been within the range 2.8 dB/km to 3.4 dB/km.)

Refractive index profiles were determined using the near-field scanning technique. Unfortunately it was not possible to measure every fibre as, towards the end of the programme, much of the near-field scanning system had been incorporated into another experiment. Nevertheless, figure 4.19 shows the superposition of the profiles measured in ten fibres. The region in which the profiles differ most is towards the edge of the core where in some cases the transition between grading out the cladding dopant and grading in the core dopant can be clearly distinguished. The outdiffusion of dopant during the collapse stage has been well compensated in almost every instance, and there is no evidence of gross perturbations of the individual profiles due to effects such as sudden transients in deposition temperature or reactant concentrations.

Pulse dispersion measurements were performed using the GaAlAs laser system described above. As the lengths of the fibres were not identical, it is not possible to assess the bandwidth performance by super-imposing the output pulse waveforms from the individual fibres. The results presented above for fibre VD230 (0.3ns/km at 0.85 μm) represent the upper range of the bandwidth performance of the fibres. At the other end of the range fwhm pulse dispersion values of up to 2.5 ns/km have been obtained.

However, the majority of fibres exhibited pulse broadening of between 0.7 ns/km and 1.5 ns/km. A typical pulse dispersion characteristic is shown in figure 4.17 for a 1140 metre length of fibre; in this case the results were read from the oscilloscope into a desktop computer which subsequently provided the hard-copy printout of the waveforms. The fwhm pulse dispersion is 1.05 ns over the 1140 metre length, giving a normalised dispersion of 0.92 ns/km. The waveforms were also transformed into the frequency domain and deconvolved to give the amplitude versus frequency response shown in figure 4.18. The 3 dB optical bandwidth is 625 MHz.km, somewhat higher than the value of 475 MHz.km obtained by assuming near-Gaussian waveforms and calculating the bandwidth from the relationship[13]:-

$$\text{3 dB bandwidth (MHz.km)} = 440/(\text{fwhm dispersion in ns/km}) \qquad (4.4)$$

In general the output pulse waveform from each fibre was single-peaked and of similar form to that given in figure 4.17.

Numerical aperture measurements were also made by measuring the far-field output distribution of the light emerging from a short length of fibre excited by a divergent beam from a tightly-focussed He-Ne laser beam. The measured NA values were found to vary by as much as $\pm$ 0.02 from fibre to fibre; this represents a variation of 18% in the core/cladding index difference. Deviations of this order can have serious consequences when jointing different fibres of nominally the same NA, and, in theory, an excess loss of up to 1.5 dB may be incurred. The NA variations have been attributed to the temperature sensitivity of the GeO_2 incorporation efficiency in the deposition process (as described in Chapter 2). Obviously one step towards the solution of this problem is to ensure that the deposition temperature is always the same from preform to preform; only then might it be possible to impose limits of $\pm$ 0.005 on the specified value of the numerical aperture.

4.2 Single-mode Fibres for Optical Communications

Compared with multimode fibres, single-mode fibres have the considerable advantage that multimode propagation effects such as intermodal dispersion are entirely eliminated, and an almost unlimited bandwidth can be achieved. In fact, bandwidth limitations are imposed principally by material dispersion, waveguide dispersion and profile dispersion[16]. In the 0.8 μm to 0.9 μm region the material dispersion dominates and would be expected to introduce pulse broadening of the order of 80 ps/nm.km; at longer wavelengths the material dispersion decreases and total dispersion of less than 20 ps/nm.km would be expected in the 1.2 μm region. It can be seen that in fibres with such wideband capabilities the measurement of fibre bandwidth is perhaps superfluous (and indeed difficult to perform). Hence in single-mode fibres the characteristics of interest are principally geometrical configuration, core/cladding index difference, normalised frequency, V, and, of course, attenuation performance. Together the normalised frequency and core/cladding index difference characterise the propagation and guidance properties of the fibre[17], and are therefore of vital importance in determining factors such as microbending resistance, launching efficiency and jointing losses.

4.2.1 Geometrical Configuration

As described in Chapter 2, the HCVD process has been applied to the manufacture of preforms for subsequent drawing into monomode fibres. Different combinations of core and cladding glasses have been evaluated in terms of ease of manufacture and optical performance of the fibre itself.

Figure 4.20a shows the cross-section of a fibre designed for monomode operation at 0.633 μm. The fibre has a borosilicate cladding with a germanosilicate core, and was drawn from the preform whose cross-section is shown in figure 4.20b.

To provide a reasonable core-diameter/overall-diameter ratio, the preform was sleeved in silica tubes before drawing. No evidence of the interface between the preform and the sleeving tubes can be detected in the fibre, and the concentricity of the structure is excellent. Unlike the multimode case, it is not possible to determine the core diameter by direct measurement on the cross-section, as the central bright region of the photograph corresponds not to the core size but to the mode size. A reasonable estimate of the core size can be obtained by measuring the diameter across the borosilicate cladding in the fibre and then scaling it by the core to cladding diameter ratio determined from the preform. Thus from the preform cross-section (fig. 4.20b)

$$a_{core} : a_{clad} = 0.24$$

and from the fibre cladding diameter of 18 μm the core diameter in the fibre is 4.3 μm.

This approach can only be considered approximate because it does not allow for the possibility of diffusion during fibre drawing; it also relies upon accurate measurement of the cladding diameter which may not be discernable in a fibre having a silica or multicomponent-glass cladding which index matches the silica substrate.

An alternative approach to the determination of fibre core diameter involves the use of a scanning electron microscope (SEM) to measure the core diameter in an etched sample of fibre. As an illustration, figure 4.21 shows an SEM photomicrograph of an etched sample of single-mode fibre having a phosphosilicate glass core in a silica cladding. The sample had been etched in dilute hydrofluoric acid prior to examination, and the higher etch rate of the phosphosilicate glass produces an etched-well which clearly delineates the core/cladding interface. Also visible at the core centre is the depletion zone where P_2O_5 outdiffusion during collapse has resulted in a reduced etch-rate and a reduced refractive index. Whilst this technique is obviously accurate it is time consuming and requires the use of sophisticated equipment.

4.2.2 Measurement of Normalised Frequency

The normalised frequency, or V-value, of a circularly symmetric fibre having a core and cladding structure is defined by the equation[18]:-

$$V = \frac{2\pi a}{\lambda} \cdot (n_1^2 - n_2^2)^{\frac{1}{2}} \qquad (4.5)$$

Where a = core radius

λ = operating wavelength

and n_1, n_2 = core and cladding indices respectively.

For monomode operation of the fibre, V must be less than the second-order mode cut-off value of 2.405. It can be seen that a knowledge of the core radius and core to cladding index difference enables the direct calculation of V at any wavelength λ. It is also very useful to know the effective numerical aperture, $(n_1^2 - n_2^2)^{\frac{1}{2}}$, since over a broad range of V-values from 1.8 to 2.4 the mode spot size depends critically on the NA[17]. In turn, factors such as launching efficiency, jointing loss and microbending loss are dependent on the mode spot size. Whilst the numerical aperture in the preform can be directly determined, it is not possible to use the same techniques in the fibre; furthermore, the assumption that the NA in the fibre will be the same as that in the preform does not take account of the quench-rate sensitivity of the refractive index of borosilicate glass, or of the dopant diffusion that may occur during drawing.

Fortunately a technique has been developed at Southampton for determining the core diameter and core/cladding index difference. The technique[19] is quick and simple and involves only the measurement of power distributions across the far-field pattern from the fibre. Inspection of the far-field pattern of a single-mode fibre reveals a mainlobe with additional sidelobes caused by diffraction, as is shown in figure 4.22. The far-field in the figure was obtained from fibre GSB2 (figure 4.20) when excited by a He-Ne laser operating at 0.633 μm. By theoretical analysis Dr. H. Matsumura demonstrated that the power distribution within the main lobe and the angular width to the first minimum depend solely upon a, n_1, n_2, and λ.

By measuring the half-power width of the main lobe and the width of the first minimum the unknown fibre parameters can be read directly from a set of universal curves.

The experimental procedure begins by preparing a short length of fibre and exciting one end using a suitable laser source. The output end is positioned perpendicular to, and at a known distance from a traversing photodiode. The diode is translated across a diameter of the far-field and the half-power and first-minimum positions are recorded. Thus, for the far-field of figure 4.22 the angles of the half-power point and the first minimum were 2.1° and 9.8° respectively, giving V = 2.4 ± 0.05, in excellent agreement with the value deduced from the preform. On the other hand the core diameter was 5 μm, rather higher than the estimated value of 4.3 μm; it is thought that this discrepancy may be caused by an enlargement of the mode spot size due to the axial refractive index depression[20], with a consequent reduction of the angular width of the half-power point from which the core size is determined. Using the deduced values of V and 'a' the effective numerical aperture is calculated using equation 4.5 to be 0.10, somewhat lower than the 0.12 value measured in the preform. Again, the discrepancy is probably caused by the enlargement of the mode size due to the index depression. The result obtained for the fibre can be considered to represent a mean value which would produce the same mode spot size in an equivalent true step-index fibre of the same NA and core size. As the mode size is determined by the effective NA of the fibre the measurement thus yields a value which is perhaps more representative of the fibres propagation characteristics than is the maximum index difference within the core. Measurements on a borosilicate-clad, silica-core fibre in which there was no axial index depression gave much closer agreement between the measured and predicted values of core size and numerical aperture.

One drawback of the far-field observation technique is that it must be performed on the far-field of the fundamental mode; if the measurement is performed at a wavelength where the fibre is multimode, it is often difficult to excite only the lowest order mode and hence the far field pattern becomes distorted.

A solution to this problem is to use a tunable wavelength laser to ensure that the test fibre is operating in or near the monomode regime.

An alternative technique for evaluating the V-value consists of measuring the loss peaks corresponding to the cut-off wavelengths of the higher-order modes in a short length of curved fibre[21]. Whilst this is a convenient technique for estimating V, particularly when a tunable laser is not available, it does not yield information on the core size or index difference. Furthermore it is prone to considerable inaccuracy due to the effects of large-scale curvature and microbending upon the loss of the higher-order modes near cut-off[22]. To illustrate this point, figure 4.23 shows the wavelength dependence of the excess loss due to a 1.5 cm radius bend in the fibre GSB2 described above. The loss peak at 520nm corresponds to the loss of the LP_{11} mode at the bend, while the sharp falling edge at 525 nm represents the point at which the LP_{11} mode no longer propagates in either the bent or straight fibre. If in a straight fibre the LP_{11} mode were lossless up to cut-off and infinitely lossy thereafter, the wavelength at which the bend loss curve falls to zero would correspond to V = 2.405. However, even in a straight fibre, microbends produce a high loss well above cut-off, thus appreciably increasing the effective cut-off frequency. Hence, in the bend-loss measurement the effective cut-off Ve occurs at a shorter wavelength than the true cut-off Vc. In figure 4.23 the bend loss curve indicates an effective cut-off Ve = 2.405 of 530nm compared with a true value of Vc = 2.405 at 633 nm, measured using the far-field observation technique; using the results of the bend loss measurement to define the V-value this introduces an error of approximately 20% in the V-value under the particular measurement conditions used in this experiment. Moreover, the effective cut-off is found to be highly sensitive to the degree of microbending, and consequently the repeatability of the measurement technique is rather poor.

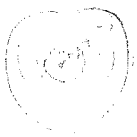

It is also worthwhile noting in the bend-loss results that the increasing attenuation at 750 nm is due to the increasing bend-loss of the fundamental HE_{11} mode with decreasing V-value. Taking the true cut-off value of 633 nm, it can be readily calculated from the figure that at $V \geqslant 2.0$ the HE_{11} mode suffers minimal excess attenuation due to the bend of 1.5 cm radius. To some extent the bend-loss measurement can thus be employed to assess a fibre's resistance to bending and microbending losses. Large core, low NA fibres have been found to be highly sensitive to bend loss at normalised frequencies as high as 2.1, whereas small-core, high NA fibres have exhibited minimal bend loss even when operating at normalised frequencies of 1.6. Although it is desirable, whenever possible, to minimise bending and microbending losses by selecting a high index difference between core and cladding. the more demanding jointing alignment tolerances demand a trade-off between microbending resistance and ease of jointing. In practice, bend-loss measurements on fibres of differing numerical apertures indicate that an index difference of $\Delta = 0.3\%$ (NA = 0.12) gives satisfactory bending resistance at V-values above 1.6.

Finally, Murakami et al[23] have reported a new technique for determining V using a method which is analogous to the bend loss technique. The measurement involves the observation of the second-order mode cut-off in the near-field of a short length of monomode fibre. One advantage of the technique is that the fibre is excited by a length of multimode fibre and is not rigidly held in mechanical clamps which introduce microbending. Furthermore, as the length of fibre under evaluation is typically 20 mm the attenuation of the LP_{11} mode near cut-off will be much lower than that in the bend-loss measurement. The difference between the effective cut-off wavelength and the true cut-off wavelength will be correspondingly reduced. Although the determination of the cut-off is rather subjective, involving visual interpretation of the near-field intensity profile, an accuracy of $\pm$ 5 nm is claimed for the determination of the cut-off wavelength Ve, and for fibre lengths in the 10 - 20 mm range Ve is within $\pm$ 5 nm of the true cut-off Vc. One shortcoming of the technique in its present form is that, like the bend loss method , it does not yield information on the core size and numerical aperture of the fibre.

4.2.3 Attenuation Characteristics

The attenuation performance of monomode fibres has been evaluated by spectral loss measurements using the same measurement equipment as for the multimode fibres (section 4.1.3). In the case of monomode fibres the spectral attenuation measurement poses particular problems which do not generally arise with multimode fibres. Firstly the smaller core size of the monomode fibres dictates the need for extremely accurate and stable alignment systems for launching into the fibre. Secondly, the power that is coupled into a monomode fibre is generally much lower than can be achieved with multimode fibres, and the dynamic range of the measuring equipment is reduced. Finally, it is essential to ensure that an effective cladding-mode stripper is employed because, at the low levels of guided power within the core, the effects of unwanted cladding modes upon detected power and attenuation are exaggerated. Whilst the launching and mode stripping problems can be overcome by careful experimental techniques, the reduced dynamic range of the measurement system is a limiting factor which must generally be overcome by performing the measurement on shorter lengths of fibre.

As true monomode operation can only be achieved at $V < 2.405$, and weak mode guidance is obtained at V values below 1.8, it is necessary to pitch the fibre's V-value such that it does not exceed these bounds over the desired range of operating wavelengths. Thus fibres may be produced for 'first-window' (0.8 to 0.9 μm), second window (1.0 to 1.3 μm) or third window operation (1.5 to 1.7 μm). Though the effects of intrinsic loss mechanisms may be the same from fibre to fibre, additional losses due to mode cut-off and bending loss will produce markedly different total attenuation levels according to the V-value at the measurement wavelength.

Figure 4.24 shows the spectral loss characteristics of a monomode fibre designed for operation in the 1.2 μm region. The fibre was characterised by an 8 μm core size, a core/cladding index difference of $\Delta = 0.24\%$, and thus had a true cut-off wavelength of 1.06 μm.

The fibre had a phosphosilicate glass core in a low-loss borosilicate cladding with a core:cladding diameter ratio of 1:4; the overall fibre diameter was 118 μm, and the loss measurement was performed on a 300 metre length of fibre. The V-values at 0.85 μm, 1.2 μm and 1.5 μm were 3.0, 2.1, and 1.7 respectively. The attenuation characteristics exhibit several interesting features. Firstly, there are three low-loss windows where the attenuation is less than 5 dB/km, namely in the 0.8 μm, 1.0 - 1.2 μm, and 1.5 μm regions. In the first window the LP_{11} mode is above cut-off and the fibre is thus multimode; the cut-off of the second-order modes produces the excess loss peak in the 0.9 μm region. Although the second-order mode cut-off produces a discrete loss of 4 dB which is independent of fibre length, extrapolation of the attenuation levels measured in the 300 metre fibre length to a normalised length of 1 km produces a 13 dB peak at 0.9 μm, and thus introduces a systematic error in the results. Similarly the peak at 0.7 μm which corresponds to the third-order mode cut-off indicates a 3 dB/km excess loss rather than a discrete loss of 1 dB. In the 1.0 μm to 1.2 μm region the fibre is operating in the monomode regime with a minimum attenuation of 2.6 dB/km at the true cut-off wavelength of 1.06 μm. Although the OH peak at 0.95 μm is barely detectable, the OH absorption bands at 1.25 μm and 1.39 μm are clearly evident and contribute significantly to the total losses in the 1.2 μm to 1.5 μm region. Indeed, the hydroxyl level of about 4 ppm is such that at 1.3 μm the interaction of the tails of the OH bands increases the attenuation to 10 dB/km. The hydroxyl impurity level is apparently much higher than that usually found in the graded-index multimode fibres, where the peaks at 1.25 μm and 1.39 μm typically introduce additional losses of 1dB/km and 12 dB/km respectively. The increased absorption losses in the monomode fibre are due to the combined effects of the hydroxyl diffusion into the barrier cladding and the increased field penetration into the cladding as V decreases with increasing wavelength. By increasing the cladding thickness and increasing the cut-off wavelength it should be possible to reduce the hydroxyl absorption to a low level.

Finally, it can be seen that at 1.5 μm the loss is only 4 dB/km even though the low V-value at this wavelength might reasonably be expected to lead to considerable microbending loss.

Obviously the higher attenuation of the monomode fibres compared with the standard graded-index fibres indicates that there is a need to investigate the sources of the excess loss and to optimise the design and fabrication of the fibres. The results achieved so far indicate that the principal problems are those of increased hydroxyl absorption and a higher level of waveguide loss. By some relatively straightforward improvements to the deposition and fibre drawing processes it should be possible to achieve results which are comparable with the remarkably low-loss fibre of 0.2 dB/km attenuation at 1.55 μm recently developed by Japanese workers using the HCVD process[24].

4.3 Single-mode Fibres for Transducer Applications

There is currently a great deal of interest in developing single-mode fibres which are capable of maintaining a defined state of polarisation during transmission. Particular applications for these fibres include the termination of fibres to integrated optical devices, laser-fibre gyroscopes, and current-sensing devices which utilise the Faraday effect. In the current transducer[25], a linearly polarised beam is launched into a monomode fibre which is wound around a current carrying conductor, and, as the fibre is lying in the plane of the magnetic field, the polarisation within the fibre is rotated in proportion to the current passing through the conductor. After suitable calibration, it is thus possible to directly determine the current in the conductor by monitoring the rotation of the polarisation at the output of the fibre. In practice the sensitivity of such devices is limited by the residual birefringence of the fibres, which introduces ellipticity in the output polarisation. A systematic study of the causes of birefringence has been undertaken with the objective of developing a fibre having insignificant residual birefringence.

4.3.1 Sources of Birefringence

An analysis of the propagation characteristics of a monomode fibre show that an ideally round, strain-free, and straight, fibre has two degenerate modes of propagation corresponding to the two orthogonal polarisations Ex and Ey[18]. Since the two modes are degenerate they have equal propagation constants and therefore conserve the polarisation state of light within the fibre. However, real fibres exhibit residual birefringence which lifts the two-fold degeneracy, and the two modes propagate with different group velocities[26]. A phase difference therefore exists between the two orthogonally polarised beams, and the polarisation state varies along the length of the fibre. In general, the light is elliptically polarised, varying between the extremes of linear and circular polarisation.

The origins of the birefringence are twofold:-

1. The core of the fibre exhibits a degree of ellipticity which establishes preferred fast and slow axes of propagation corresponding to the minor and major axes of the elliptical core. The linear retardation which results depends on the ellipticity present and the fibre propagation parameters.

2. In general a high level of stress occurs within the fibre owing to the thermal-expansion mismatch between the core and cladding glasses. Any asymmetry in the stress distribution, caused for example by core ellipticity, will lead to a transverse stress-optical birefringence which contributes to the observed retardation in a similar manner to the core ellipticity.

4.3.2 Design of Fibres for Low Birefringence

Dr. M.J. Adams analysed the propagation characteristics of elliptical-core monomode fibres for various core/cladding index difference values, and derived a set of design curves giving the phase retardation $\delta\beta$ as a function of core ellipticity for various values of index difference, as shown in figure 4.25.

It may be seen that the tolerance on core circularity can be relaxed by choosing a small index difference and, by inference, a large core diameter. However the bending requirements of monomode fibres in transducer applications may be more demanding than those in telecommunications usage, and a minimum core/cladding index difference of $\Delta = 3 \times 10^{-3}$ would be satisfactory. For the current transducer application a retardation of $< 3°$/metre is required, corresponding to a phase difference of 2π between fast and slow modes in a length of 120 m (the 'periodic length'). From the design curves it can be seen that for $\Delta = 3 \times 10^{-3}$ the core ellipticity must be less than 0.1%, a geometrical perfection which has hitherto been difficult to achieve.

A rigorous analysis of the state of stress within a clad glass fibre having circular symmetry shows that in the core the radial, tangential and axial stresses are independent of position and that furthermore the radial and tangential stresses are equal[27]. On the other hand, the radial and tangential stresses in the cladding are at a maximum at the core/cladding interface and decrease with increasing radius; as in the core, the axial stress in the cladding is constant. Calculation of the stress anisotropy required to produce a transverse birefringence of 3°/m in fused silica yields a value of less than 1 kN/m^2 for the stress differential between orthogonal planes; this is three orders of magnitude less than the axial stress level in a typical silica-clad, phosphosilicate-core monomode fibre. Clearly the demands on stress anisotropy are as demanding as those upon core ellipticity!

4.3.3 Fibre Manufacture and Characteristics

Analysis of the core circularity and stress uniformity requirements made it clear that a dual approach to developing a low birefringence fibre would be necessary. An experimental fibre manufacturing programme was undertaken with the aims of reducing not only the core ellipticity but also the total core stress levels.

A number of fibres were manufactured using both the HCVD process and the rod-in-tube technique. During the course of this programme some particularly interesting features were discovered, and led to the final solution of the problems[28]. The characteristics of five experimental fibres are given in Table 4.1, and their properties are described below:-

Fibre VD214: This borosilicate-clad, silica-core fibre was made by HCVD inside a high-quality silica tube. To relax the circularity requirement a low index difference was chosen, thus giving an 8.5 μm core diameter in the fibre at a cut-off wavelength of 633 nm. Measurement of the deviation from core circularity was made by examining etched samples of fibre on a high-power optical microscope, and in all cases less than 1% ellipticity was found.

Birefringence measurements were made on a straight length of fibre using a He-Ne laser operating at 633 nm as source. At this wavelength the V-value had been found to be exactly 2.4 using the far-field observation technique. As is shown by the retardance versus length curve for this fibre in figure 4.26, the fibre behaved as a linear retarder, the specific retardance being 126°/m. As this figure was considerably in excess of the predicted value it was concluded that even at the low B_2O_3 doping level used in the fibre the stress levels due to thermal mismatch were too high.

Fibre SV1: In an effort to reduce the residual stress levels a rod-in-tube preform having a synthetic-silica core and a Vycor cladding was drawn into a monomode fibre having V = 2.5 at 633 nm. Vycor is a 96% SiO_2, 4% B_2O_3 glass having an expansion coefficient close to that of silica, and a somewhat lower refractive index. Measurements on etched fibre samples again revealed that the ellipticity was better than 1%, indicating an expected retardance of about 2°/m. The retardance measurements revealed that, as with fibre VD214, SV1 behaved as a linear retarder, but in this case the improved value of 66°/m was obtained for the specific retardance, as can be seen from curve SV1 in figure 4.26.

Fibre SV2: From the results of fibre SV1 it was concluded that the large cladding:core area ratio was resulting in a core stress level which was still excessive. The rod-in-tube preform was thus sleeved in a silica tube and drawn into fibre of the same core diameter and V-value as SV1. By sleeving the fibre in this way it was thought that the core stress level would be significantly reduced, and the cladding stress level would be accordingly raised.

The retardance measurements, figure 4.26, revealed that the retardance of the fibre had in fact increased to 86°/m as a result of the outer silica jacket. From this result it was suggested that the stress within the cladding, and, more specifically, the stress at the core/cladding interface played an important role in determining the stress birefringence in the fibre. It was also felt that increased field penetration into the cladding could lead to increased birefringence.

Fibre SV3: To test the last hyopthesis a second length of sleeved SV1 preform was drawn to have V = 2.2 at 633 nm. Again measurement of core ellipticity by etching revealed that the ellipticity was below 1%. As can be seen from the retardance measurement results (figure 4.26), decreasing the V-value as predicted led to an increased retardance which was found to be 115°/m. It was thus confirmed experimentally that the retardance was a function of not only the cladding stress level but also the V-value of the fibre.

4.3.4 Low-birefringence Fibre GSB2

In order to reduce the rapidly changing stress levels at the core/cladding interface and to obtain a more uniform stress distribution within the cladding, it was realised that by balancing the expansion coefficients of the core and cladding glasses in an HCVD preform, the core and cladding would be indistinguishable from a mechanical viewpoint. Whilst having very different optical characteristics the glasses would be subjected to the same stress levels which would be invariant with radius within both the core and cladding.

Additional benefit would be gained from the fact that the total area of deposited glass would be increased, thereby reducing the tensile stress level within the core.

Borosilicate glass was the obvious choice of cladding material and germanosilicate glass was chosen for the core because a low doping level could be employed to give an acceptable core/cladding index difference. As the previous fibres had been susceptible to excessive microbending loss due to their relatively low numerical aperture, it was decided to increase the core/cladding index difference to give an improved handling performance. Also by employing a numerical aperture of 0.12 in the fibre the B_2O_3 doping level would be sufficiently high to permit deposition of many cladding layers without excessive shrinkage of the silica substrate tube. Equating the expansion coefficients of the two glass sytems it was calculated that to achieve a 0.12 NA and exact thermal expansion matching, doping levels of 1.34 m/o GeO_2 and 2.77 m/o B_2O_3 were necessary in the core and cladding respectively.

A preform was thus produced by HCVD using a standard Heralux silica substrate tube having a 14 mm overall diameter and a 1.2 mm wall thickness. Tne borosilicate cladding layers were deposited prior to the single germanosilicate core layer. A transverse cross-section through the preform has already been given in figure 4.20b and the fibre drawn from the sleeved preform is shown in figure 4.20a. Excellent core and cladding circularity was obtained, as is seen from the transverse cross-sections of core and cladding shown at different magnification in figures 4.27a and 4.27b; in the preform the core ellipticity was again well below 1% and it has been assumed to be no worse in the fibre. The fibre was characterised by a V-value of 2.4 at the 633 nm wavelength although the fibre NA obtained by the far-field observation technique was 0.10, somewhat less than expected.

The birefringence measurements on the fibre revealed that the specific retardance had been dramatically reduced to a level which was difficult to measure in short lengths.

As can be seen from the experimental results, plotted in figure 4.26, the retardance was only 2.6°/m, and as with the other fibres the retardation was linearly dependent upon length. It was thus confirmed that by careful control of circularity and stress levels within both the core and cladding of a monomode fibre, it was possible to attain retardation levels which were three orders of magnitude lower than in typical fibres. Though this result was obtained in 1977, it still represents the lowest reported value for the birefringence of a monomode fibre.

The matched expansion coefficients also appeared to reduce the temperature sensitivity of the birefringence, thus ideally suiting the fibre to use in current measuring instrumentation. Such was the success of this fibre that it has been employed in a prototype current transducer which has been installed and successfully operated within the CEGB generating station at Fawley, Hants. Long-term tests on the effects of pressure, vibration and temperature have yet to be completed, but initial results are favourable and indicate that the fibre characteristics make such a device a practical reality.

4.4 References to Chapter 4

1. Gambling, W.A., Payne, D.N., Hammond, C.R. and Norman, S.R.: 'Optical fibres based on phosphosilicate glass'. Proc IEE, 123 (1976), pp 570 - 576.

2. Gardner, W.B.: 'Microbending losses in optical fibres', B.S.T.J.,54(1975). pp 457 - 465.

3. Horiguchi, M., and Osanai, H,: 'Spectral losses of low OH content optical fibres', Electron. Lett., 12(1976), pp 310 - 311.

4. Pinnow, D.A., Rich, T.C., Ostermayer, F.W., and DiDomenico, M.: 'Fundamental optical attenuation limits in the liquid and glassy state with application to fibre optical waveguide materials', App.Phys.Lett., 22(1973), pp 527 - 529.

5. Inada, K.: 'A new graphical method relating to optical fibre attenuation', Opt.Commun., 19(1976), p 437.

6. Kaiser, P.: 'Drawing-induced colouration in vitreous silica fibres', J.Opt.Soc.Am., 64(1974), pp 475 - 481.

7. Dodd, D.M., and Fraser D.B.: 'Optical determination of OH in fused silica', J. App. Phys., 37(1966), p 3911.

8. Payne, D.N., and Gambling, W.A.: 'Zero material dispersion in optical fibres', Electron. Lett., 11(1975), pp 176 - 178.

9. Osanai, H., Shioda, T., Moriyama, T., Araki, S., Horiguchi, M., Izawa, T. and Takata, H.: 'Effect of dopants on transmission loss of low OH content optical fibres', Electron. Lett., 12(1976), pp 549 - 550.

10. Edahiro, T., Horiguchi, M., Chida, K., and Ohmori, Y.,: 'Spectral loss characteristics of GeO_2-P_2O_5 - doped silica graded-index fibres in long wavelength band', Electron. Lett., 15(1979), pp 274 - 275.

11. Olshansky, R., and Keck, D.B.,: 'Pulse broadening in graded-index optical fibres', App. Opt., 15(1976), pp 483 - 491.

12. Midwinter, J.E.,: 'Optical fibre communications' John Wiley and Sons, New York 1979, p 398.

13. Versluis, J.W., and Peelen, J.G.T.,: 'Optical communication fibres. Manufacture and properties', Philips Telecomm. Rev., 37(1979), pp 215 - 230.

14. Hartog, A.H.,: Private communication.

15. Olshansky, R., and Oaks, S.M.: 'Differential mode delay measurement', Prog. 4th European Conference on Optical Communications, Genoa 1978, pp 128 - 132.

16. Gambling, W.A., Matsumura, H., and Ragdale, C.M.,: 'Mode dispersion, material dispersion and profile dispersion in graded-index single-mode fibres', Microwaves, Optics and Acoustics, 3 (1979), pp 239-246.

17. Gambling, W.A.: and Matsumura, H.: 'Simple characterisation factor for practical single-mode fibres', Electron. Lett., 23(1977), pp 691 - 693.

18. Gloge, D.: 'Weakly guiding fibres', App. Opt. 10(1971), pp 2252 - 2258.

19. Gambling, W.A., Payne, D.N., Matsumura, H., and Dyott, R.B.: 'Determination of core diameter and refractive index difference of single-mode fibres by observation of the far-field pattern', Microwaves. Opt. and Acoust., 1(1976), pp 13 - 17.

20. Gambling, W.A., Matsumura, H., and Ragdale, C.M.: 'Wave propagation in a single-mode fibre with dip in the refractive index', Opt. Quant. Electr. 10(1978), pp 301 - 309.

21. Katsuyama, Y., Tokuda, M., Uchida, N., and Nakahara, M.: 'New method for measuring V-value of a single-mode optical fibre', Electron. Lett., 12(1976), pp 669 - 670.

22. Gambling, W.A., Payne, D.N., Matsumura, H., and Norman, S.R.: 'Measurement of normalised frequency in single-mode optical fibres', Electron. Lett., 13(1977), pp 133 - 135.

23. Murakami, Y., Kawana, A., and Tsuchiya, H.: 'Cut-off wavelength measurements for single-mode optical fibres', App. Opt., 18(1979), pp 1101 - 1105.

24. Miya, T., Terusuma, Y., Hosaka, T., and Miyashita, T.: 'Ultimate low-loss single-mode fibre at 1.55 um', Electron. Lett., 15(1979), pp 106 - 108.

25. Smith, A.M.: 'Polarisation and magneto-optic properties of single-mode optical fibres', App. Opt., 17(1978), pp 52 - 56.

26. Marcatili, E.A.J.: 'Dielectric rectangular waveguide and directional coupler for integrated optics', B.S.T.J., 48(1969), pp 2071.

27. Bananin, V.I.: 'Radial and tangential stresses in clad glass fibres', Translated from Izvestiya Akademii Nauk SSSR, 4(1968), pp 2223 - 2228.

28. Norman, S.R., Payne, D.N., Adams, M.J., and Smith, A.M.: 'Fabrication of single-mode fibres exhibiting extremely low polarisation birefringence', Electron. Lett., 15(1979), pp 309 - 311.

FIBRE NO. :	VD214	SV1	SV2	SV3	GSB2
Core composition	SiO_2	SiO_2	SiO_2	SiO_2	GeO_2-SiO_2
Core Diameter μm	8.5	9.0	9.0	8.0	4.0
Cladding composition	B_2O_3-SiO_2	Vycor	Vycor	Vycor	B_2O_3-SiO_2
Cladding diameter μm	36	-	140	123	16.5
Substrate tube	Silica	Vycor	Silica	Silica	Silica
Overall fibre diameter μm	140	140	180	158	85
Relative index difference Δ	7.6×10^{-4}	7.4×10^{-4}	7.4×10^{-4}	7.4×10^{-4}	3.4×10^{-3}
V-value at 633 nm	2.4	2.5	2.5	2.2	2.4

Table 4.1: Characteristics of a series of monomode fibres fabricated to investigate the effects of residual stress and core ellipticity upon birefringence.

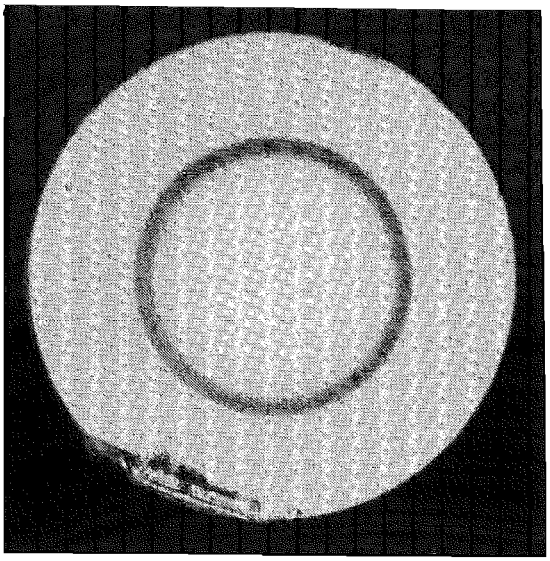

a) CROSS-SECTION OF "STANDARD" GRADED-INDEX FIBRE

Core diameter	= 63 um
Fibre diameter	= 125 um
Cladding thickness	= 4 um
Core Glass	: P_2O_5-GeO_2-SiO_2
Cladding Glass	: B_2O_3-SiO_2

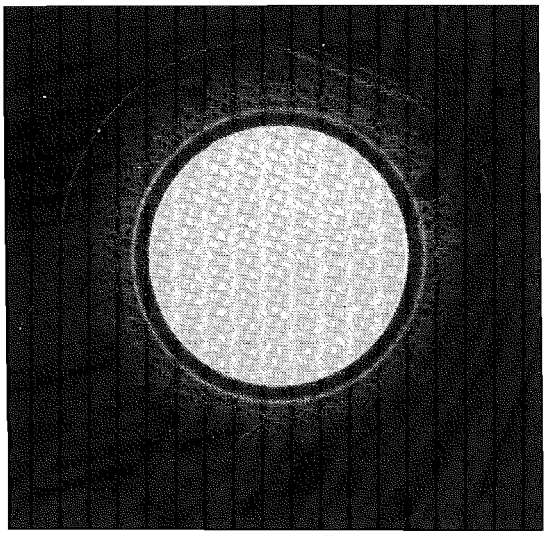

b) CROSS-SECTION OF "LARGE-CORE" GRADED-INDEX FIBRE

Core diameter	= 75 um
Fibre diameter	= 125 um
Cladding thickness	= 4 um
Core Glass	: P_2O_5-GeO_2-SiO_2
Cladding Glass	: B_2O_3-SiO_2

FIGURE 4.1

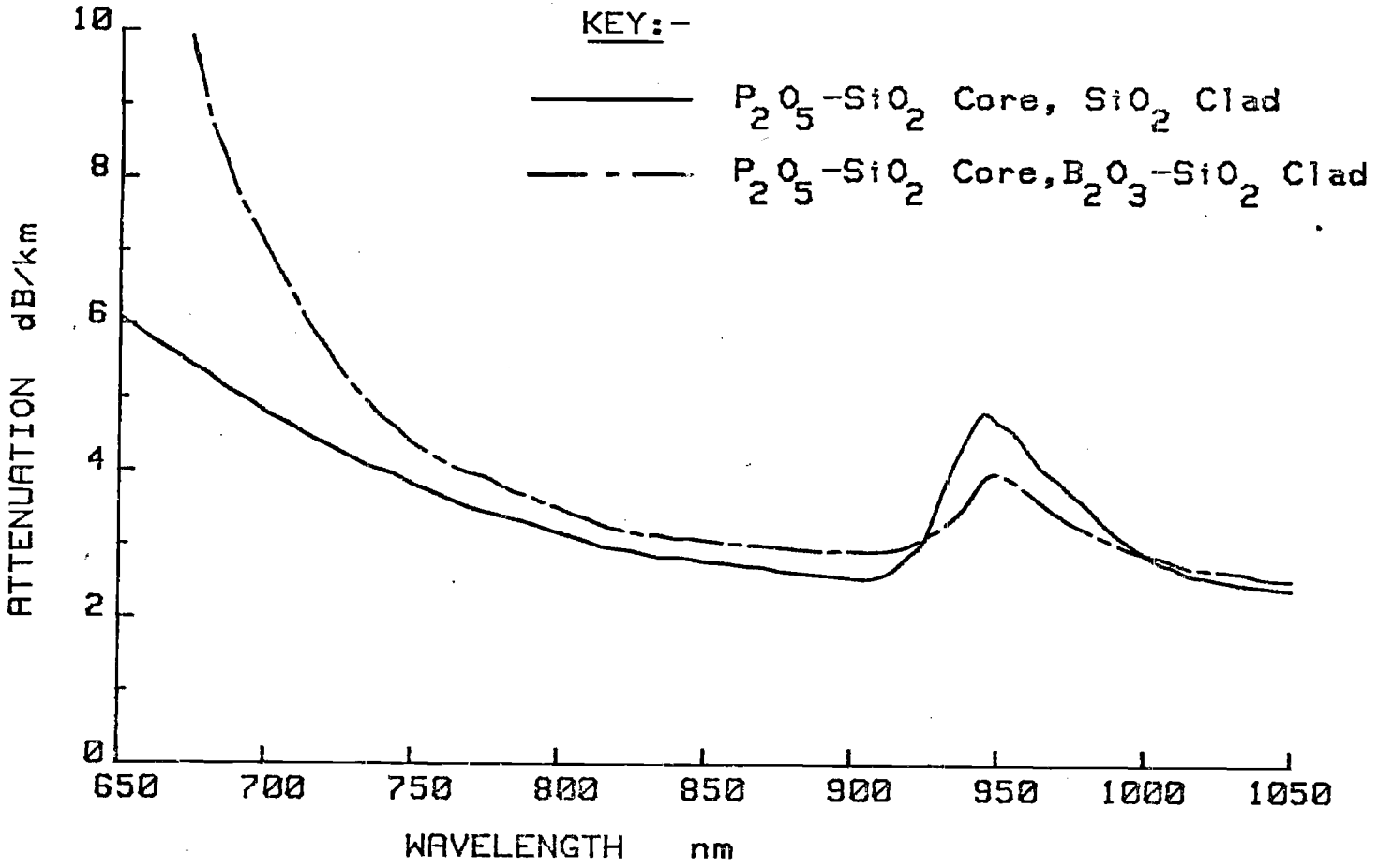

SPECTRAL LOSS CHARACTERISTICS OF GRADED-INDEX FIBRES HAVING A PHOSPHOSILICATE-GLASS CORE IN SILICA OR BOROSILICATE CLADDING.

FIGURE 4.2

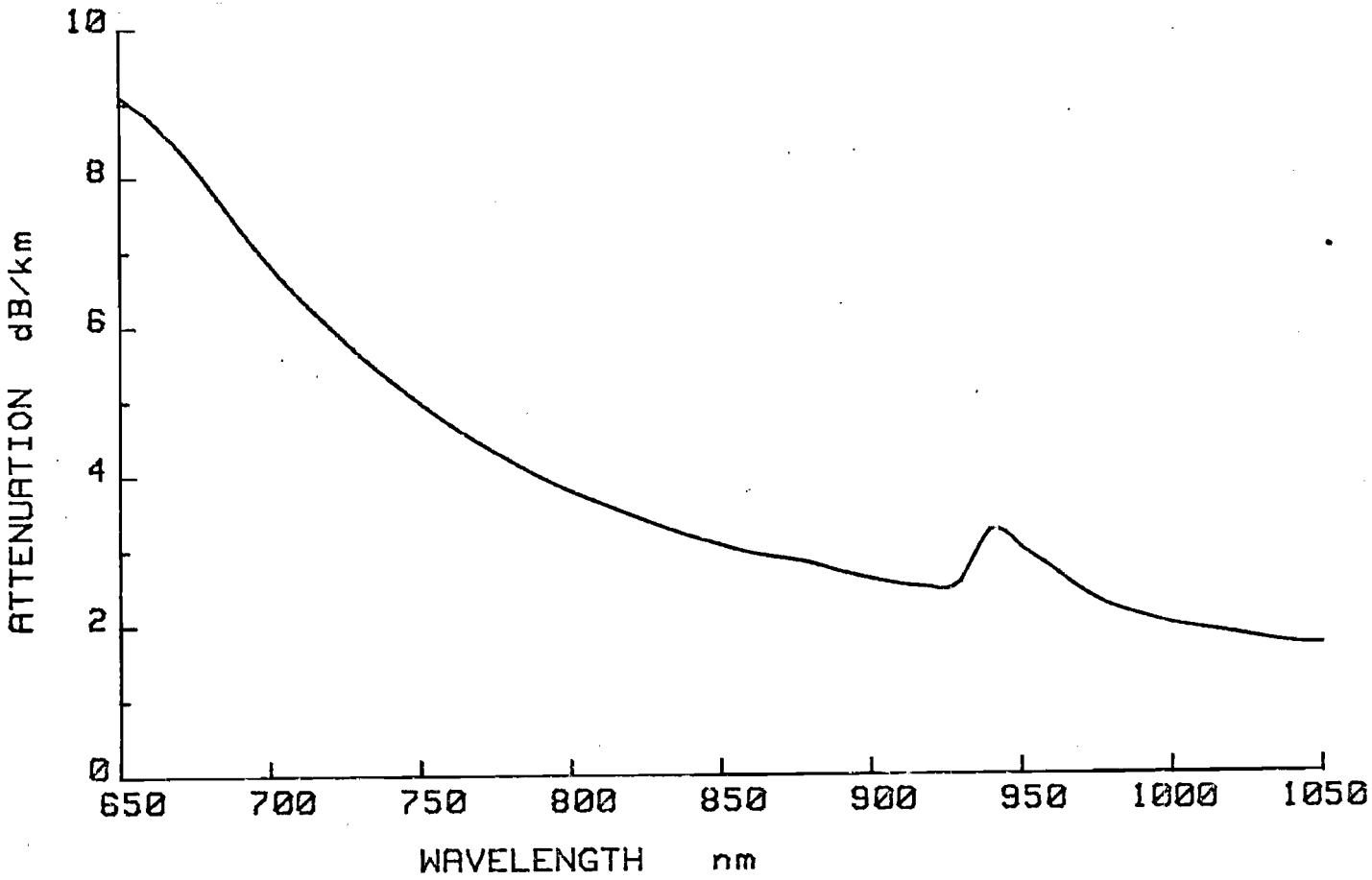

SPECTRAL ATTENUATION OF TYPICAL P_2O_5-GeO_2-SiO_2 GRADED INDEX FIBRE OVER THE WAVELENGTH RANGE 650nm TO 1050nm.

FIGURE 4.3

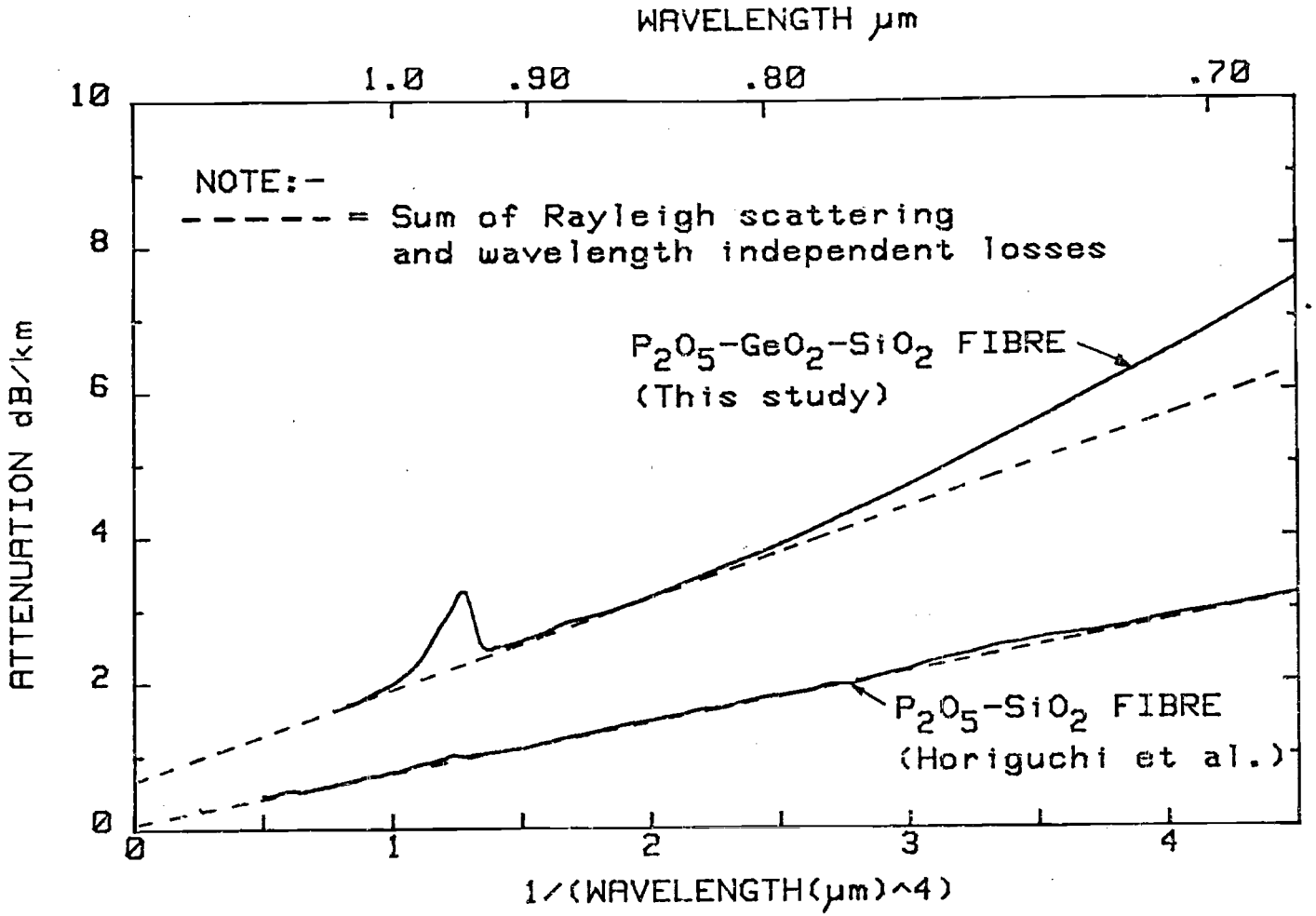

SPECTRAL ATTENUATION OF P_2O_5-GeO_2-SiO_2 AND P_2O_5-SiO_2 FIBRES PLOTTED ON (WAVELENGTH)$^{-4}$ SCALE.

FIGURE 4.4

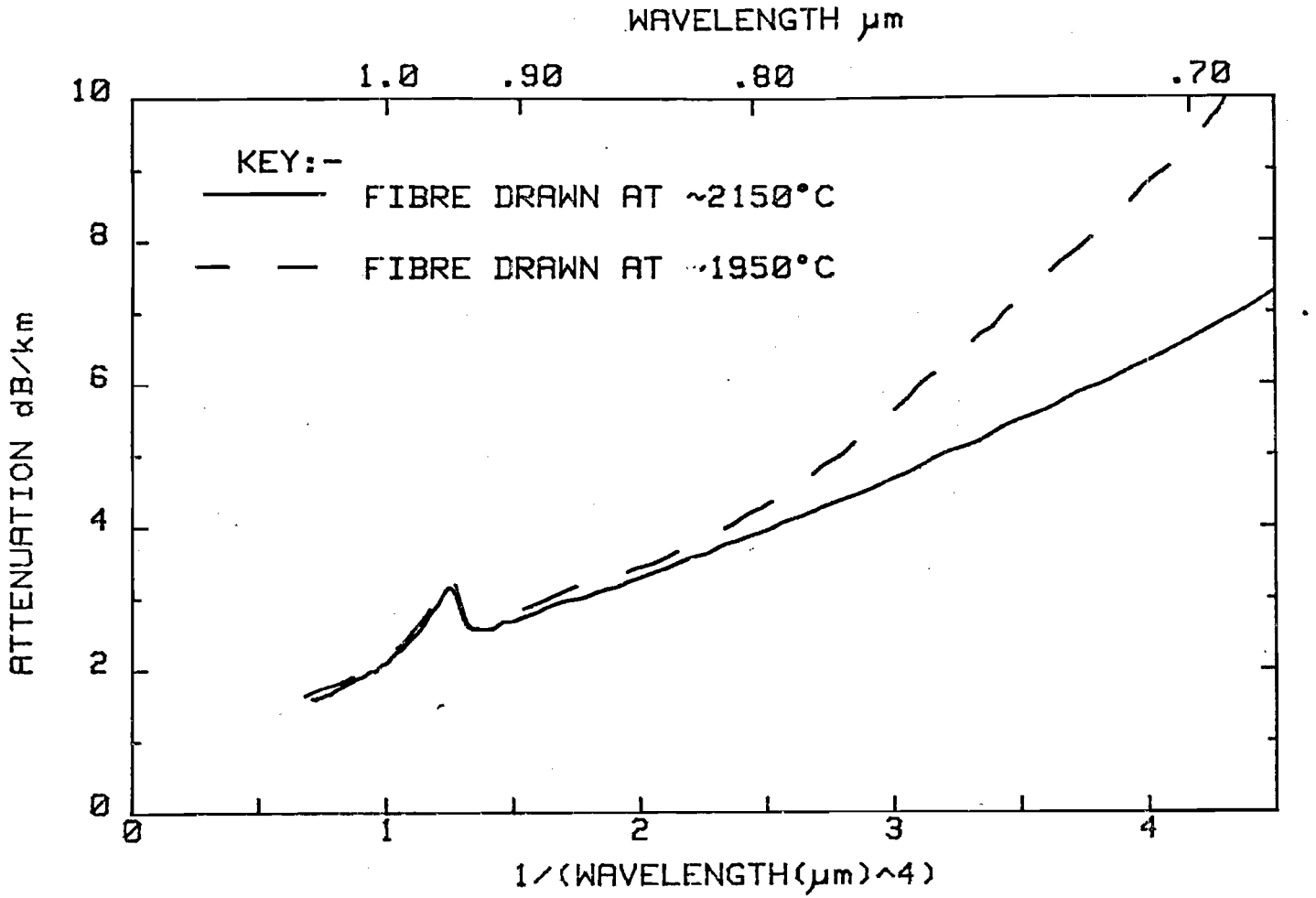

SPECTRAL ATTENUATION CHARACTERISTICS OF TWO LENGTHS OF FIBRE DRAWN AT DIFFERENT TEMPERATURES FROM THE SAME PREFORM.

FIGURE 4.5a

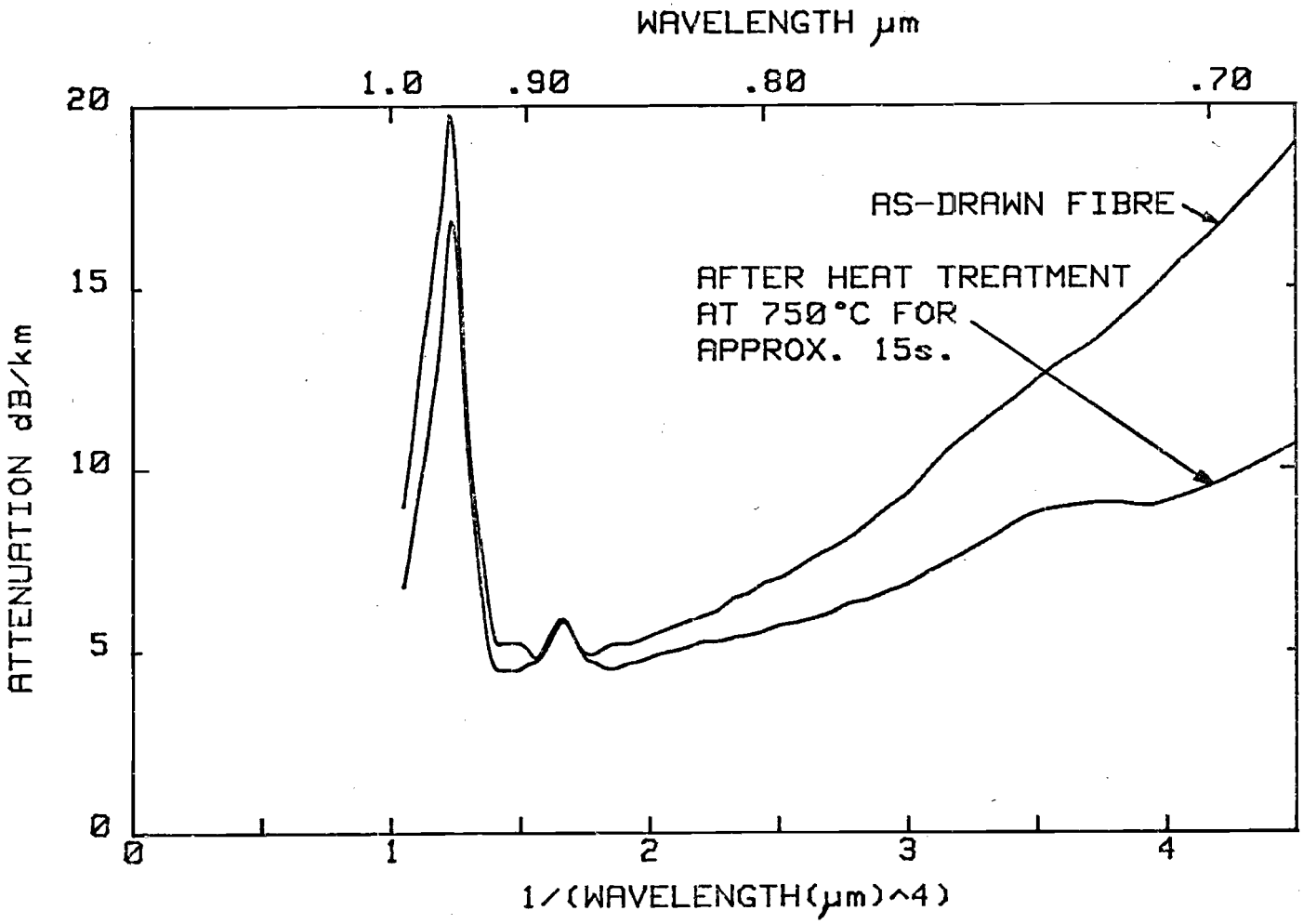

EFFECT OF HEAT-TREATMENT UPON THE SPECTRAL ATTENUATION OF P_2O_5-GeO_2-SiO_2 GRADED-INDEX FIBRE.

FIGURE 4.5b

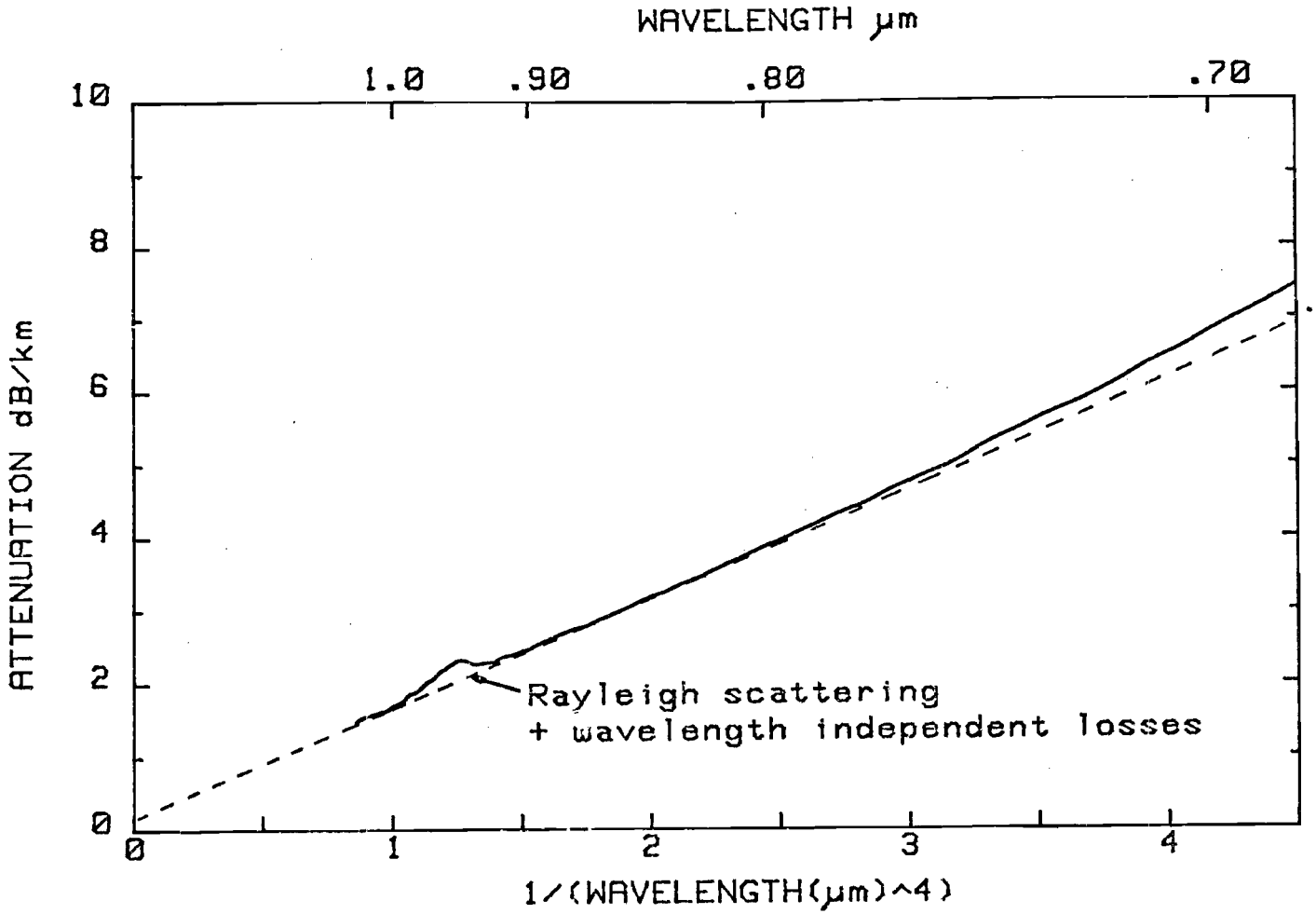

SPECTRAL ATTENUATION OF FIBRE VD280 PLOTTED ON (WAVELENGTH)$^{-4}$ SCALE. The diameter variations along the fibre were less than $\pm 1\mu m$.

FIGURE 4.6

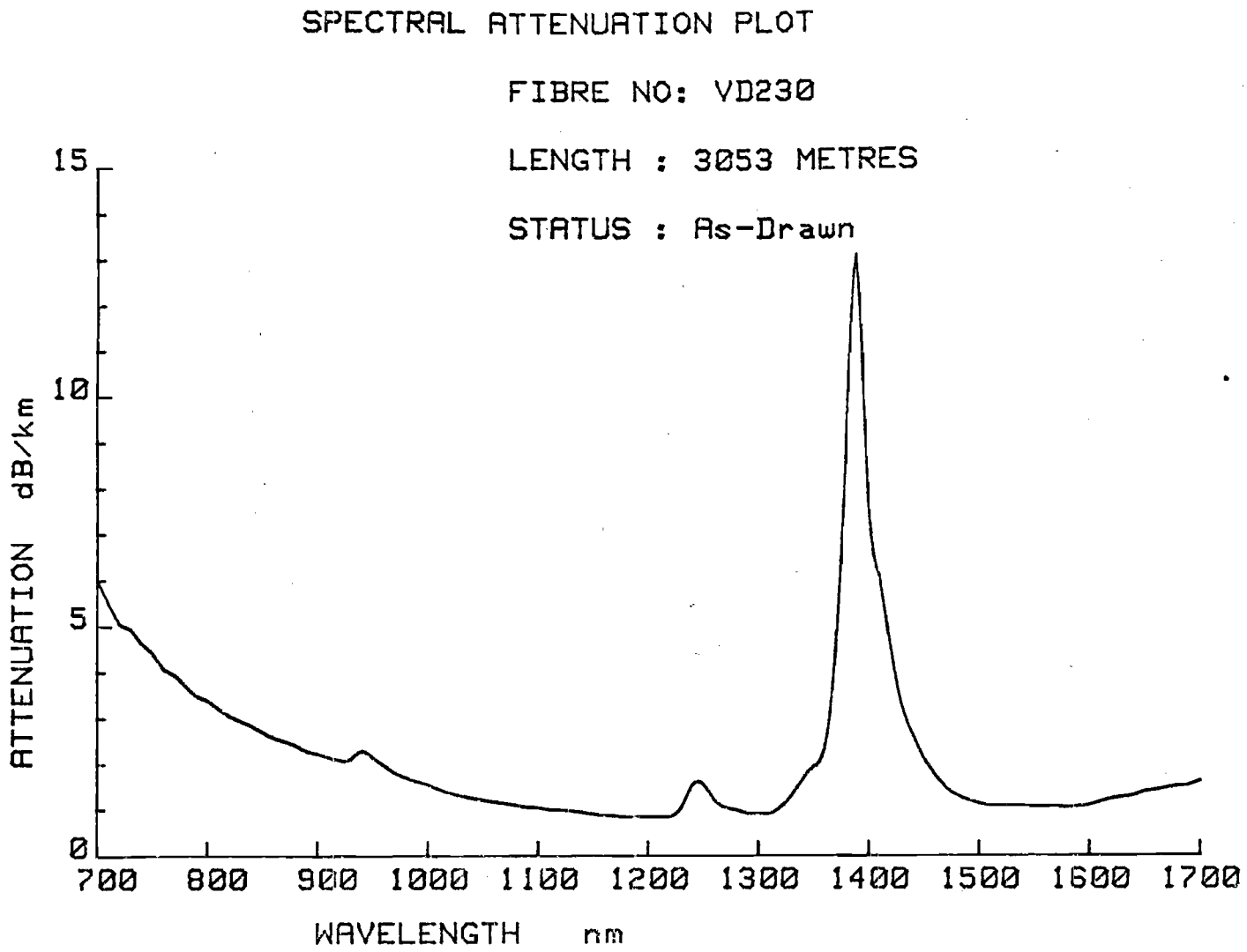

SPECTRAL ATTENUATION OF GRADED-INDEX FIBRE OVER THE WAVELENGTH RANGE 700nm TO 1700nm. The measurement was made with the fibre fully excited.

FIGURE 4.7

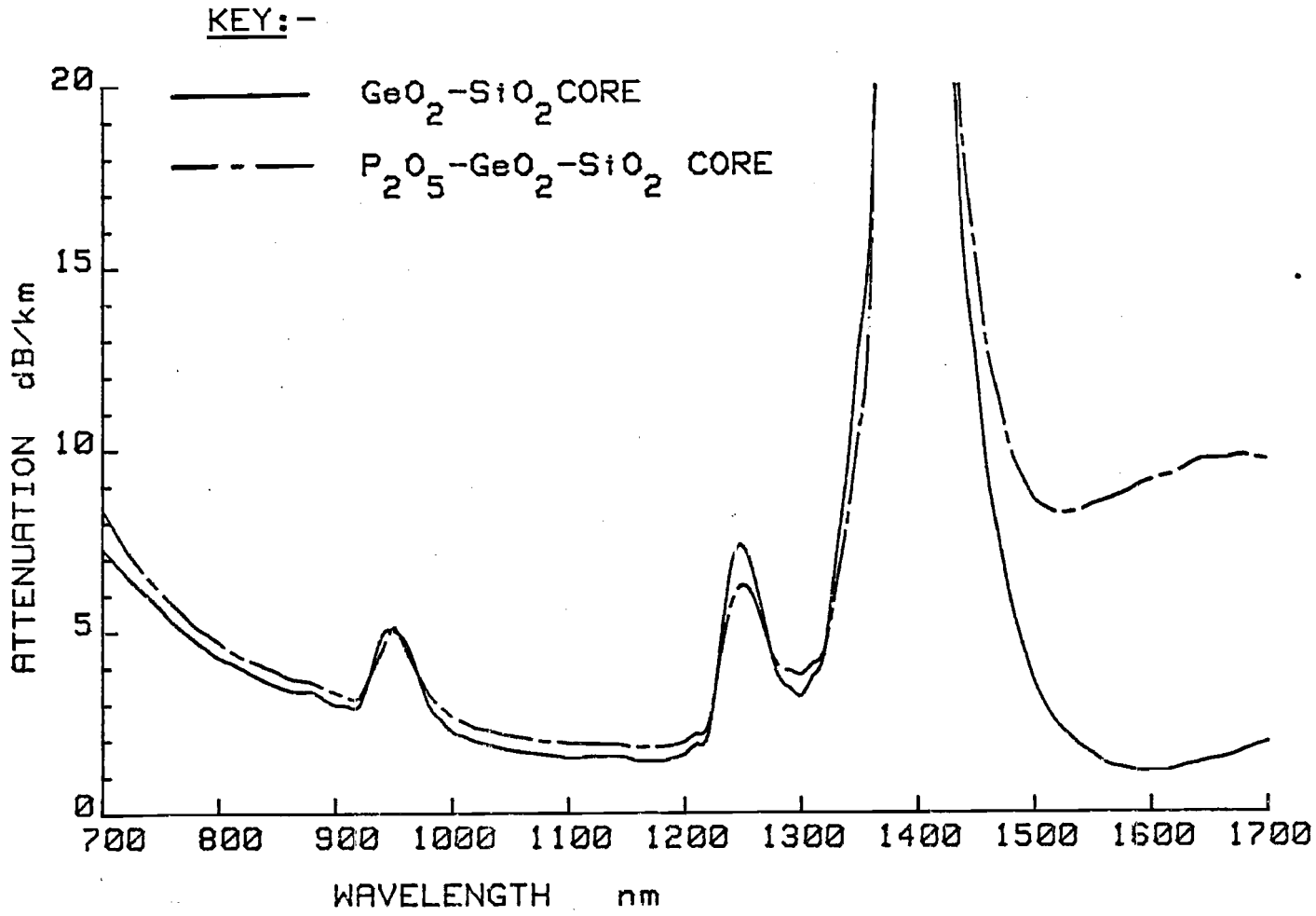

LOSS SPECTRA OF HIGH OH-CONTENT GeO_2-SiO_2 AND P_2O_5-GeO_2-SiO_2 GRADED-INDEX FIBRES OVER THE WAVELENGTH RANGE 700nm TO 1700nm.

FIGURE 4.8

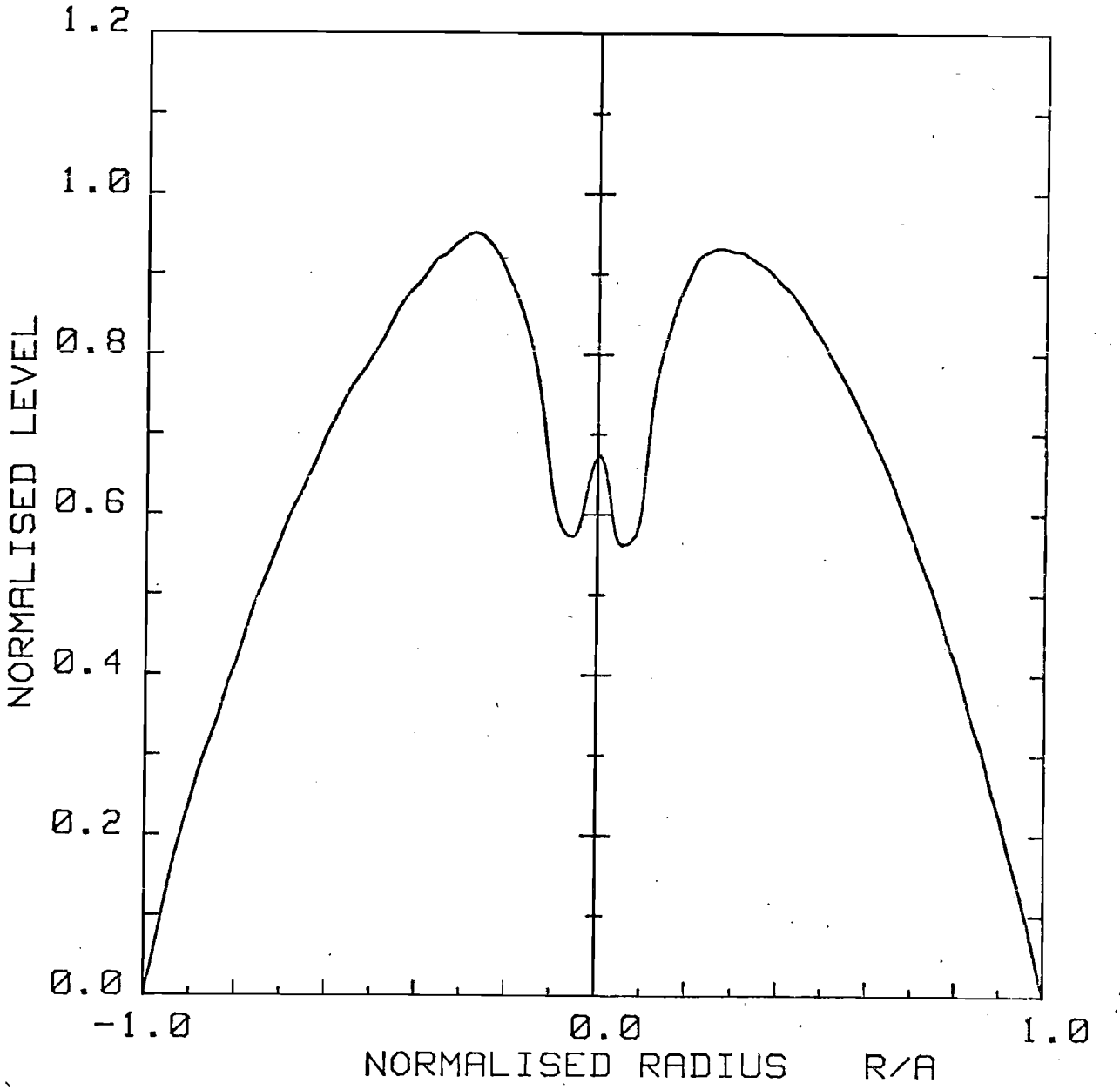

Refractive index profile of phosphosilicate-core, borosilicate-clad, graded-index fibre. Outdiffusion of dopant has been partially compensated during the preform collapse.

FIGURE 4.9

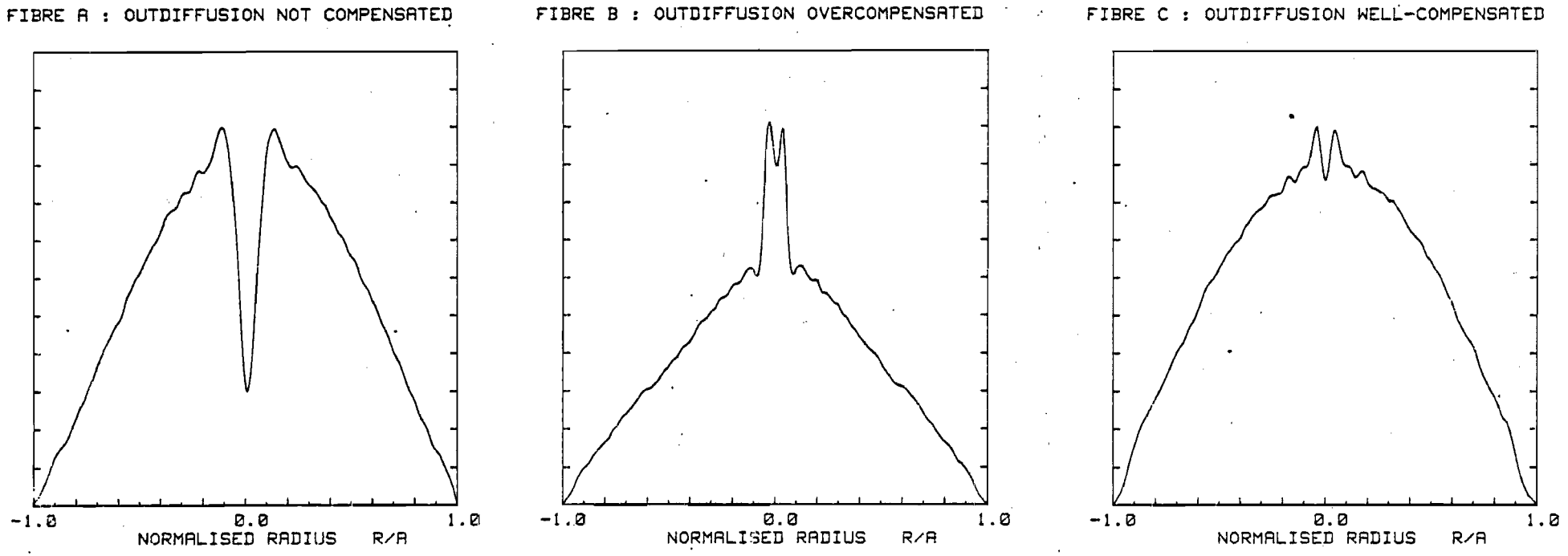

REFRACTIVE INDEX PROFILES OF THREE GRADED-INDEX FIBRES IN WHICH DIFFERENT DEGREES OF COMPENSATION FOR THE OUT-DIFFUSION OF DOPANT DURING COLLAPSE WERE EMPLOYED. Compensation was achieved by creating a germania-rich atmosphere in the closure-zone during the preform collapsing operation.

FIGURE 4.10

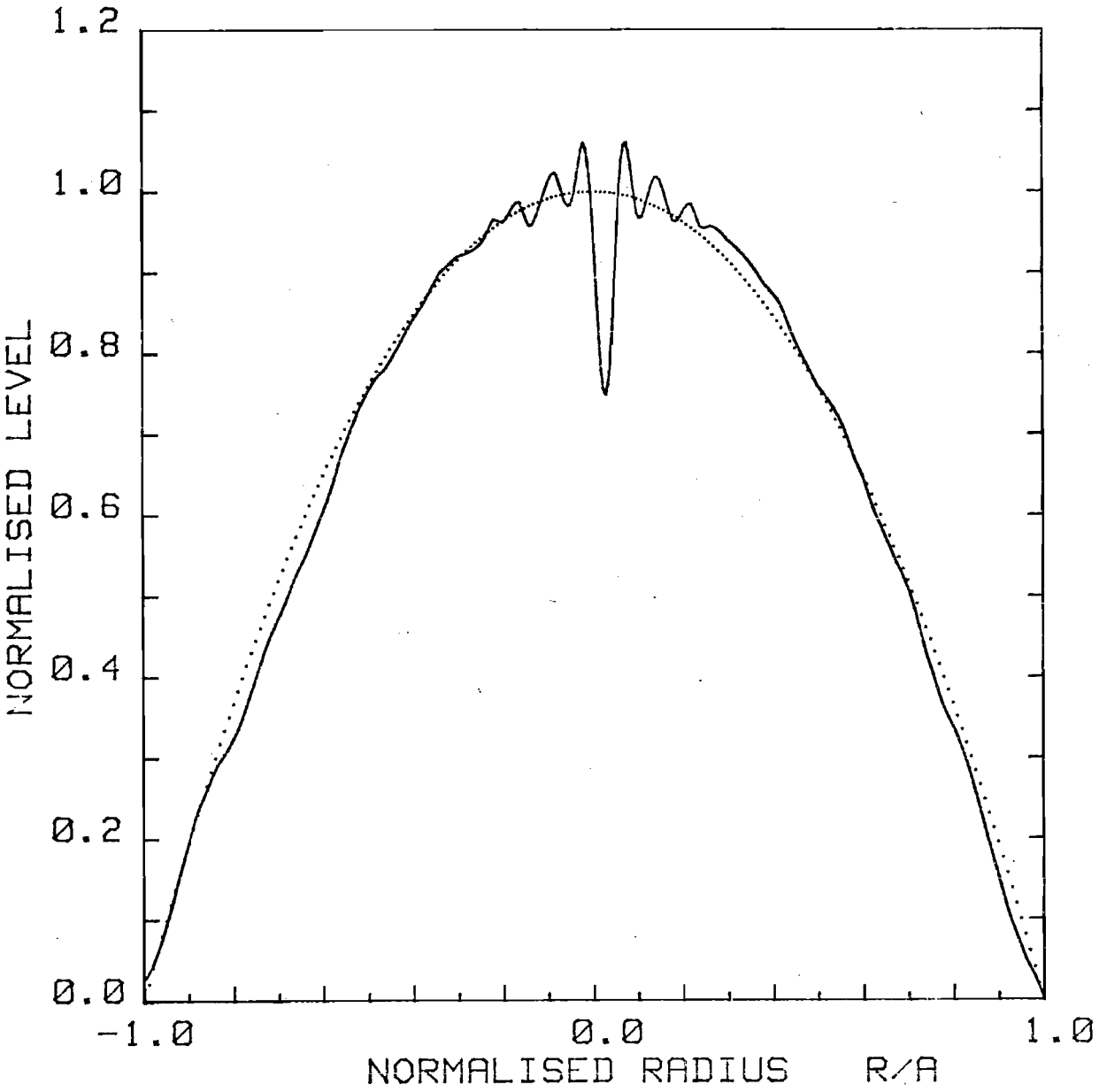

REFRACTIVE INDEX PROFILE OF P_2O_5-GeO_2-SiO_2 GRADED-INDEX FIBRE VD230 [Solid line]. The broken line describes an alpha-profile of exponent 2.05.

FIGURE 4.11

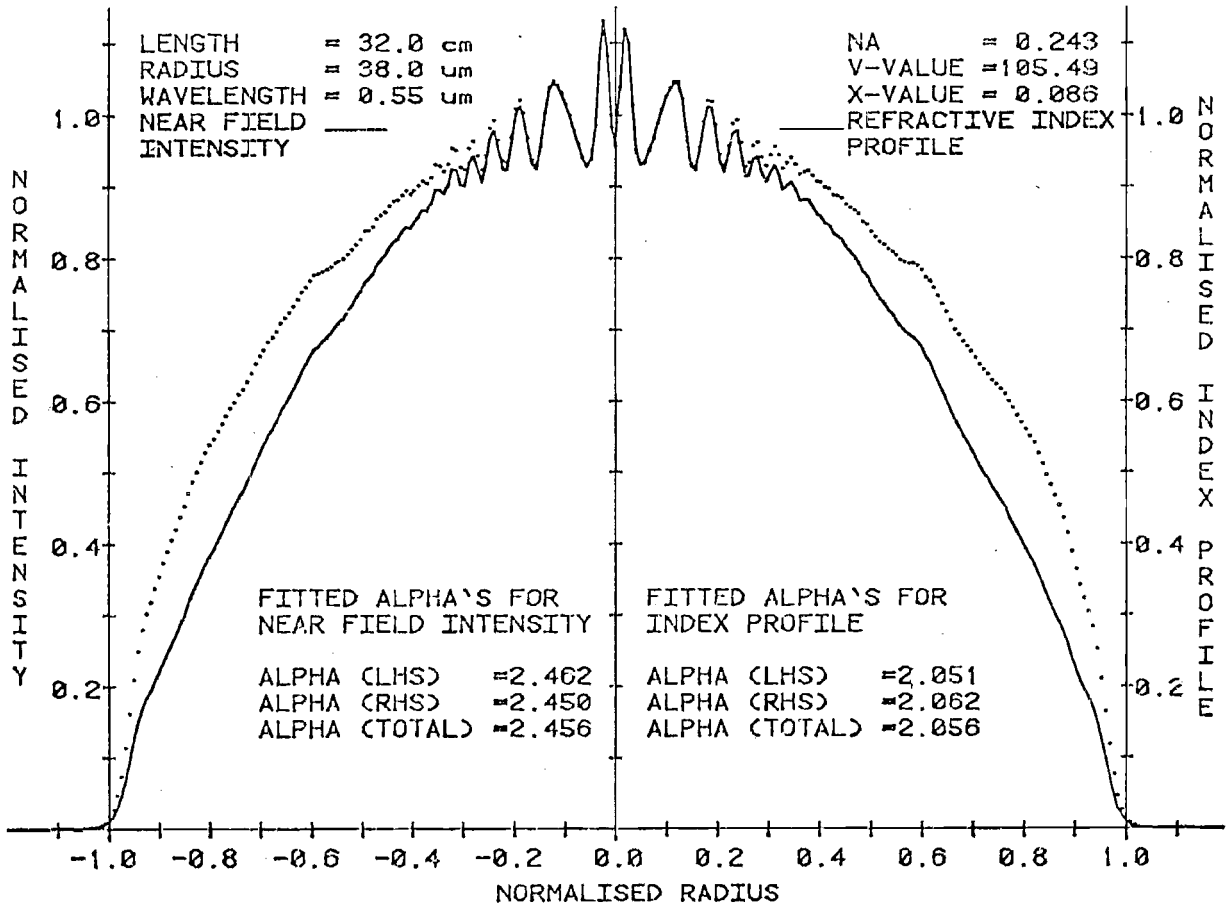

Near-field intensity distribution (dotted line) and deduced refractive index profile (solid line) of a graded-index phospho-germanosilicate-cored fibre. The equivalent alpha-values for the near-field and index profile are also shown. The symmetry of the profile is excellent, and the index profile is near-optimal for 0.85 μm operation.

FIGURE 4.12

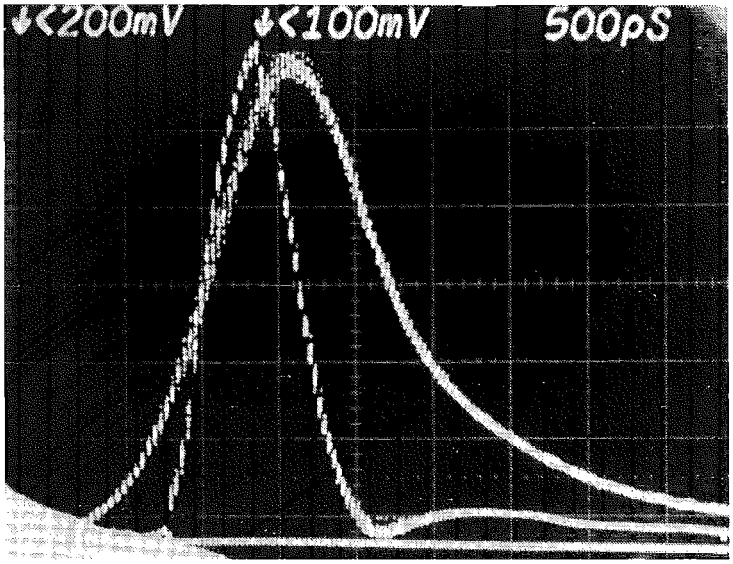

Timebase = 0.5 ns/div.

Input pulse-width = 0.65 ns FWHM

Output pulse-width = 1.28 ns FWHM

FWHM pulse dispersion = 1.1 ns over 3.03km

= 0.36 ns/km (including material dispersion)

Measurement wavelength = 850 nm

Laser source linewidth ~ 2 nm

PULSE DISPERSION IN 3.03km LENGTH OF GRADED-INDEX FIBRE VD230 .

FIGURE 4.13

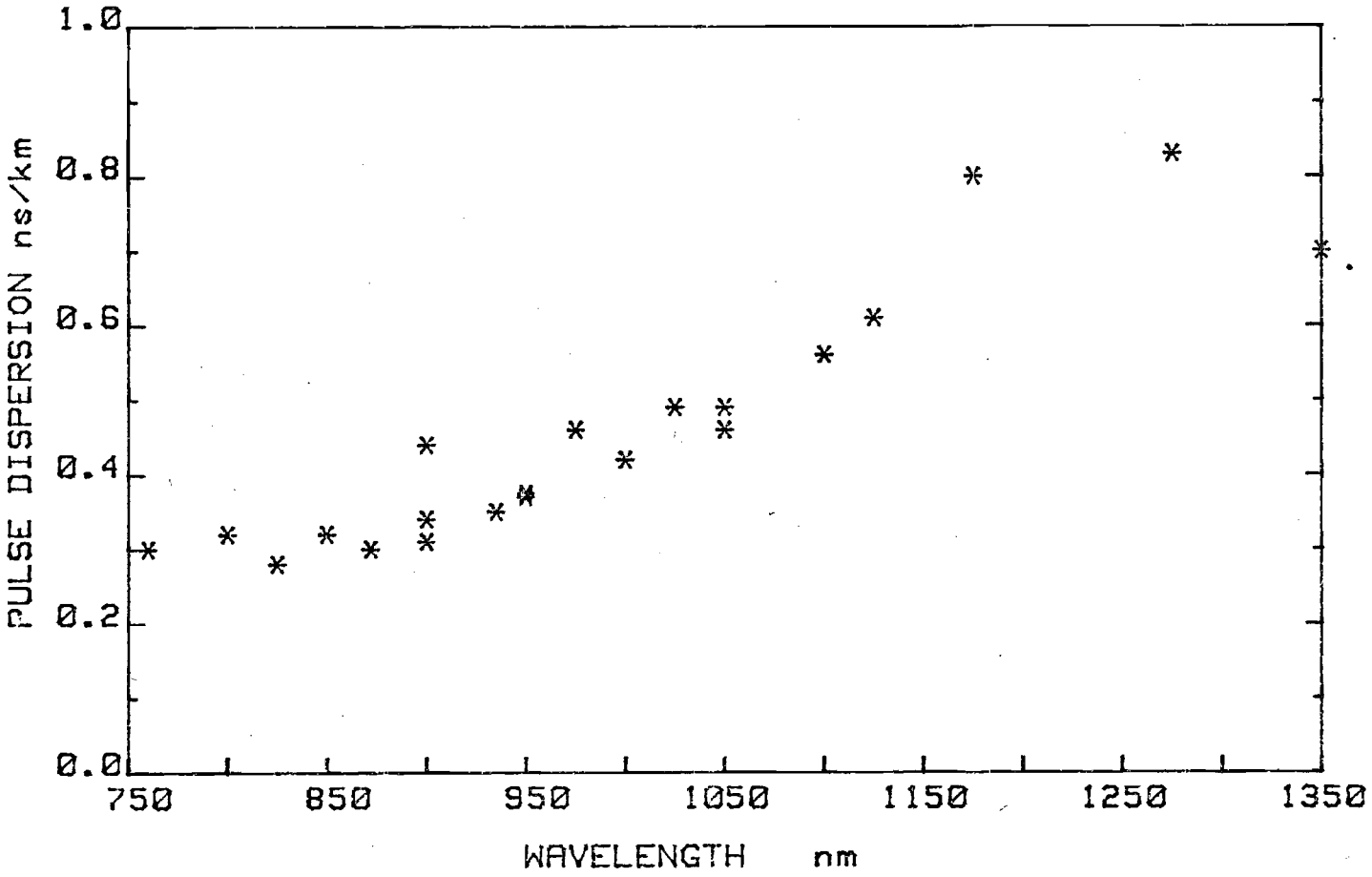

PULSE DISPERSION AS A FUNCTION OF WAVELENGTH IN P_2O_5-GeO_2-SiO_2 GRADED-INDEX FIBRE VD230 .

FIGURE 4.14

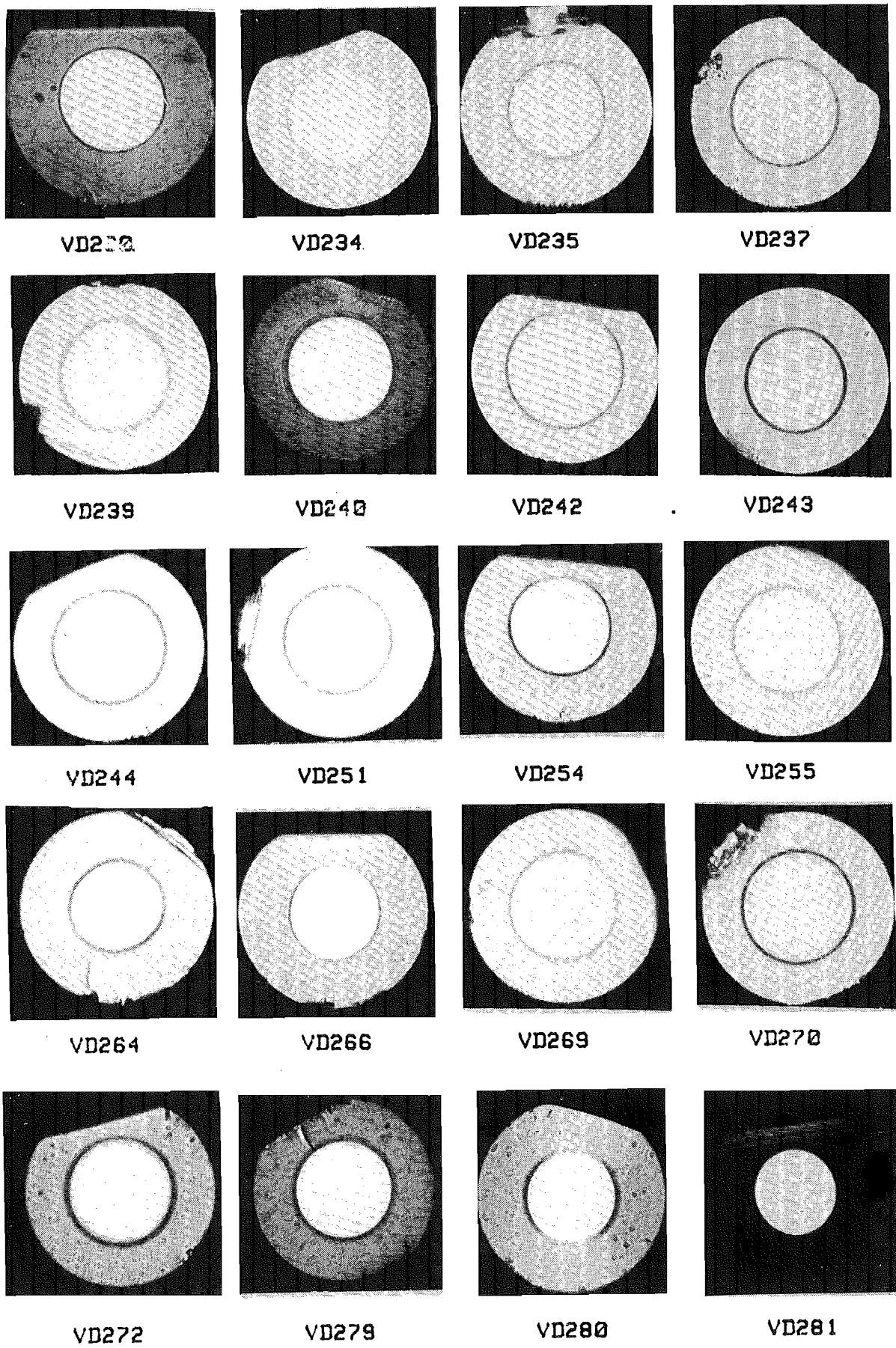

TRANSVERSE CROSS-SECTIONS OF TWENTY P_2O_5-GeO_2-SiO_2 GRADED-INDEX FIBRES MANUFACTURED UNDER NOMINALLY IDENTICAL CONDITIONS

FIGURE 4.15

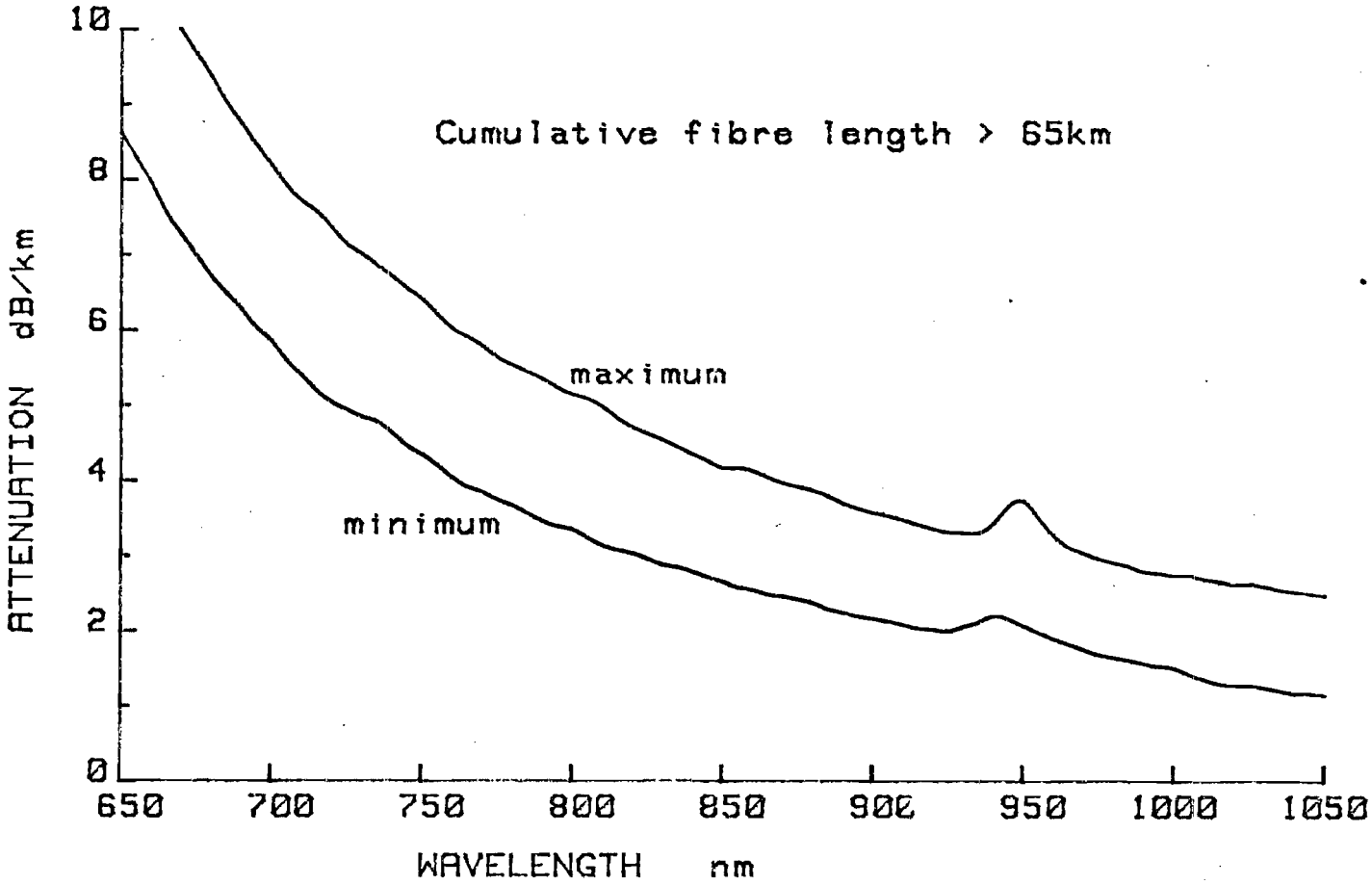

COMPOSITE LOSS SPECTRUM OF TWENTY P_2O_5-GeO_2-SiO_2 GRADED-INDEX FIBRES MANUFACTURED UNDER NOMINALLY IDENTICAL CONDITIONS.

FIGURE 4.16

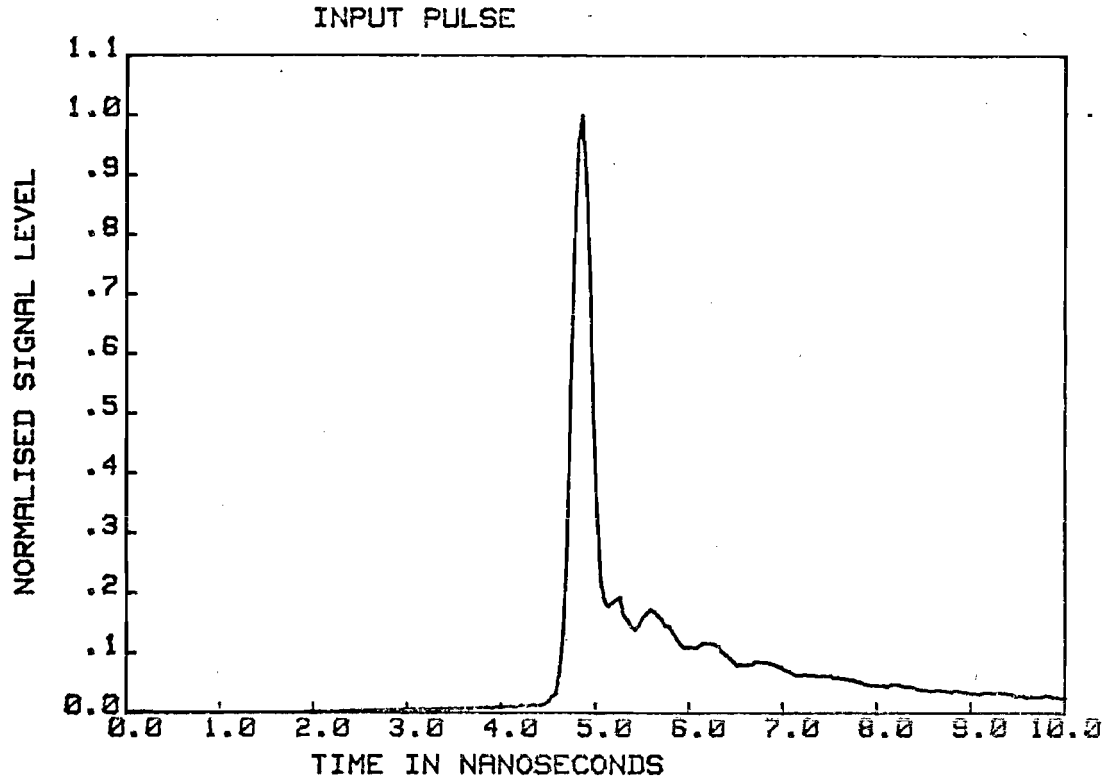

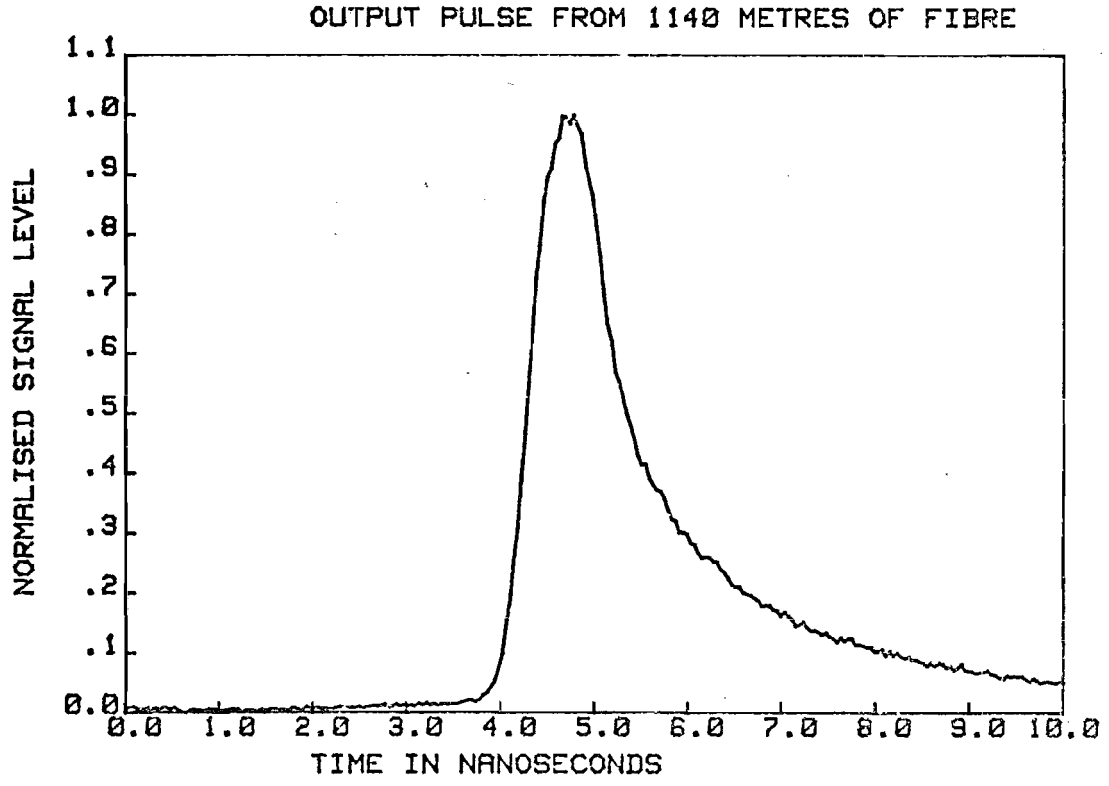

Measurement wavelength = 850nm ; Source = Laser
Fibre length = 1140m

PULSE DISPERSION CHARACTERISTICS OF TYPICAL

P_2O_5-GeO_2-SiO_2 GRADED-INDEX FIBRE.

FIGURE 4.17

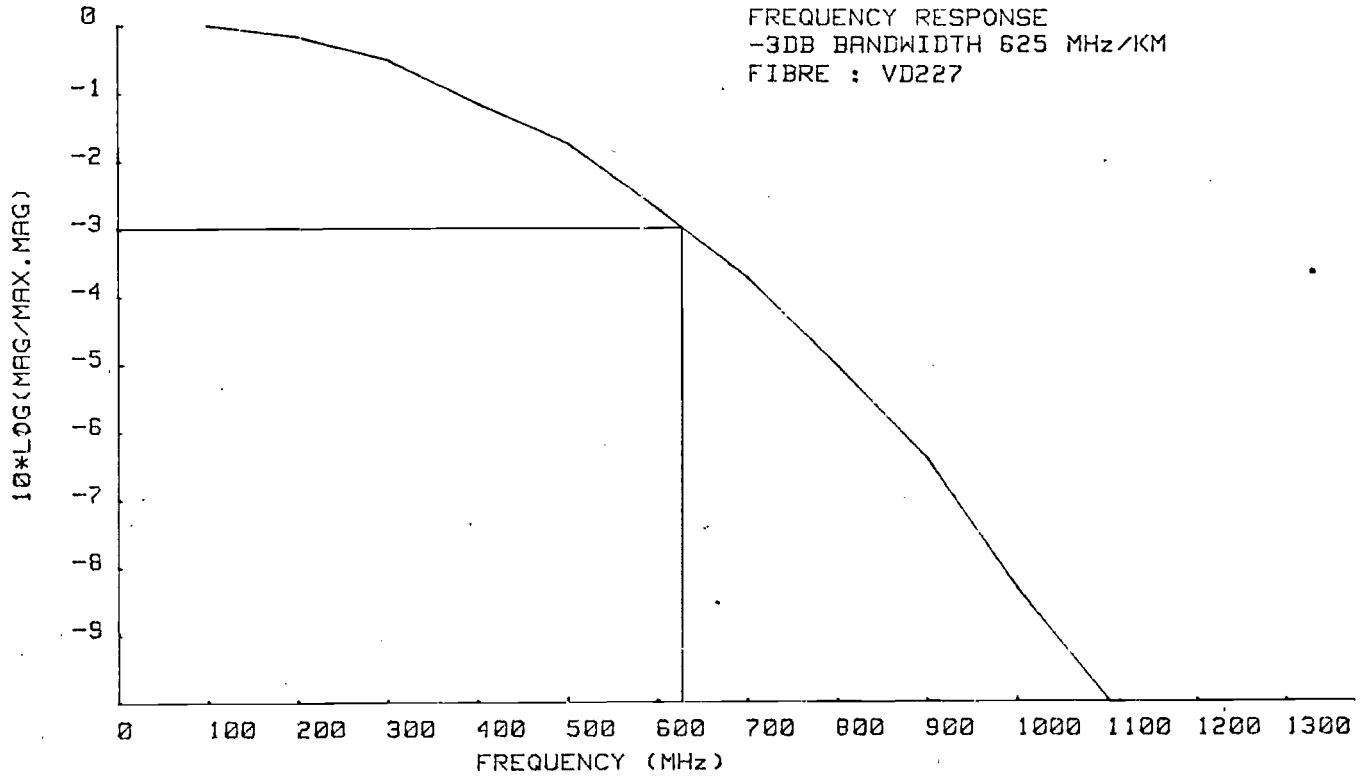

FREQUENCY RESPONSE OF TYPICAL P_2O_5-GeO_2-SiO_2 GRADED-INDEX FIBRE.

The results were computed by FFT from the pulse dispersion characteristics of the fibre (see Figure 4.17)

FIGURE 4.18

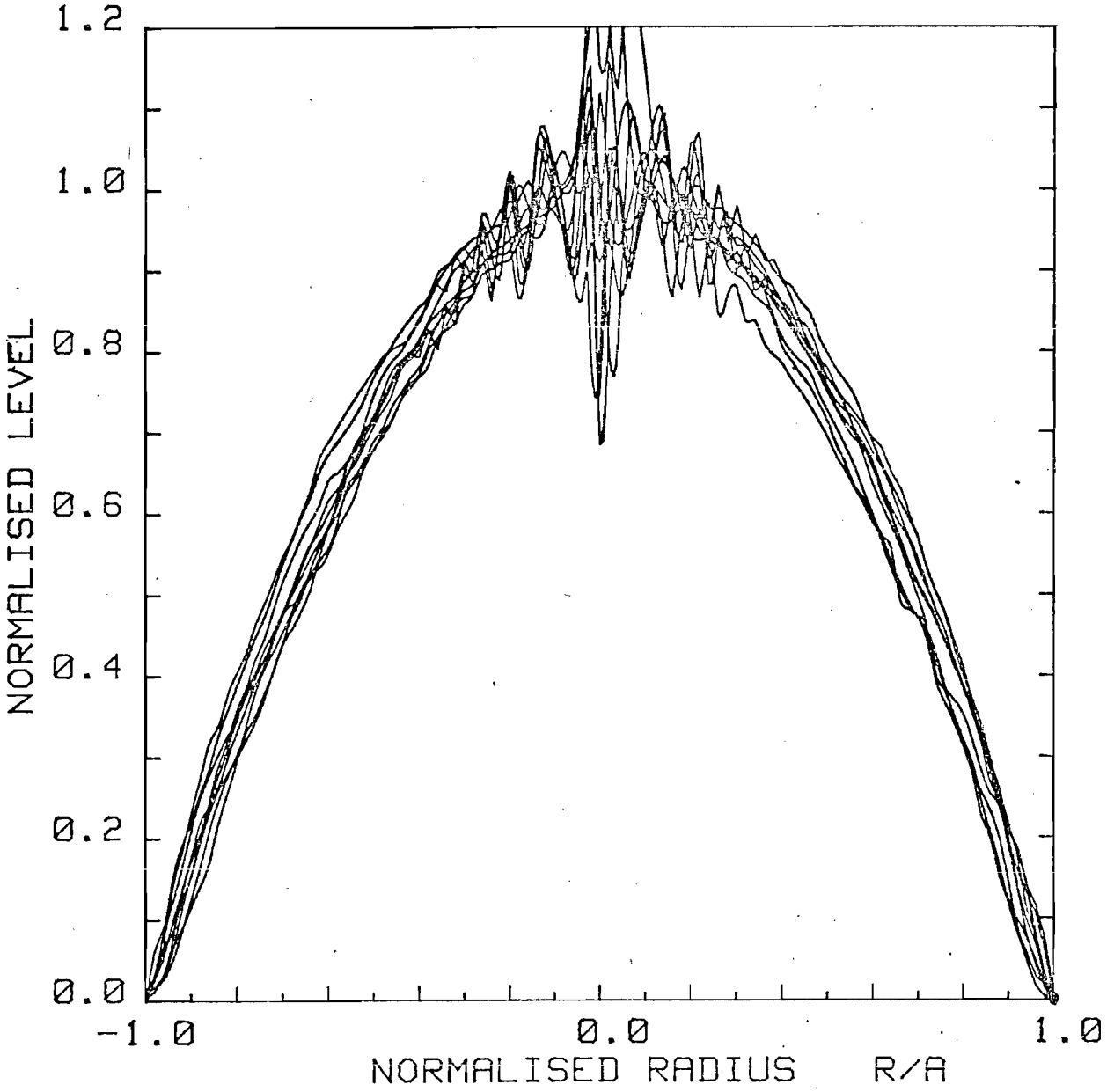

Refractive index profiles of 10 graded-index fibres manufactured under nominally identical conditions .

FIGURE 4.19

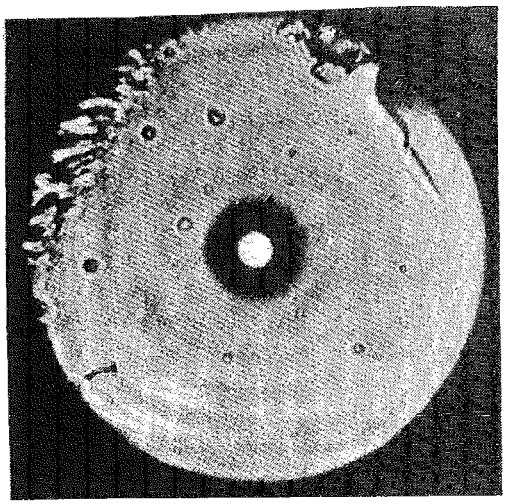

A: CROSS-SECTION OF MONOMODE FIBRE WITH V=2.4 AT 0.633μm.
The fibre has a germanosilicate core in a borosilicate cladding.
Core diameter, 2a ~ 4μm
Clad diameter = 18 μm
Fibre diameter = 90 μm

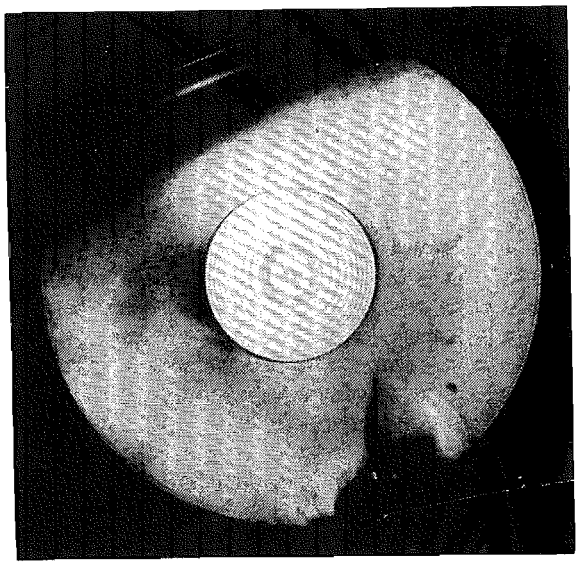

B: CROSS-SECTION OF PREFORM FROM WHICH THE ABOVE FIBRE WAS DRAWN.
Core : Cladding diameter ratio = 0.24

FIGURE 4.20

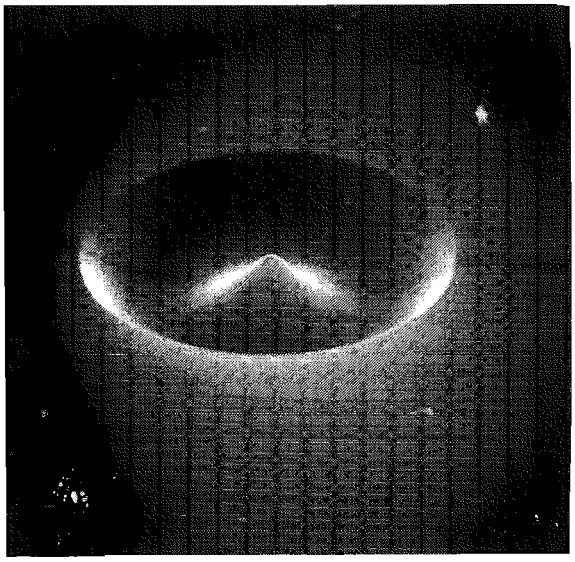

ETCHED CORE OF PHOSPHOSILICATE-CORE, SILICA-CLAD SINGLE-MODE FIBRE. SEM ×700mag.
The depletion of P_2O_5 from the core-centre is shown. Core diameter = 6μm

FIGURE 4.21

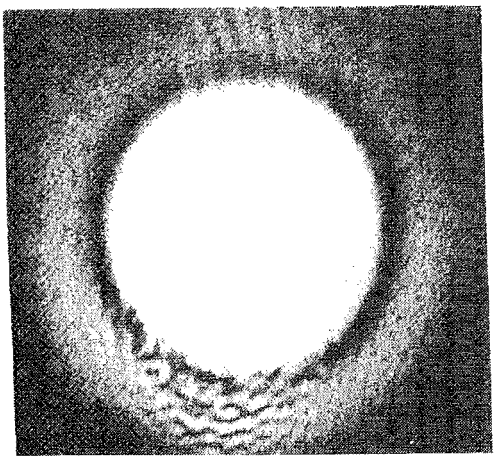

FAR-FIELD RADIATION PATTERN OF MONOMODE FIBRE.
The central Gaussian-spot and first side-lobe are clearly distinguishable.

FIGURE 4.22

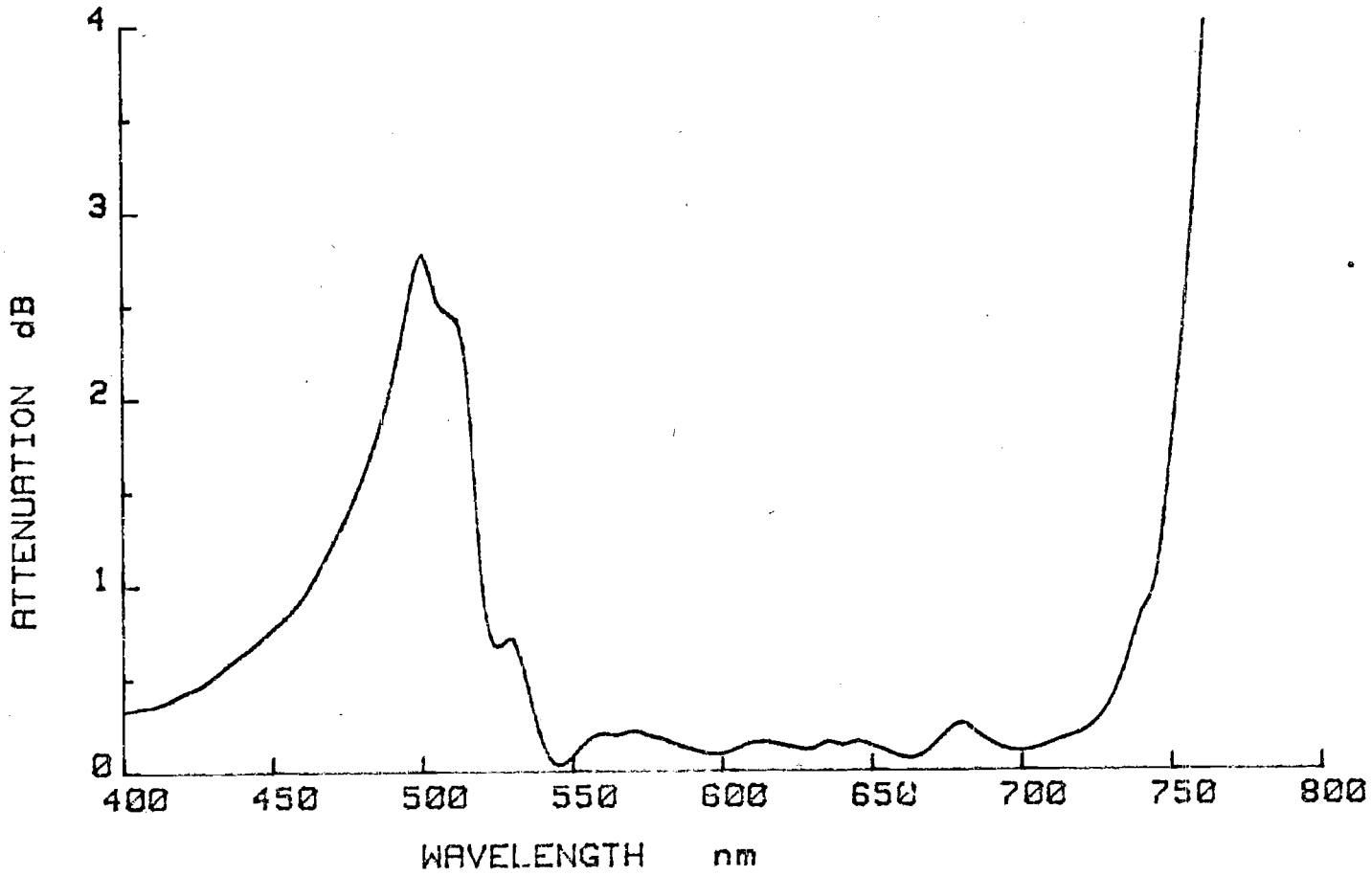

WAVELENGTH DEPENDENCE OF EXCESS LOSS DUE TO 1.5cm RADIUS BEND IN SINGLE-MODE FIBRE GSB2.

FIGURE 4.23

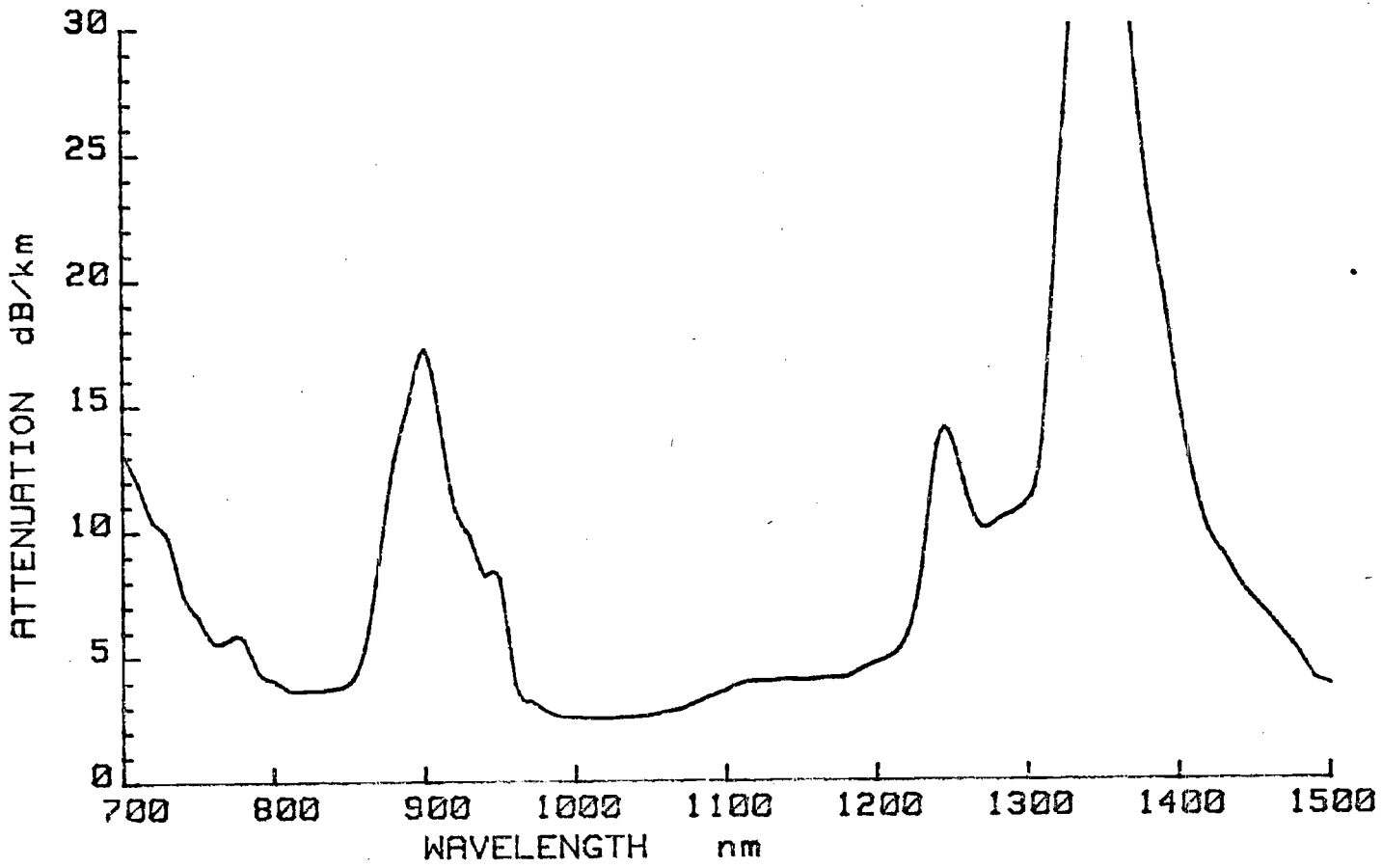

SPECTRAL ATTENUATION CHARACTERISTICS OF P_2O_5-SiO_2 CORE, B_2O_3-SiO_2 CLAD SINGLE-MODE FIBRE. True cut-off wavelength = 1060nm.

FIGURE 4.24

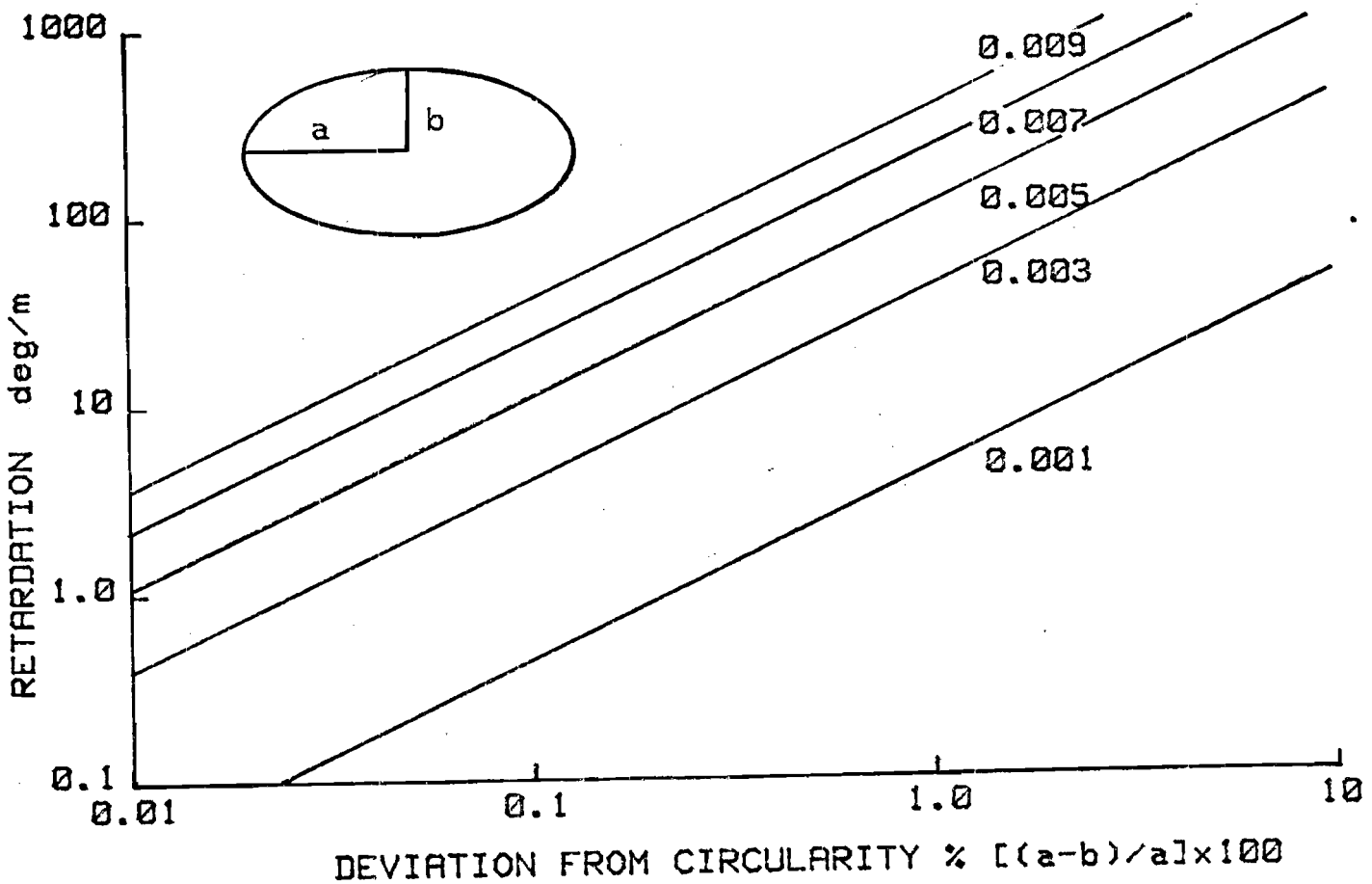

RETARDATION AS A FUNCTION CORE CIRCULARITY IN A FIBRE HAVING V = 2.4 AT 633nm. Curves are for the values of relative index difference Δ shown.

FIGURE 4.25

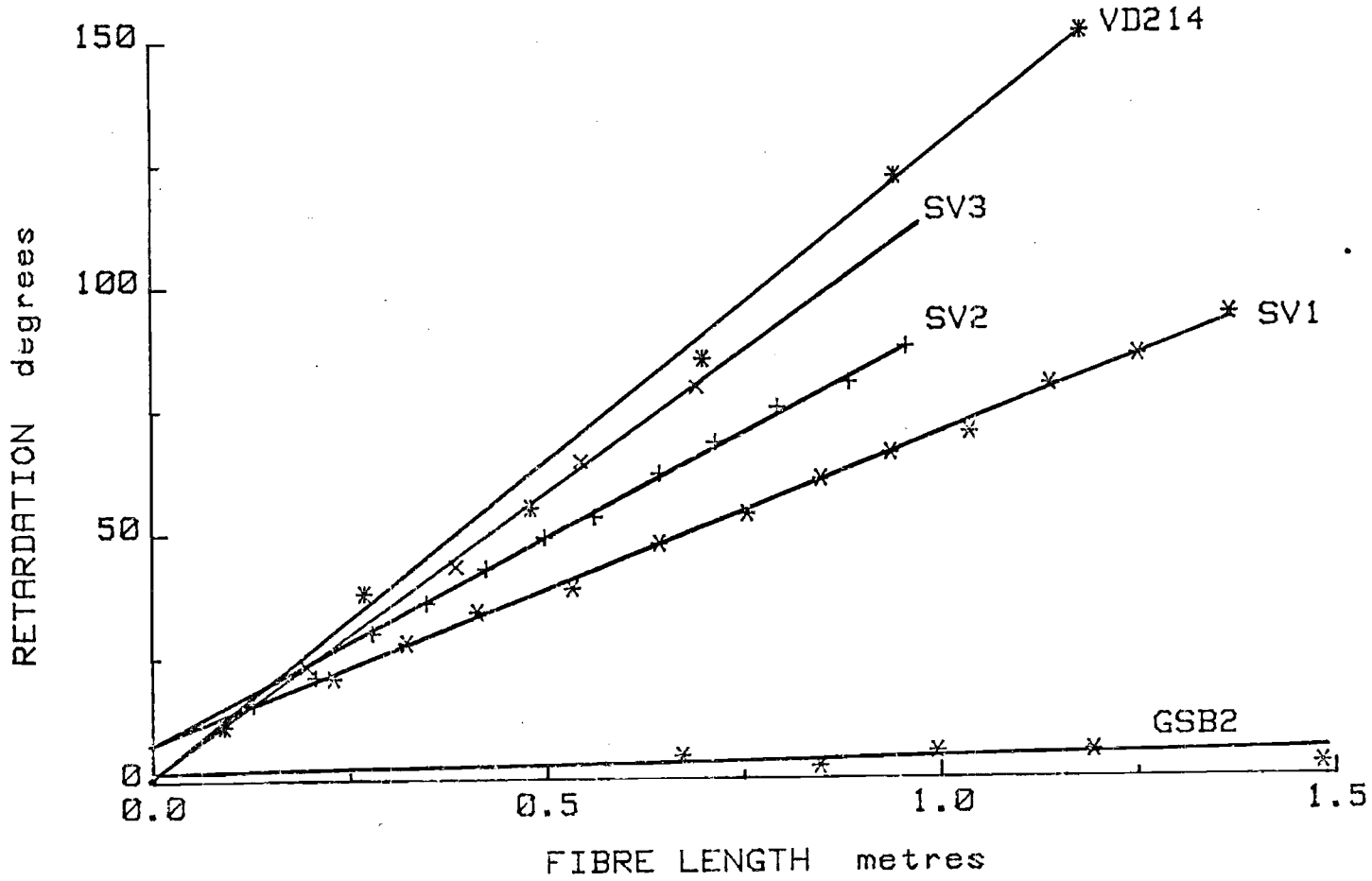

PHASE RETARDATION AS A FUNCTION OF LENGTH IN THE FIBRES SHOWN. Specific retardance values are:- VD214: 126°/m, SV1: 66°/m, SV2: 86°/m, SV3: 115°/m, GSB2: 2.6°/m.

FIGURE 4.26

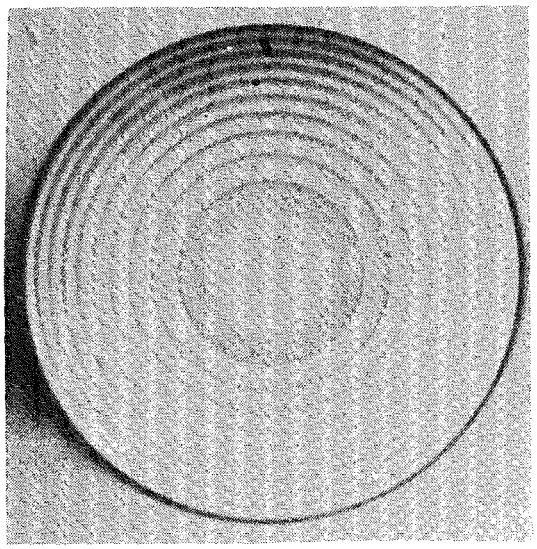

A: DEPOSITED REGION ×25mag.

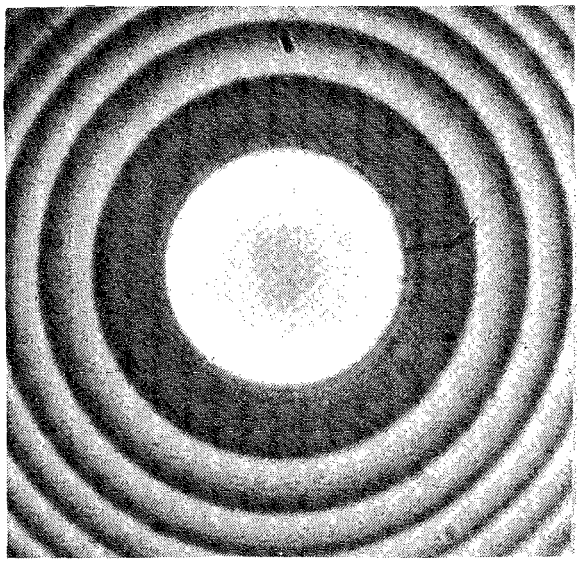

B: CORE AND INNER CLADDING LAYERS ×50mag.

CROSS-SECTION OF DEPOSITED CORE AND CLADDING

OF PREFORM GSB2.

The annular rings are the borosilicate cladding layers, and the central bright region is the germanosilicate core.
CORE ELLIPTICITY < 1%

FIGURE 4.27

CHAPTER 5 PROTECTIVE COATINGS FOR OPTICAL FIBRES

For optical fibres to be successfully employed in telecommunications cables it must be possible to package and cable them in such a manner that their mechanical integrity is guaranteed without degrading their optical properties. Whilst glass is an inherently strong material it is also extremely brittle, and when stress-concentrating defects are present on its surface it will fail under low tensile stresses. It is well known that the high-temperature fibre-drawing operation can produce a pristine fibre surface, and that freshly-drawn fibres can exhibit strengths approaching 7 GN/m^2 [1]. One technique to optimise the mechanical strength of optical fibres is to apply a protective coating to the fibre as it is drawn, thereby preventing the introduction of flaws due to abrasion and atmospheric attack during subsequent handling. In the first section of this chapter a programme of work on the application of in-line or 'primary' coatings to optical fibres is described. The requirements of the coating have been defined and a number of materials have been assessed; using a thermosetting coating of silicone rubber, fibre strengths have been increased by an order of magnitude over the bare-fibre strength.

For the low loss potential of the HCVD fibres to be fully realised in a cable structure, the fibres must be free of externally-applied lateral forces which cause distortion of the fibre, or 'microbending' within the cable. In a theoretical analysis of the effects of lateral pressure on a fibre lying on a rough surface[2], it was found that surprisingly small lateral forces could produce microbending losses of the order of 100 dB/km in an unprotected fibre. Gloge proposed that the fibres should be incorporated into a composite plastic jacket which decoupled the fibre from the external environment, and suggested a number of jacket configurations which would provide the necessary mechanical isolation.

These jacketing configurations were subsequently adopted by laboratories throughout the world and have been used to produce low-loss cables. Whilst Gloge's analysis was quite specific about the jacketing configuration, there were no recommendations regarding the materials to be employed in the jacket, and so many jacketed-fibre designs have proliferated. The second part of this chapter describes the development of a jacketing process for use with the HCVD graded-index fibres. Though the jacket configuration complies with Gloge's suggestions, the use of nylon 6 as the hard outer shell of the composite structure is novel and has not been reported elsewhere. It is shown that, in comparison with other jacketing materials, nylon 6 provides superior mechanical and optical protection and is easily applied to the primary-coated fibres.

5.1 Primary Coatings for Optical Fibres

Two major problems associated with the cabling of low-loss optical fibres are breakage of the fibres due to tensile forces applied during cabling and installation, and static fatigue during service resulting from flaw growth due to atmospheric attack under uniform tensile loading[3]. Since glass is a brittle material, glass fibres fail catastrophically without previous yield or permanent deformation, the failure always resulting from a tensile component of stress. Theoretical calculations based on the binding energy of the Si-O bond predict ultimate tensile strengths of the order of 18 GN/m^2 for pure silica, although the highest figures practically attained are of the order of 7 GN/m^2. The reduction in strength generally results from stress-concentrating Griffiths microcracks present on the surface of the glass; the widespread scatter in experimental strength data is attributable to the randomness of occurences and severity of the flaws. In this respect the strength of glass is essentially a statistical phenomenon and the strength of glass optical fibres thus depends primarily on the size and frequency distribution of the flaws along the length of the fibres.

A study of the factors affecting the ultimate strength of bulk fused silica revealed that the flaw distribution is considerably reduced in fire polished or freshly-drawn silica fibre samples[4], and tensile strengths approaching the theoretical prediction can be obtained at low temperature (78°K).

Similarly, in the drawing of HCVD preforms into fibre, the viscous flow at the drawing temperature produces a pristine fire-polished surface and the freshly-drawn fibres exhibit considerable strength. In practice the strength is limited by defects such as bubbles, stones, and particulate matter within the bulk of the glass and also by new surface flaws introduced by contaminants such as dust and metallic vapours within the fibre-forming zone[5]. Nevertheless, it can be seen that if a protective coating can be applied to the fibre without introducing additional flaws, the 'as-drawn' strength of the fibre can be preserved, and will provide a greater safety margin against fibre breakage in subsequent handling.

5.1.1 Coating Requirements

The type and volume of coating material that can be applied on the draw is limited largely by the dimensional restrictions of the fibre drawing machine and the form of material application. On the Southampton University fibre-drawing tower the distance between the pulling drum and the graphite furnace is less than 1.5 metres. The need for diameter monitoring before primary coating leaves less than 1.25 metres of space in which to apply the protective coating; at the typical drawing speed of 0.5 m/s this allows 2.5s in which to apply and harden the coating. Clearly the volume of material which can be applied in this period is limited and will depend upon whether the coating is applied from solvent solution, as a thermosetting resin, or as an extruded thermoplastic. At an early stage in the programme it was decided that the on-line coating should be considered only as a thin primary coating to protect the fibre's surface and that a thick secondary coating should be applied off-line.

The requirements of the coating were considered with regard to the properties of the coated fibre and the limitations imposed by the drawing process, and are summarised below:-

1. Fibre Properties

a) The coating must not degrade the optical properties of the fibre.

b) The coating should be uniform, continuous, and resistant to abrasion.

c) The coating should provide an effective moisture barrier and should be stable over the fibre's range of operating temperatures.

2. Drawing Operation

a) The coating must be applied in approximately 2 seconds.

b) To facilitate application the coating material should 'wet' the glass surface.

c) To prevent excessive fibre wastage the coating process should not require a long warm-up period and should reach equilibrium conditions rapidly.

Furthermore, although it was not an essential requirement, it was considered desirable that the fibre should adhere to the glass surface matrix and also possess a high modulus of elasticity. In this way any surface defects present in the glass would be bridged, and under tensile loads the coating would carry some of the load across the defect, thereby reducing the stress concentration[6].

5.1.2 Coating Materials

The selection of a coating material cannot be made independently of the selection of the application technique; for example, thermoplastic coatings are most sensibly applied using extrusion techniques. The physical restrictions of the fibre-drawing machine and the high cost of extrusion equipment unfortunately precluded the use of an extruder, and thus thermoplastic coatings were not investigated as coating materials. However, experience in other laboratories indicates that coatings applied from the melt are difficult to control and that the high initial strength of the fibre decreases rapidly after coating[7]. Attention was therefore devoted to materials which could be applied at low temperature from a solvent solution, in dispersion form, or as a multi-component thermosetting mixture.

Many materials were considered including conventional magnet-wire coatings such as polyamides, polyamide-imide and polyesters, all of which are generally applied from heavy solvent solutions. However of the many materials considered, silico-organic compounds exhibited some particularly interesting properties; Firstly, they have a strong chemical affinity for silicates, and thus form strong bonds with the surface matrix of silica. Secondly, they are hydrophobic and resistant to chemical attack; once cured they are chemically inert and are thermosetting compounds. Whilst conventional siloxanes form only monomolecular films on the glass surface and are thus unsuitable for use as a primary coating, a family of partially-polymerised organo-polysiloxanes were particularly attractive. The materials were designed for use with glass-fibre matting and were therefore well suited to use with silica. The partially-polymerised resins are soluble in light solvents such as acetone and are applied to the surface to be treated in solution. Having driven off the solvents by heating, the resins are subsequently cross-linked to form a stable co-polymer. The materials, known commercially as 'Glass Resin Polymers' can be applied in thicknesses of up to 15μm in one pass, and when cured exhibit excellent physical properties, some of which are tabulated in Table 5.1.

In particular the films are flexible, exhibit elongations of greater than 10% before failure, adhere strongly to the substrate, and are abrasion resistant. The materials were thus selected for experimental evaluation.

As will be seen in later sections, some difficulty was experienced in driving off the solvents from the coating without introducing 'blisters' and 'pinholes' and so attention was switched to a group of silicone elastomers. The second group of materials were designed for use as encapsulants which could be cured in thick sections at room temperature. The materials are applied as a two-component high-viscosity silicone which, when cross-linked, cures to a flexible silicone rubber. The curing time can be greatly reduced by the application of heat, the curing time at 400°C being of the order of 1s compared with 8 hours at 20°C. Thus, as the resins are not solvent-based they have considerable potential as a fibre-coating material which can be applied and cured in a straightforward manner. The disadvantages of these materials are, firstly, that the Young's modulus of the cured elastomer is extremely low and secondly, that the materials do not form strong bonds with a silica substrate; there is no possibility of improvement of fibre strength by the primary coating carrying tensile loads across a flaw.

5.1.3 Experimental Equipment

To enable a range of coatings to be applied and cured on the draw, a number of coating applicators and a curing oven were designed and constructed.

5.1.3.1 Drying and Curing Oven

A tube furnace was constructed for use as a drying and curing oven which could operate over a wide range of temperatures up to 650°C. A schematic illustration of the furnace construction is shown in figure 5.1.

The heating element is based on nichrome wire wrapped around a threaded silica tube, and is encased in a stainless steel body. Temperature control is effected by means of a thermocouple and thyristor controller unit. The furnace has a very low thermal mass and can be brought to temperature in a very short time. To reduce the 'chimney' effect common in vertical furnaces, variable aperture iris diaphragms are fitted at each end of the furnace, and are used to constrict the convection currents through the furnace. The furnace was fitted to the fibre-drawing machine on swinging arms which permit it to be swung away from the line of the fibre when not in use.

5.1.3.2 Coating Applicators

Two applicators were designed for use with the glass resin polymers which were applied from low-viscosity solutions. The first of these utilised the conventional approach of passing the fibre through spring-loaded felt pads which were impregnated with the coating solution. As the fibre passes through the pads a boundary layer of coating solution adheres to the fibre, the thickness of the layer increasing with the viscosity of the solution. In practice it was found that the maximum coating thickness was limited to about 3 μm when applied at the recommended solids concentration of 40% by weight. In addition, the high temperature of the fibre at the point of application caused the resin in the felt near the glass/felt interface to cure and thus prevent the flow of the solution onto the fibre.

To overcome these problems a second applicator of novel design was constructed and is shown in figure 5.2. Two contra-rotating wheels of 5 cm diameter are driven at an angular frequency of about 1 revolution per second. The periphery of each wheel passes through a reservoir of coating solution and picks up a boundary layer of liquid on its circumferential face. Lateral translation of the wheels is obtained by using a swinging arm and turnbuckle arrangement.

Hence, by drawing the two wheels sufficiently close, the two films of coating solution converge and form a liquid meniscus which bridges the small gap between the rollers. The flow characteristics of the situation are such that the gravitational forces on the liquid are balanced by the upward shear forces exerted by the rollers. In addition the liquid forming the meniscus is continually replaced and replenished by fresh material from the reservoirs. Thus by drawing the fibre through the meniscus, as shown in the figure, a uniform, concentric coating is applied to the fibre without it having come into contact with any solid surface which may abrade or weaken the glass. Since the coating process is essentially one of 'dip-coating' the thickness of material applied to the fibre is governed only by the viscosity and solids content of the coating solution, both of which are readily controllable. Finally, to allow accurate alignment with the fibre, the applicator was mounted on precision translation units which permit lateral and axial movement.

As the viscosity of the silicone elastomers before curing is at least two orders of magnitude greater than that of the siloxane solutions, it was impracticable to apply the silicone resins using either of the above techniques. A coating bath was therefore constructed and is shown diagrammatically in figure 5.3. The fibre passes vertically through the bath, which contains the pre-mixed resin, and draws on a thick coating of material, most of which is wiped off as the fibre exits the bath through a sizing die. The silicone resin wets the fibre as it enters the bath and a 'vortex' flow of resin is established which ensures uniform exposure of the resin to the hot fibre throughout the drawing operation. To facilitate the start-up operation, the coating bath and coating die were made in accurately mating halves; the fibre would be aligned with the coating channel of one half of the split die before fitting the second half of the bath and die, and then adding the resin. By means of a suitable adaptor which replaces the split-die it is possible to use tapered nozzle coating tips of the form developed by Hart et al[8]; using the tapered nozzles an improvement of the concentricity between the fibre and the coating can be obtained due to the hydrodynamic centering forces in the converging flow field.

5.1.4 Experimental Results and Discussion

5.1.4.1 Polyorgano-siloxanes

Initial coating trials with the cross-linkable poly-organo-siloxanes using the felt-wipe applicator brought two major problems to light. Firstly, the high temperature of the fibre at the coating zone was curing the coating within the felt pads and also scorching the pads themselves. Secondly, there was little evidence of a strength improvement in the fibres; it was concluded that the contact between the wipes and the fibre was creating flaws on the glass surface, and that a non-contacting applicator was necessary.

An immediate improvement in coating quality was obtained by use of the double-roller applicator. It was found that uniform concentric coatings could be applied in thicknesses of up to 15 μm at drawing speeds in the range of 0.25 m/s to 0.75 m/s. At higher coating thicknesses the surface tension forces of the liquid coating were sufficient to form 'beads' along the length of the fibre, and thus, after curing, the solid coating exhibited a similar modulation of the coating thickness.

Figure 5.4 shows an S.E.M. photomicrograph of a coated fibre sample at x 500 magnification. The sample consisted of a silica fibre of 140 μm diameter having a coating of about 10 μm radial thickness; the sample had been prepared by cleaving the coated fibre using the 'score-and-break' technique. The excellent adhesion of the coating to the silica substrate is evident from the glass/coating interface along the line of the break. Also of note is the plastic flow of the coating in the high energy region of the fracture.

Spectral attenuation measurements on lengths of coated and uncoated fibre showed that the application of the coating had not degraded the optical characteristics of the fibres.

Strength measurements on the siloxane-coated samples gave mean breaking stresses of about 0.9 GN/m^2 compared with about 0.4 GN/m^2 for bare fibre, but the results fell rather short of expectations.

Subsequent SEM examination of the test samples revealed the presence of microscopic pinholes in the coating which would provide sites for atmospheric attack of the fibre surface. The pinholes were attributed to the rapid drying and curing process which, it was supposed, had led to solvent entrapment within the coating due to surface-skinning of the coating during solvent evaporation. At the curing temperature of 350°C the vapour pressure of the trapped solvent would be sufficient to rupture the outer skin and thus leave a small hole in the coating.

In an effort to overcome this problem mixed solvent solutions were employed having a low boiling point solvent and a high boiling point solvent. Thus, in the drying operation, the high boiling point solvent would diffuse slowly out of the coating, ensuring a uniform surface finish. Because of the slower drying process it was necessary to subject the coating to a second off-line heat treatment at 450°C to ensure complete cross-linking of the co-polymers. A further improvement in fibre strength was obtained and mean breaking strengths of 1.6 GN/m^2 were measured; there was still considerable scatter in the results and the extreme values of 2.3 GN/m^2 and 1.0 GN/m^2 were obtained in a sample population of only 20. Again SEM examination of coated fibre samples revealed that pinholing was still occurring although there was evidence that some flow of the resin had occurred during the post-cure process, as can be seen from the SEM photomicrograph in figure 5.5a. Clearly in this sample there were a great number of coating pinholes which have to some extent healed themselves during the cross-linking heat treatment; unfortunately the healing of the defects does not guarantee that the fibre surface has remained free of flaws.

A number of subsequent attempts to reduce the pinhole level and to attain strengths of the order of 7 GN/m^2 were fruitless. Increasing the proportion of the high-boiling-point solvent had little effect on the coating quality, and reducing the drying temperature produced smooth coatings which, although pinhole free, were uncured and prone to crazing. In addition to these problems another type of defect was observed, as shown in figure 5.5b. Here the coating has obviously not wetted the fibre surface over a significant area.

It was not clear whether this was due to bubbles in the coating, the flow characteristics of the coating, or the surface condition of the fibre itself. Although defects of this kind were not common, the occurrence of a few defects along the length of a fibre would severely reduce the strength of long gauge-length samples.

In an effort to determine whether the low strength of the coated fibres was inherent to the fibres or to the solvent-evaporation problems it was decided to investigate solventless coatings such as the silicone elastomers and to return to the development of the polyorgano-siloxanes at a later date.

5.1.4.2. Silicone Elastomers - Coating Geometry and Uniformity

As was anticipated, the solventless nature of the Dow Corning Sylgard elastomers made the curing of the resin particularly easy. It was found that, at the normal range of pulling speeds, coatings of up to 350 μm overall diameter could be applied over 140 μm diameter fibres. Curing of the resin was possible over a broad temperature range from 300°C to 450°C; if the resin was not fully cured, final cure would occur at room temperature over a period of about 24 hours. An immediate improvement of the mean strength of the coated fibres was achieved compared with the best results of the siloxane-coated fibres.

Figure 5.6a shows a photomicrograph of a transverse cross-section of silica fibre coated with Sylgard 184; the sample was prepared by the score-and-break technique and is shown under transmitted-light illumination. The diameter of the fibre was 125 μm and the diameter over the silicone rubber coating (the region of intermediate brightness) is 263 μm. The coating is not concentric with the fibre, and the minimum radial coating thickness is 43 μm. The eccentricity of the coating was similar at both ends of the 1700 metre length, as can be seen in figure 5.6b. The eccentricity found in this fibre is typical, even though the coating cup was accurately aligned with the fibre. It was also found that increasing the diameter of the primary coating often resulted in increased eccentricity of fibre and coating; this was attributed to a reduction of the centering forces on the fibre passing through the coating-sizing die.

The upper limit on the overall coating diameter is posed by the onset of beading of the coating between the coating bath and the curing oven. This effect is illustrated diagramatically in figure 5.7a and is shown on actual fibre samples in figure 5.7b. As the diameter of the coating is increased relative to the fibre (which is assumed to be of constant diameter), the surface tension forces of the liquid coating overcome the viscous body forces and cause the fluid to accumulate from both directions in periodic beads, ultimately pinching-off individual droplets along the fibre as the minimum energy configuration. Increasing the fibre diameter within the coating increases the surface tension forces at the fibre/coating interface, and also increases the shear stress which must be applied across the coating to produce pinch-off. Thus whilst 350 μm diameter coatings of Sylgard 184 can be applied to 140 μm fibre, the maximum uniform diameter that can be achieved with 125 μm fibre is less than 300 μm. The tendency towards beading is increased when the lower viscosity Sylgard 182 is used as the coating. To provide a reasonable working margin between the correct coating conditions and the pinch-off conditions 125 μm diameter fibres are usually coated to approximately 250 μm overall diameter.

The maximum coating speed is limited by two effects: Firstly, at speeds above 0.75 m/s the body forces required to maintain the vortex within the coating cup exceed the adhesive forces between the resin and the fibre, and the coating vortex collapses; although a coating is still applied its diameter uniformity is often poor. Secondly, at higher speeds the temperature of the fibre when it enters the coating bath produces partial polymerisation of the resin, and an accumulation of this material forms in the sizing-die. Eventually the material solidifies in the die, and effectively reduces the die size to that of the fibre passing through it. For 125 μm diameter fibre, pulling speeds of 0.3 m/s to 0.5 m/s are normally employed, and give uniform coating finishes free of the above effects.

Tapered-nozzle coating tips have been used in preference to the split-die tip in an attempt to reduce the eccentricity between the fibre and its coating.

The tips were moulded in silicone rubber using the techniques described by Hart[8], and were fitted to the coating bath by means of an extension tube which was located in the seating previously used for the split-die. Measurements of eccentricity on coated fibre samples confirmed Hart's observation that the degree of self-alignment between the fibre and its coating is strongly dependent on the ratio of the tip exit diameter to the fibre diameter. Other factors which influenced the eccentricity were the angle at which the tip was cut and the degree of misalignment between the tip and the axis of the fibre.

In figure 5.8 the effect of a lateral offset between tip and fibre on the coating eccentricity is shown for a 125 μm fibre coated at 0.4 m/s using a 250 μm tip exit size. Initial alignment of the fibre axis with the tip was achieved using a plumb-line. For the conditions used in this experiment it can be seen that if the coating eccentricity is to be kept below 25% (47 μm minimum coating thickness) then the unidirectional lateral offset must be less than 1.3mm. The shape of the curve indicates that the centering action of the tip obviously has a beneficial effect and that only at offsets above 2mm does the eccentricity increase sharply with increasing offset. The 14% initial eccentricity in the coating shows that the centering forces were not sufficient to produce perfect concentricity at a coating:fibre diameter ratio of 2:1. Reducing the ratio increases the centering forces and provides greater tolerance in the lateral offset for a constant eccentricity. Thus, by using a 200 μm tip size it is possible to obtain well-centred coatings, such as that shown in figure 5.9, without having to accurately align the tip beforehand; whether any benefit is gained is dubious because the reduction in overall diameter means that the minimum radial coating thickness of 35 μm is comparable to that in a 250 μm coating having a coating eccentricity of 40%!

Samples of coated fibre have been examined for voids and non-uniformities using the scanning electron microscope. In all cases the silicone coating was found to be free of pinholes, and there was no evidence of the bubbles which are sometimes present in the resin bath being drawn into the fibre coating.

Figure 5.10 shows an SEM photomicrograph of a typical coated fibre sample of 250 μm overall diameter. The remarkable feature of the coating is that although it is soft and easily torn, it is not damaged by normal handling, rewinding and jacketing operations where it passes over stationary guides at speeds of up to 100 m/min. Yet, as seen in the figure, the coating can be readily cleaved in the same manner as the fibre to produce a plane end-face which does not leave any residue on the fibre itself. Although the development of the silicone primary-coating was undertaken 'in isolation' during the period 1975/1976, the attractions of the silicone elastomers have also been recognised by other workers, and today the materials are in widespread use in fibre-manufacturing plants throughout the world.

5.1.4.3. Strength Characteristics of Silicone-coated fibres

The use of silicone elastomers instead of siloxanes as the primary coating material led to a dramatic improvement is the mean breaking strength of the primary coated fibres, and a marked reduction in the distribution of breaking loads. Breaking loads of the order of 60 N were readily attained in 1 metre gauge lengths of 125 μm HCVD fibre; ultimate tensile strengths of 4.8 GN/m^2 were thus approaching the 7 GN/m^2 target value. The improvement in strength meant that the fibres could be subjected to smaller bend radii before breaking ; a minimum bend radius of the order of 1mm can be sustained without breakage of the fibre or damage to the silicone coating.

Although the breaking strength of individual fibre samples is of interest, the characteristics of the flaw distributon in long lengths is of far greater importance to the cable maker. The strength of long lengths of fibre may be assessed by tensile testing of a small number of very long gauge length samples, or by testing a large population of short gauge length samples and using statistical relationships to extrapolate to longer gauge lengths. A number of models for characterising the flaw distributions of glass fibres are available, but of these the model according to Weibull is most widely applied[9]:-

Let the number of flaws per unit length which cause failure between the tensile stress levels σ and $\sigma + d\sigma$ be $n(\sigma)d\sigma$, thus defining the flaw distribution $n(\sigma)$

Let $F(\sigma,L)$ = probability of length L failing below stress σ

$S(\sigma,L)$ = " " " L surviving below stress σ

Then the cumulative failure probability $F(\sigma,L)$ is related to the cumulative survival probability $S(\sigma,L)$ by

$$F(\sigma,L) + S(\sigma,L) = 1 \tag{5.1}$$

The probability of failure in the stress interval $[\sigma, \sigma + d\sigma]$ is then

$$p = F(\sigma + d\sigma, L) - F(\sigma, L) \tag{5.2}$$

but p is also the probability of a sample surviving stress σ and failing in the interval $[\sigma, \sigma + d\sigma]$.

Hence $$p = [n(\sigma)d\sigma L] \cdot S(\sigma,L) \tag{5.3}$$

Equating (5.2) and (5.3) gives

$$F(\sigma + d\sigma,L) - F(\sigma,L) = [n(\sigma)d\sigma L]\, S(\sigma,L) \tag{5.4.}$$

From (5.1) $$\frac{dF(\sigma,L)}{d\sigma} = -\frac{dS(\sigma,L)}{d\sigma} \tag{5.5}$$

and from (5.4) $$\frac{dS(\sigma,L)}{d\sigma} = -L\, n(\sigma)\, S(\sigma,L) \tag{5.6}$$

If we write the cumulative number of flaws which cause failure at or below stress σ as

$$N(\sigma) = \int_0^{\sigma} n(\sigma^1)\, d\sigma^1 \tag{5.7}$$

then integrating (5.6) with respect to σ gives the survival distribution:-

$$S(\sigma,L) = \exp\,[-LN(\sigma)] \tag{5.8}$$

Weibull proposed a flaw distribution of the form

$$N(\sigma) = \left[\frac{(\sigma - \sigma_{min})}{(\sigma_o - \sigma_{min})}\right]^m \qquad (5.9)$$

Where σ_{min} = tensile stress below which no break will occur

σ_o = normalising factor

m = Weibull modulus, which is parameter related to the flaw size distribution.

Setting $\sigma_{min} = 0$ and substituting (5.9) in (5.8) gives the Weibull survival distribution.

$$S(\sigma, L) = \exp\left[-L\left(\frac{\sigma}{\sigma_o}\right)^m\right] \qquad (5.10)$$

Using equation (5.10) it is thus possible to extrapolate strength data obtained on short gauge length samples to longer gauge length samples. The values of σ_o and m are determined empirically by plotting $\ln [1/L \ln 1/S(\sigma, L)]$ against $\ln\sigma$: if a Weibull distribution applies, the graph will be a straight line of gradient m intercepting the $\ln [1/L \ln \frac{1}{S}]$ axis at $-m \ln\sigma_o$. It should be noted that the sample size and the value of 'm' affect the accuracy of the extrapolation; for example, at m = 10 sample sizes of less than 50 can introduce errors in excess of 10% in the predicted values of S[10]. To gain a realistic estimate of the strength distribution in fibres it is important therefore to examine a large sample population.

A tensile testing machine has been designed specifically for use with high strength optical fibres and has been constructed by Pirelli General Cable Works. The machine employs capstan grips to eliminate 'end-effects' due to the clamping of the fibre, a variable-speed geared-motor to elongate the sample and a torque transducer to monitor the tensile load. The machine was designed to permit rapid mounting and testing of the samples, and can accommodate samples from 0.25m to 2.5m gauge length.

Tensile tests have been performed on eighty samples of graded-index fibre coated with Sylgard 184 to an overall diameter of 250 μm. The samples were taken at random from spooled fibres which had been drawn several months previously; a 1 metre gauge length was employed. A mean breaking load of 60 N was obtained for the complete sample population, giving a mean ultimate tensile strength (UTS) of 4.9 GN/m^2. In figure 5.11 the strength distribution is characterised by plotting the cumulative percentage of samples which failed at stress $\bar{\sigma}$ or below. The median strength is 5.17 GN/m^2 and the distribution exhibits a characteristic low-strength tail, with a much narrower high-strength region above the median level.

Transposing the results to a plot of the Weibull failure probability, as shown in figure 5.12, gives a bimodal strength distribution characterising the low-strength tail and the high-strength region. The flaw population changes its character at a stress level of about 4.9 GN/m^2 where the gradient of the Weibull plot changes rapidly from ~ 10 to ~ 25. Such a compound distribution can be described as the sum of two separate Weibull populations[9]:-

$$N(\bar{\sigma}) = \left(\frac{\bar{\sigma}}{\bar{\sigma}_A}\right)^{m_A} + \left(\frac{\bar{\sigma}}{\bar{\sigma}_B}\right)^{m_B} \qquad (5.11)$$

In this analysis it is assumed that each of the flaw distributions extends over the total range of measured stresses. At low strengths the flaw population is dominated by the population having the lower gradient, whilst at higher strengths the steeply sloping population is dominant. An approximate fit has been made to the data and is shown by the solid lines in figure 5.12. Decomposing the data into two separate Weibull populations gives:-

$\bar{\sigma}_A = 5.5$ GN/m^2 $\qquad$ $m_A = 10.6$

$\bar{\sigma}_B = 5.25$ GN/M^2 $\qquad$ $m_B = 23.4$

Although single-moded flaw distributions have been observed in laser-drawn synthetic-silica fibres[11], the bimodal distribution observed here is commonly found in fibres drawn from fused-quartz rods or HCVD preforms using a less clean heat source[9]. The two distinct flaw populations result from flaws introduced by dust in the drawing environment, and flaws intrinsic to the starting materials. Thus, by using a CO_2 laser as a clean heat-source, Miller et al were able to eliminate the low-strength tail in very long fibres coated with silicone rubber. The gradient of the high-strength region reflects the spread of the flaw sizes intrinsic to the material; synthetic silica rod exhibits a narrower distribution of intrinsic flaws than does fused-quartz rod, and the value of $_B$ is consequently higher for the synthetic-silica fibres.

As the low-strength tail will limit the strength of long lengths of fibre, it is of interest to apply the Weibull survival distribution using $m = 10.6$ and $\sigma_o = 5.5$ GN/m^2 to calculate the strength of a 1km sample. Hence, using the equation

$$S(\sigma,L) = \exp\left[-L\left(\frac{\sigma}{5.5}\right)^{10.6}\right] \qquad (5.12)$$

gives a stress level of 1.85 GN/m^2 for a 99% survival probability, equivalent to a tensile load of 23 N on a fibre of 125 μm diameter. Whilst this represents a strength reduction, at the 1% failure level, of only 36% of the strength of a 1 metre sample, calculations for a 50% failure give a drastic reduction from 5.1 GN/m^2 to 2.8 GN/m^2 applied tensile stress; the influence of the low-strength tail upon the overall performance of the fibre is clearly evident. Obviously, there is considerable scope for further improvement of the strength performance, particularly by narrowing the size distribution of the flaws which cause failure at the low stress levels. Despite this need, it should be emphasised that the present-day results are more than acceptable to permit the cabling of the fibres with confidence; as typical fibre-cabling machinery applies less than 1 N tensile load on the fibre during stranding, the probability of failure during stranding is less than 1 in 10^8!

5.2 Secondary Coating of Optical Fibres

To be able to take full advantage of the very low loss of HCVD fibres, the incorporation of the fibres into a cable structure should introduce minimal excess attenuation. In a theoretical analysis of the effects of random bends in the axis of a fibre, Gloge[2] found that such perturbations need not be of large amplitude to cause losses of several decibels per kilometre. In particular it was found that this 'microbending loss' was greatest when the spatial wavelength of the axial deformation corresponded to the difference in phase constant between adjacent modes in the fibre. For a typical graded index fibre, a narrow band of wavelengths centred on a critical wavelength of about 1mm are important; experimental verification of this sensitivity was obtained by Gardner[13]. It is therefore essential to provide a cable environment where the optical fibre is mechanically isolated from distortions on this scale.

5.2.1 Jacketed Fibre Structures

A most effective way of protecting the fibre from externally applied transverse forces is to apply a jacket which provides mechanical isolation by decoupling the fibre from the contact forces on the jacket. Gloge proposed a number of jacketing configurations but, of these, two preferred designs evolved which both employ composite coatings of soft and hard materials: In the first structure the fibre is protected by a shell of hard material over which a layer of soft material is applied. In the second structure a soft coating is applied to the fibre and a hard outer shell is then added. If the materials have the correct elastic moduli and relative dimensions there is little difference in the performance of each configuration.

Bearing in mind the low modulus of the silicone rubber primary coating, the second configuration is the obvious choice for use with our fibres. The application of a hard outer shell is of additional benefit in that it protects the silicone primary coating from the rigours of the cabling process. Whereas in the fibre-drawing process the use of an extruded thermoplastic primary coating was considered undesirable, the application of the hard outer shell, or 'secondary coating', is well suited to extrusion techniques. Also, there is an almost unlimited range of thermoplastic materials available for extrusion.

However, the application of an extruded over-jacket is not in itself a straightforward operation and can induce microbending loss within the coated fibre[14]. The attenuation increment due to jacketing is strongly influenced by physical properties of the coating material such as surface roughness and thermal expansion behaviour. The latter property can most seriously affect the low-temperature attenuation of the fibre: the difference of thermal expansion coefficient between the high-silica optical fibre and the thermoplastic coating lead to compressive forces on the fibre, causing it to buckle within the jacket, thereby introducing microbending losses. An extrusion line has been constructed for use with optical fibres and a number of thermoplastics have been evaluated with the objective of developing a jacket structure exhibiting superior performance with the HCVD graded-index fibres.

5.2.2 Secondary Coating Extrusion Line

Conventional extrusion lines for the insulation of metallic conductors for telecommunications cables are unsuitable for use with optical fibres for a number of reasons. Firstly, insulating lines run at speeds of up to 2000 m/min and employ high-inertia spooling systems; the inevitable 'snatch' loads, which produce a small plastic elongation of the metallic conductor, would certainly lead to breakage of glass fibres. Secondly, even if it were possible to run the lines at lower linear speeds, the minimum extrudate throughput would typically be 10 kg/hour which is an order of magnitude greater than that required to coat a fibre to 1mm diameter at a linespeed of 25 m/min.

To overcome these difficulties it was necessary to develop an extrusion line for coating optical fibres. The line, shown schematically in figure 5.13, was designed by the author and commissioned at the Pirelli General Cable Works. Briefly, the equipment consists of an extruder having an 18mm screw diameter with a minimum throughput of about 0.2kg/hr and a maximum throughput of 2kg/hr. The primary-coated fibre is fed into the extrusion line from a low-tension, low-inertia traversing pay-off unit (2). The fibre passes through the extruder's crosshead where the secondary coating is applied, and into a cooling trough (3) where cooling water in the temperature range 5°C to 90°C may be circulated.

Having passed through an optical diameter monitor (4), the fibre passes around a driven capstan (5), which controls the linespeed, and onto a take-up bobbin (7) via an accumulator (6). The accumulator compensates for speed variations between the capstan and the take-up, to ensure that the fibre is wound on to the bobbin at a constant tension; by attaching weights to the dancing carriage of the accumulator it is possible to apply a proof-testing tensile load to the coated fibre. The linespeed is controlled to maintain the diameter of the jacketed fibre at a preset value by means of a feedback loop incorporating the optical diameter gauge and the capstan speed controller. The tension of the fibre between the pay-off bobbin and the capstan can be adjusted by varying the current through a constant-torque motor to which the pay-off bobbin is coupled; line tensions of 0.5 N are typical. Linespeeds of up to 60 m/min are possible, and the capstan's rotational speed is controlled to better than 0.1%.

The thermoplastic coating is applied to the fibre using a cross-head arrangement and tubing dies as shown in figure 5.14. In the tubing technique the fibre to be coated passes through a core tube that extends to the die exit; sufficient clearance is allowed to preclude contact between the primary-coated fibre and the internal surface of the core tube. The polymer is extruded as a completely independent tube around the fibre, and, as the linespeed is higher than the linear speed of the extrudate, the polymer tube is drawn down onto the fibre whilst still molten. To assist the draw-down process an internal vacuum may be applied to the extrudate tube by means of a vacuum line connected to the core tube. The dimensions of the extruded tube are typically 2.5mm outside diameter and 1.25mm internal diameter, giving a draw-down ratio of about 25 for a fibre jacketed to an overall diameter of 0.5mm. The tubing technique was chosen in preference to the conventional 'smear' coating technique because the free-tubing process produces a smooth surface finish with low contact forces between the primary-coated fibre and the extruded secondary coating.

5.2.3. Initial Materials Evaluation

The choice of plastic material to be used as the hard outer shell of the composite jacket is of great importance. The essential requirements of the material can be summarised as:-

1. High tensile modulus, E
2. Smooth surface finish on solidified extrudate.
3. Low shrinkage due to cooling after extrusion, e
4. Low coefficient of thermal expansion, α_T
5. Long-term stability.

The first two requirements are dictated by the resistance to microbending that is desired in the jacketed fibre. The last three considerations are governed by the needs to introduce minimal excess attenuation due to jacketing and to have stable optical performance with temperature and time. A number of materials were considered in terms of their physical properties, ease of processing and cost; the characteristics of some potential coating materials are tabulated below:-

Material	Youngs Modulus E, GN/m^2	Linear Shrinkage e %	Thermal Expansion $x10^{-5}$ $°C^{-1}$ α_T
High-density polyethylene (HDPE)	0.4 -- 1.25	2 -- 5	12
Polypropylene copolymer (PPC)	0.7 -- 1.2	1 -- 2.5	9.5
Thermoplastic polyester (TPE)	1.9	1.5 -- 2	9.5
Nylon 6	2.8	0.6 -- 1.4	8.0
Nylon 11	1.3	1.2	10.0
Nylon 12	1.25	0.3 -- 1.5	10.0
Tefzel	0.8	3 -- 4	9.3

Although quantitative data are not available, experience shows that the surface finish of the harder polymers is generally better than that of the low-modulus materials. Hence from the above table, HDPE would not be a suitable jacketing material because it only fulfills condition (5) above; its low modulus would be expected to give poor microbending resistance, its high linear shrinkage would produce retraction and microbending in the coated fibre, and its high thermal expansion coefficient would give poor low-temperature performance. Similarly, PPC would be somewhat superior to HDPE but would clearly be inferior to Nylon 6 which not only possesses a very high modulus but also has excellent shrinkage and thermal expansion properties. It is interesting to note that the fluoropolymer, Tefzel, has very high linear shrinkage and a very low modulus, and should only be considered as a coating material in situations where high-temperature stability is required.

On the basis of the data produced in the table, Nylon 6 is the preferred jacketing material. To verify this theory extrusion tests were performed on four of the seven materials, namely PPC, TPE, Nylon 6 and Nylon 12. Lengths of primary-coated graded-index fibre were coated to an overall diameter of 500 μm using one of the selected materials. Attenuation measurements were performed on the fibres at room temperature before, and after, coating in order to determine the incremental loss due to coating. At 0.85 μm the following results were obtained.:-

	Attenuation dB/km at 0.85 μm		
Material	Before coating	After coating	Increment
PPR	5.1	180	175
TPE	3.5	8.4	4.9
Nylon 6	3.1	3.12	0.02
Nylon 12	3.5	4.1	0.6

Examination of the polypropylene-jacketed fibre revealed that there were no fibre breakages, and that the high excess loss was due to the large retraction of the polypropylene on cooling. Furthermore the longitudinal retraction appeared to be accentuated by the orientation of the polymer as a result of the draw-down process. A similar, but less drastic, effect was observed in the thermoplastic polyester where retraction of the jacket on cooling had produced an additional loss of 4.9 dB/km; as with the polypropylene coating the extrudate did not have a highly-polished surface finish. In contrast, the results for both nylon coatings were very encouraging, and in particular the result for nylon 6 confirmed the initial predictions. Both nylon polymers were found to produce highly-smooth coatings with no evidence of retraction; examination of the draw-down zone revealed that solidification of the extrudate occurred some distance after the point at which the coating closed on to the fibre, and it was likely that residual elongation stresses would be annealed prior to solidification.

The low-temperature attenuation characteristics of the TPE-, nylon 6- and nylon 12-coated fibres were then evaluated by using a low-temperature cell and the spectral attenuation measuring system to monitor the variation of output signal from each fibre as a function of temperature. In this way the attenuation increment from the starting point could be readily determined; the results over the temperature range +20°C to -20°C are plotted in figure 5.15. Again the nylon 6 coating gave the best temperature performance, but even so an attenuation increase of 0.7 dB/km occurred over the range + 20°C to - 20°C. Measurement of the spectral attenuation at the temperature limits revealed that the excess loss was independent of wavelength. Although there was a 2 dB/km attenuation increment in the fibre coated with nylon 12 the attenuation increase was greatest over the range +20°C to -4°C and was almost constant from -4°C to -20°C. The performance of the thermoplastic polyester coating was very poor, giving a loss increase of 23 dB/km at 0°C over the room temperature loss. Whilst it was realised that, by paying attention to the extrusion conditions, it might have been possible to improve the performance of the nylon 12 and TPE coatings, the attenuation performance and physical properties of the nylon 6 coating were so obviously superior that it was selected for further evaluation and development.

5.2.4. Further Aspects of Nylon 6 Coatings

5.2.4.1 Effect of Extrusion Conditions on Low-temperature Performance

In a study of the effects of coating and cabling upon the optical performance of step-index fibres [14], it was observed that the low-temperature attenuation characteristics of tightly-jacketed fibres was dependent upon the cooling conditions of the molten extrudate; by employing air-cooling instead of cold-water cooling the creation of voids at the secondary-coating/primary-coating interface was diminished, with an attendant reduction in the microbending loss at low temperature.

To determine whether the nylon 6 coatings were sensitive in the same manner, extrusion trials were performed under different cooling conditions. Figure 5.16 shows the temperature dependence of the excess loss of two lengths of the same fibre, VD236, jacketed to an overall diameter of 500 μm with nylon 6; in one length cold-water cooling was employed whilst in the second length the extrudate was cooled in air. The slower cooling rate of the second length produced a significant improvement of the low-temperature attenuation compared with the rapidly cooled sample. For example, at 850nm the attenuation of the air-cooled length was only 3.2 dB/km at 20°C, and over the range +20°C to -15°C the attenuation increase was less than 0.1 dB/km, giving a thermal coefficient of attenuation of only 0.003 dB/km.deg.C; although the room-temperature attenuation of the rapidly-cooled fibre was comparable, the mean thermal coefficient of attenuation was somewhat higher at 0.014 dB/km.deg.C.

The spectral attenuation characteristics of the air-cooled length are shown in figure 5.17 for the as-drawn fibre, the jacketed fibre at 20°C and the jacketed fibre at -20°C. The difference between the measurements on the jacketed length are barely discernable, and are certainly within the limits of the measurement accuracy. The attenuation of the jacketed fibre is apparently below that of the as-drawn fibre over the full spectral range: This effect is most probably due to the fact that the microbending loss incurred by jacketing is less than the microbending loss in the as-drawn fibre, which was measured whilst wound in multiple layers on an expanded-polystyrene spool.

In each case, plotting the attenuation on a (wavelength)$^{-4}$ basis reveals that the wavelength-independent loss due to the combined effects of waveguide loss and microbending loss is less than 0.6 dB/km. Another interesting feature of the attenuation curves is the somewhat lower attenuation of the jacketed fibre at short wavelengths when compared with the as-drawn fibre. This effect is not peculiar to this set of measurements and is common to most jacketed graded-index fibres. The exact cause of this difference is unknown and warrants further investigation; possible causes are annealing of the drawing-induced losses within the fibre during the extrusion process, or a wavelength-dependence of the microbending losses in the as-drawn fibre. The annealing effect might be possible at the extrusion temperature of 250°C, and examination of the (wavelength)$^{-4}$ attenuation plots, figure 5.18, shows that the attenuation is closer to the Rayleigh scattering limit in the jacketed fibre, as would be expected if an annealing effect had occurred. By subjecting a length of primary-coated fibre to a heat treatment at the extrusion temperature (250°C) it will be possible to determine whether annealing occurs during the extrusion process.

Using air-cooling of the extrudate, more than 150km of fibre has been jacketed with nylon 6 to an overall diameter of 500 μm. By the acquisition of a temperature-controlled environmental chamber it was possible to perform attenuation measurements over the range of temperatures from -40°C to 100°C. Figure 5.19 shows a typical attenuation versus temperature characteristic for a fibre over the range -40°C to +60°C. Cooling the fibre to -40°C does not introduce significant loss increase, and over the full measurement range the attenuation changed by less than $\pm$ 0.1 dB/km. The variation of performance from fibre to fibre is so small that the measurement of the temperature performance of each fibre is no longer thought to be essential in a production environment.

5.2.4.2. Colour-coding of Fibre by Jacket Pigmentation

It is desirable to colour-code the jacketed fibres to enable easy identification of the fibres within a cable. With extruded thermoplastics such as nylon 6, colour coding is most simply effected by the addition of colouring pigments to the plastic granules in the plastic manufacturing process; a wide range of coloured grades of nylon 6 are thus available from the manufacturer[15].

However employing these materials as a direct replacement for the unpigmented material used in previous experiments led to a serious degradation of the optical performance of jacketed fibres at low temperature. For example, figure 5.20 shows the temperature performance of a fibre coated to 500 μm diameter with a heavily-pigmented blue nylon 6. The attenuation/temperature characteristic was similar in shape to that obtained using nylon 12, and the excess loss was found to be a function not only of temperature but also of time. Thus at -20°C the excess losses 4,7, and 18 days after jacketing were 6.0, 1.7 and 0.8 dB/km respectively.

Normally the extrusion coating of nylon 6 is cooled sufficiently slowly to minimise the difference between the degree of crystallinity on the surface and inner layers of the secondary coating[16]. The addition of pigment increases the degree of crystallinity and the crystallisation rate, thereby creating a greater stress imbalance within the coating (as in the case of water-cooling of the extrudate), and a corresponding degradation of the low temperature attenuation performance. Absorption of moisture from the atmosphere increases the molecular mobility and promotes re-ordering of the partially-crystalline material towards a reduction of the stress levels within the coating; the water-activated annealing thus produces an improved performance with time.

To overcome the problems associated with the use of fully-pigmented coatings, experiments were carried out on diluted mixtures of pigmented and non-pigmented material. It was found that by employing a 1:10 pigmentation ratio the performance of the coloured fibres at low temperature was essentially the same as that of the fibres coated with non-pigmented material, and readily identifiable colouration was achieved.

5.2.4.3 Load-bearing Capability of Secondary Coating

The above results relate to fibres coated to an overall diameter of approximately 500 μm, which was selected as the minimum coating diameter for reasonable microbending resistance during cabling. Multilayered winding of jacketed fibre under tension on a 20cm diameter spool produced negligible loss increase, empirically confirming that the coating thickness was sufficient to permit cabling of the fibres.

However, a question that remained unanswered was 'what part does the coating play in carrying tensile loads on the jacketed fibre?'

The high elastic modulus of nylon 6 compared to the other secondary coating materials can be used to advantage in reducing tensile loads on the optical fibre itself. Figure 5.21 shows the theoretical improvement in load-bearing ability of a jacketed fibre as a function of coating thickness. Although the modulus of nylon 6 is more than an order of magnitude less than that of the silica fibre, the difference in relative areas of the two can contribute a significant strength improvement at coating diameters of 500 μm or more. Thus at 500 μm the nylon coating will carry 32% of the tensile load per unit strain and a 48% improvement in load-bearing capacity is obtained. At larger coating diameters the improvement is more dramatic, and at 700 μm coating diameter the fibre itself will bear less than 47% of the applied tensile load.

The improvement offered by the use of a 700 μm jacket diameter was considered worthwhile provided that the increased coating thickness did not lead to a degradation in the transmission properties of the fibres. Using the same extrusion conditions as for the 500 μm coatings it has been possible to achieve high-quality coatings of pigmented and non-pigmented material which do not affect the performance of the fibres over the temperature range -40°C to +60°C. As an illustration figure 5.22 shows 'state-of-the-art' results on a 2.4km length of graded-index fibre jacketed with pigmented nylon 6 (1:10 pigmentation ratio). Not only was the attenuation of the fibre unaffected by jacketing but also the attenuation change during temperature cycling over the range -40°C to +60°C was less than 0.05 dB/km at the measurement wavelength of 850 nm. At this wavelength the attenuation of the jacketed fibre was 2.8 dB/km and the pulse dispersion was less than 0.5 ns/km. Of course, in a structure where there is negligible microbending loss due to jacketing, the pulse dispersion characteristics were similarly unaffected by the jacketing process. Exhaustive tensile strength measurements have yet to be performed on the fibre, but in a 2 metre gauge length, tensile breaking loads in excess of 75 N were obtained in all of ten test samples.

5.3 References to Chapter 5

1. Morley, J.G., Andrews, P., and Whitney, I.: 'Strength of fused silica fibres', Symposium on the strength of glass and ways of improving it, Florence 1965, pp. 417-445.

2. Gloge, D.: 'Optical fibre packaging and its influence on fibre straightness and loss', B.S.T.J., 54(1975), pp. 245-262.

3. Kalish, D., and Tariyal, B.K.: 'Probability of static fatigue in optical fibres', App.Phys.Lett., 28(1976),pp. 721-723.

4. Hillig, W.B.: 'The factors affecting the ultimate strength of bulk fused silica', Symposium on the strength of glass and ways of improving it, Florence 1965, pp. 295-325.

5. Maurer, R.D.: 'Effect of dust on glass fibre strength'. App.Phys.Lett., 30(1977), pp. 82-84.

6. Nakahara, T., Tsukamoto, A., Kumamaru, H., and Hoshikawa, M.: 'Transmission and mechanical properties of protected optical fibres for use in optical fibre cables', PROC IEE, 123(1976), pp. 603-608.

7. McDonnel, D.: Private communication.

8. Hart, A.C., and Alberino, R.V.: 'An improved fabrication technique for applying coatings to optical fibre waveguides', Second Conference on Optical Fibre Transmission, Williamsburg, U.S.A. 1977, Paper TuB2.

9. Olshansky, R., and Maurer, R.D.: 'Tensile strength and fatigue of optical fibres', J.App.Phys., 47(1976), pp. 4497-4499.

10. Trustrum, K., and Jayatilaka, A.: 'On estimating the Weibull modulus for a brittle material', J.Mat.Sci., 14(1979), pp. 1080-1084.

11. Miller, T.J., Hart, A.C., Vroom, W.I., and Bowden, M.J.: 'Silicone- and ethylene-vinly-actate-coated laser-drawn silica fibres with tensile strength 3.5 GN/m^2 in 3km lengths', Electron. Lett., 14(1978), pp. 603-605.

12. Maurer, R.D.: 'Effect of dust on glass fibre strength', App.Phys. Lett., 30(1977), pp. 82-84.

13. Gardner, W.B.: 'Microbending loss in optical fibres', B.S.T.J., 54(1975), pp. 457-465.

14. Rokunohe, M., Shintari, T., Yajima, M., and Utsumi, A.: 'Stability of transmission properties of optical fibre cables', Proceedings of the Second European Conference on Optical Communications, Paris 1975, pp. 183-188.

15. British Industrial Plastics' 'Beetle Nylon 6' Materials selection guide.

16. Russell, D.P., and Beaumont, P.W.R.: 'Structure and properties of injection-moulded nylon 6', J.Mat.Sci., pp. 197-207.

a) Fully-Cured Films

Youngs Modulus, E = 1.4 GN/m^2
Elongation to failure $\sim$10%
Flexibility - 180° bend over 2.5mm mandrel
Hardness = 7H on pencil scale
Refractive index = 1.45
Adhesion to glass substrate - excellent
Solubility - unaffected by most common organic solvents
Weatherability - excellent

b) Coating Solution of Partially-Cured Resin

Viscosity of 40% solution in xylene $\sim$50 cps.

Table 5.1 Physical properties of polyorganosiloxane primary coatings.

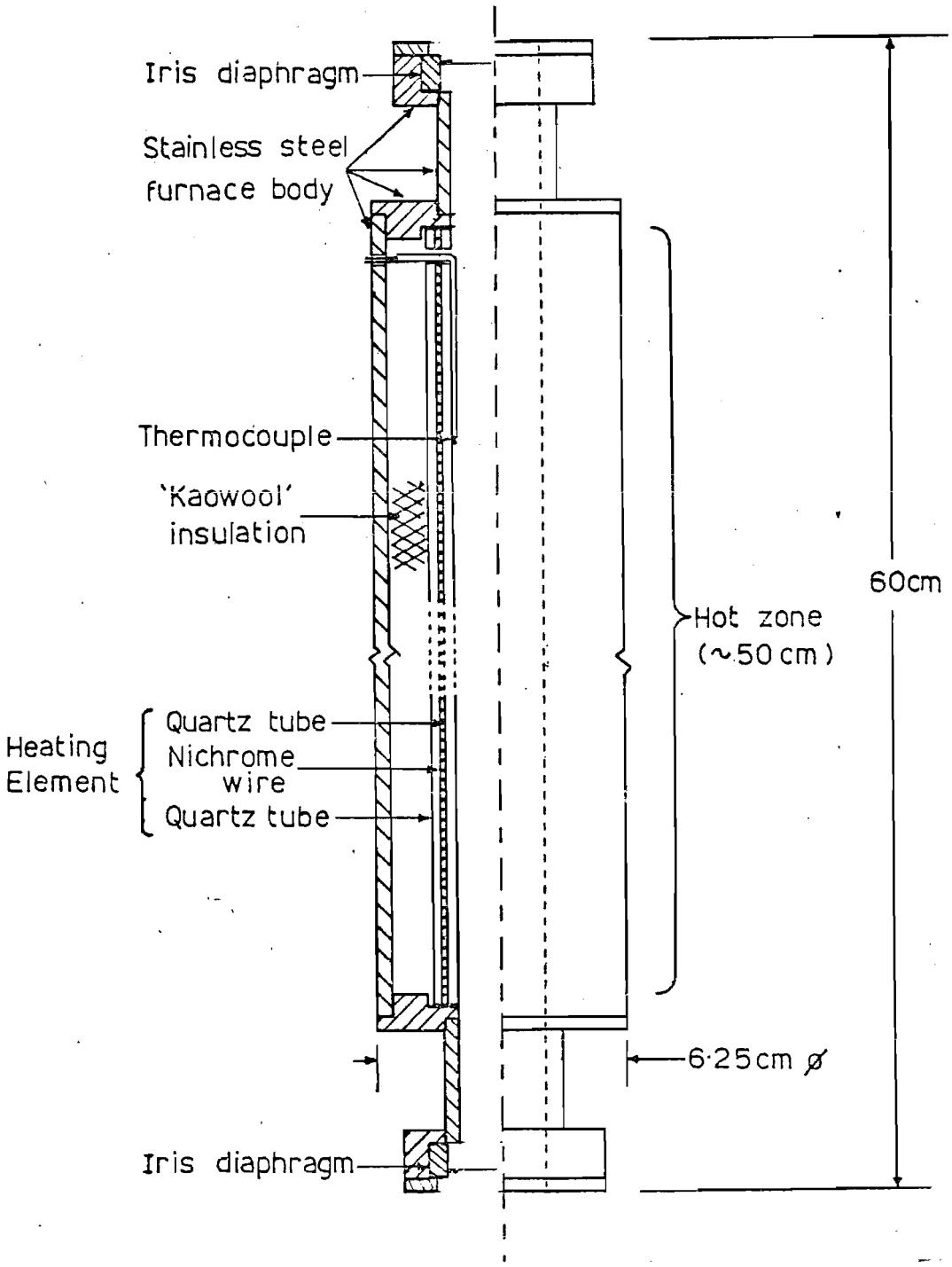

Tubular furnace for drying / curing of primary coatings in-line with fibre drawing.

FIGURE 5.1

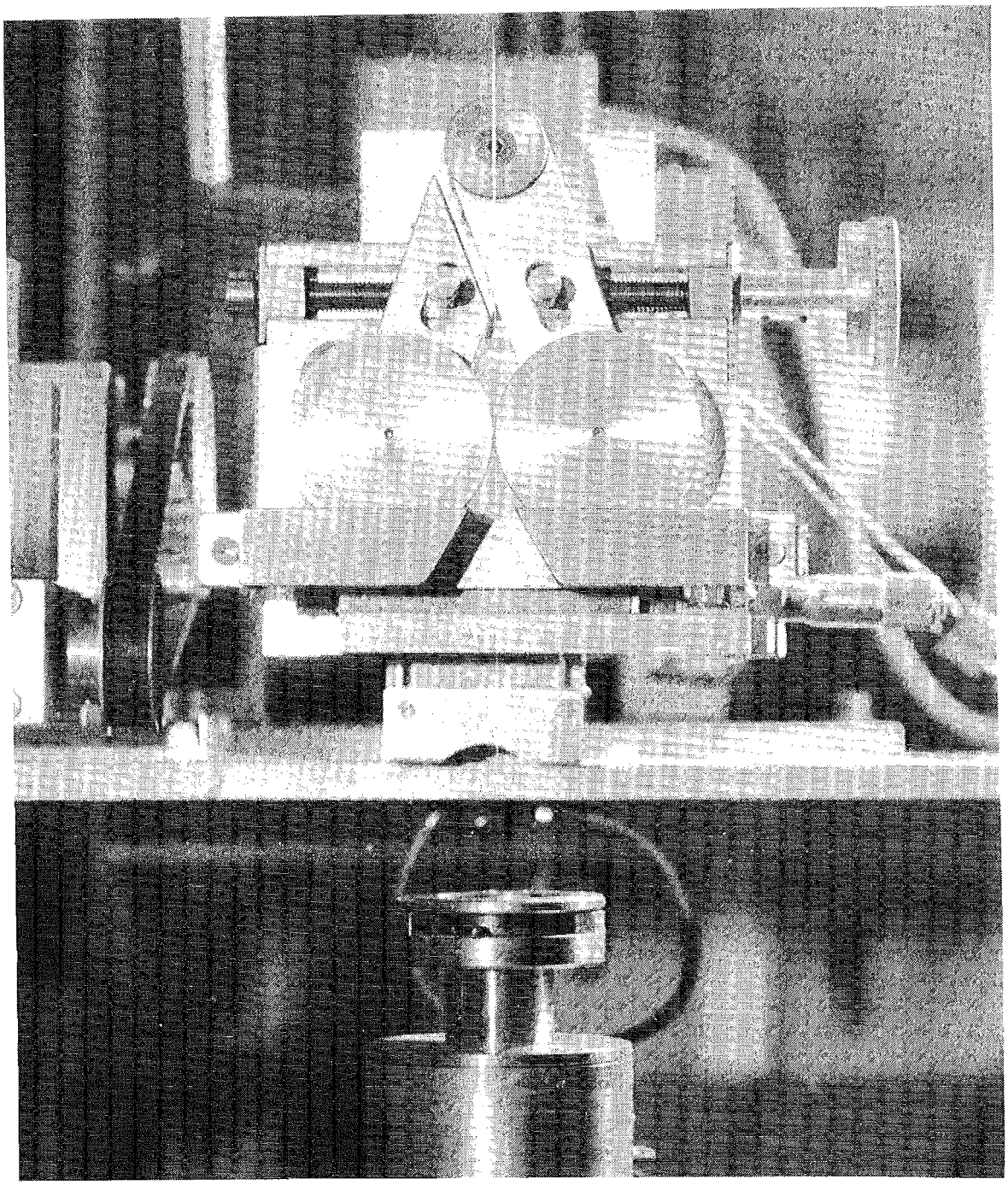

Novel applicator for low-viscosity primary-coating materials.

FIGURE 5.2

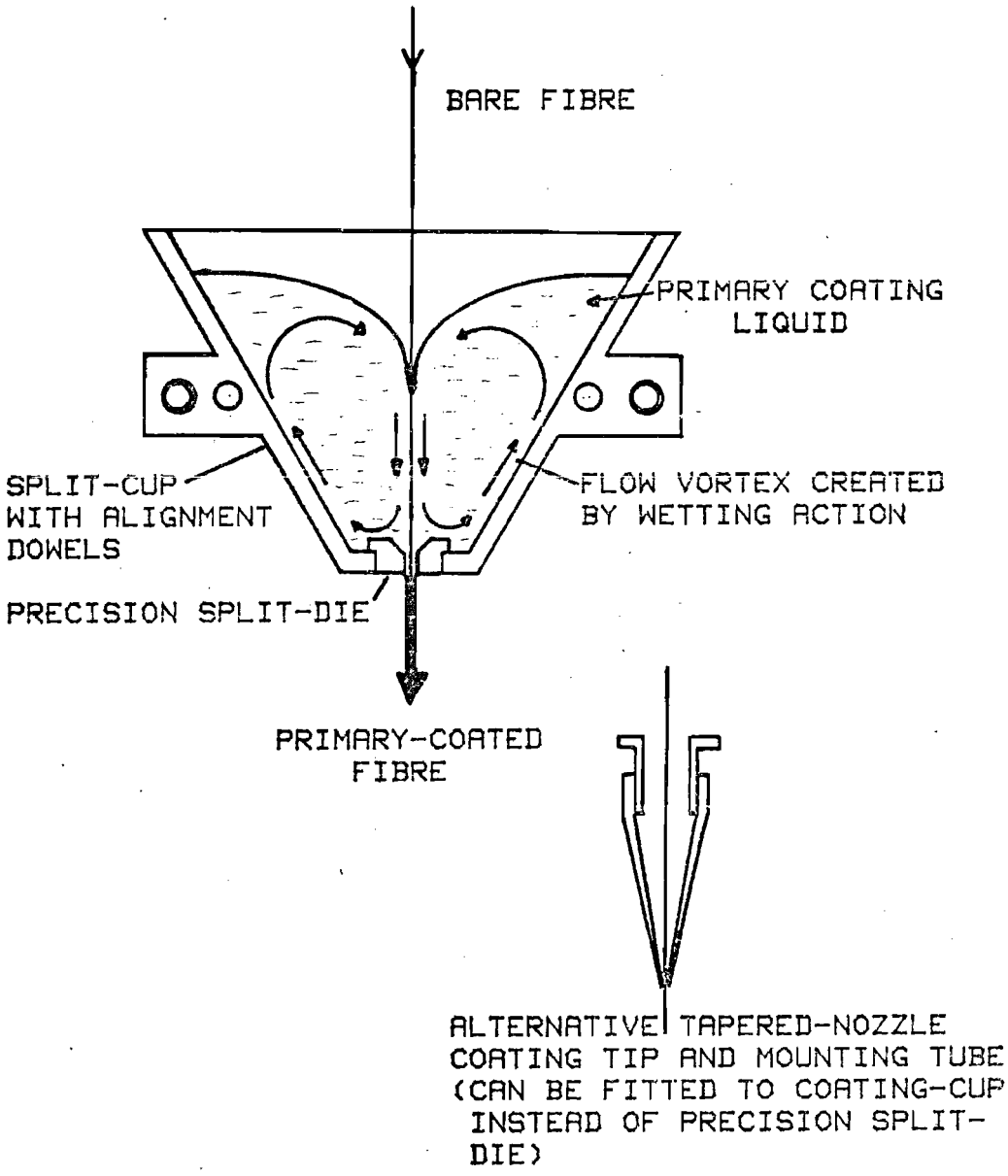

SECTIONAL VIEW THROUGH SPLIT-CUP FOR APPLICATION OF MEDIUM-VISCOSITY PRIMARY COATINGS

FIGURE 5.3

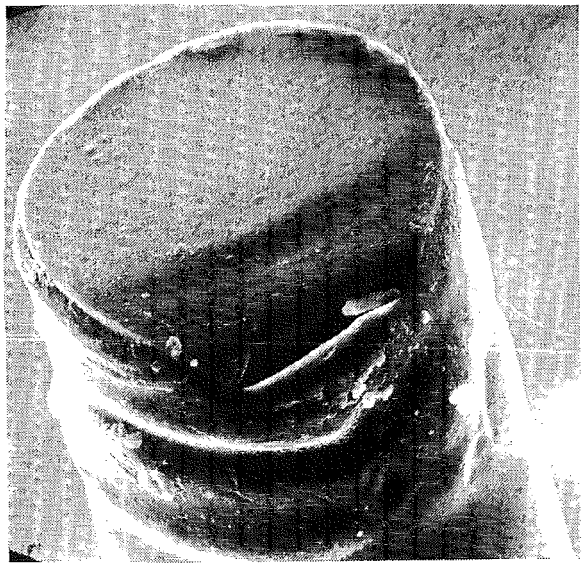

SILOXANE COATING ON 140μm
SILICA FIBRE
S.E.M. ×400 mag.

FIGURE 5.4

"PINHOLES " IN SILOXANE
COATING APPLIED FROM
MIXED-SOLVENT SOLUTION
S.E.M. ×400 mag.

FIGURE 5.5a

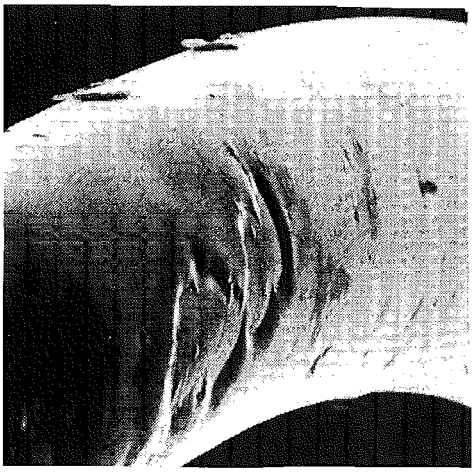

INCOMPLETE "WETTING" OF
SILICA FIBRE BY SILOXANE
PRIMARY-COATING APPLIED
FROM MIXED-SOLVENT SOLUTION
S.E.M. ×400 mag.

FIGURE 5.5b

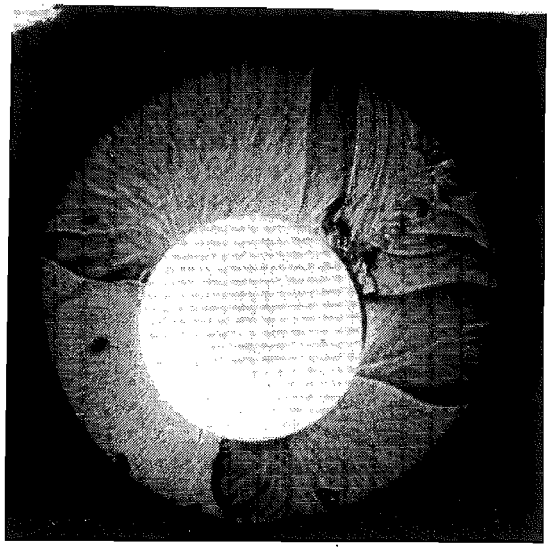

Silicone rubber primary coating on 140μm silica fibre Coating diameter = 280μm. Minimum radial coating thickness = 45μm.

FIGURE 5.6a

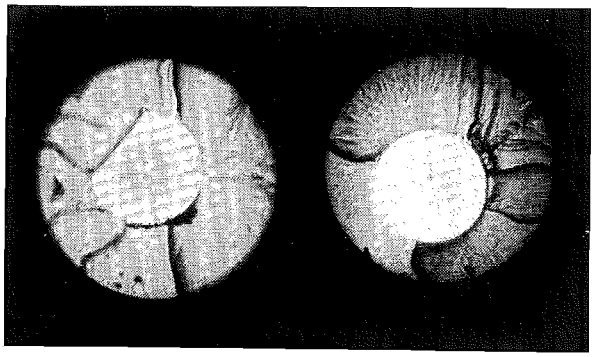

Coating geometry at each end of 1700m length of fibre shown in FIGURE 5.6a . The coating eccentricity did not vary along the length.

FIGURE 5.6b

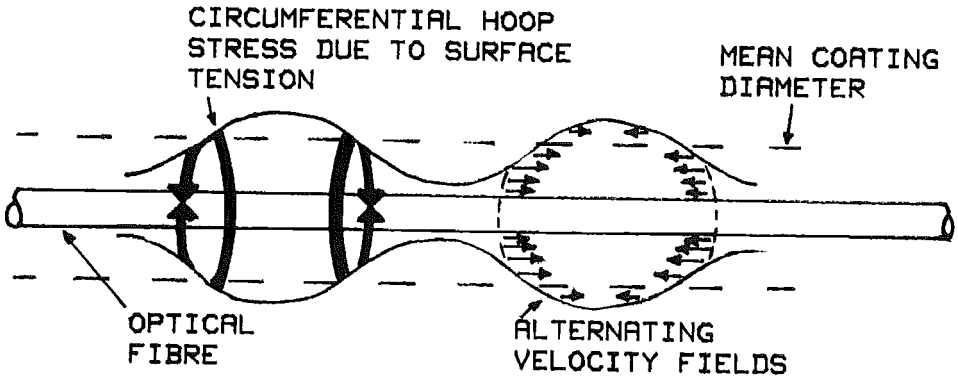

SCHEMATIC ILLUSTRATION OF PERIODIC "BEADING" EFFECT INDUCED BY SURFACE TENSION FORCES IN LIQUID PRIMARY-COATING MATERIALS.

FIGURE 5.7a

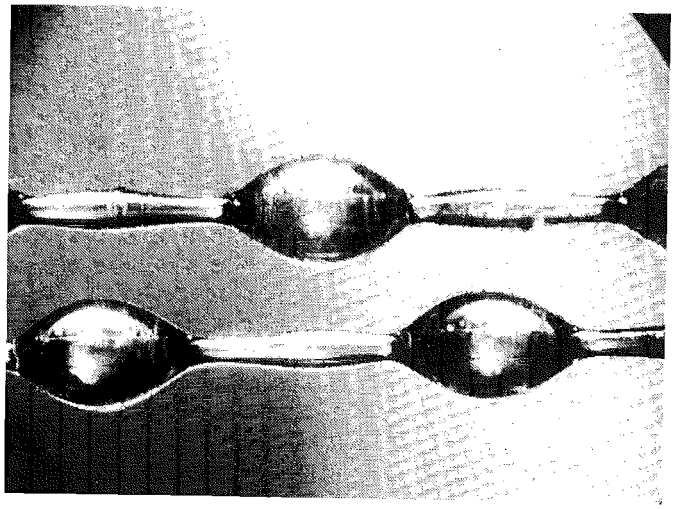

SEVERE "BEADING" OF SILICONE RUBBER PRIMARY-COATING ON 125μm HCVD FIBRE. ×25 mag.

Coating material : Sylgard 184

FIGURE 5.7b

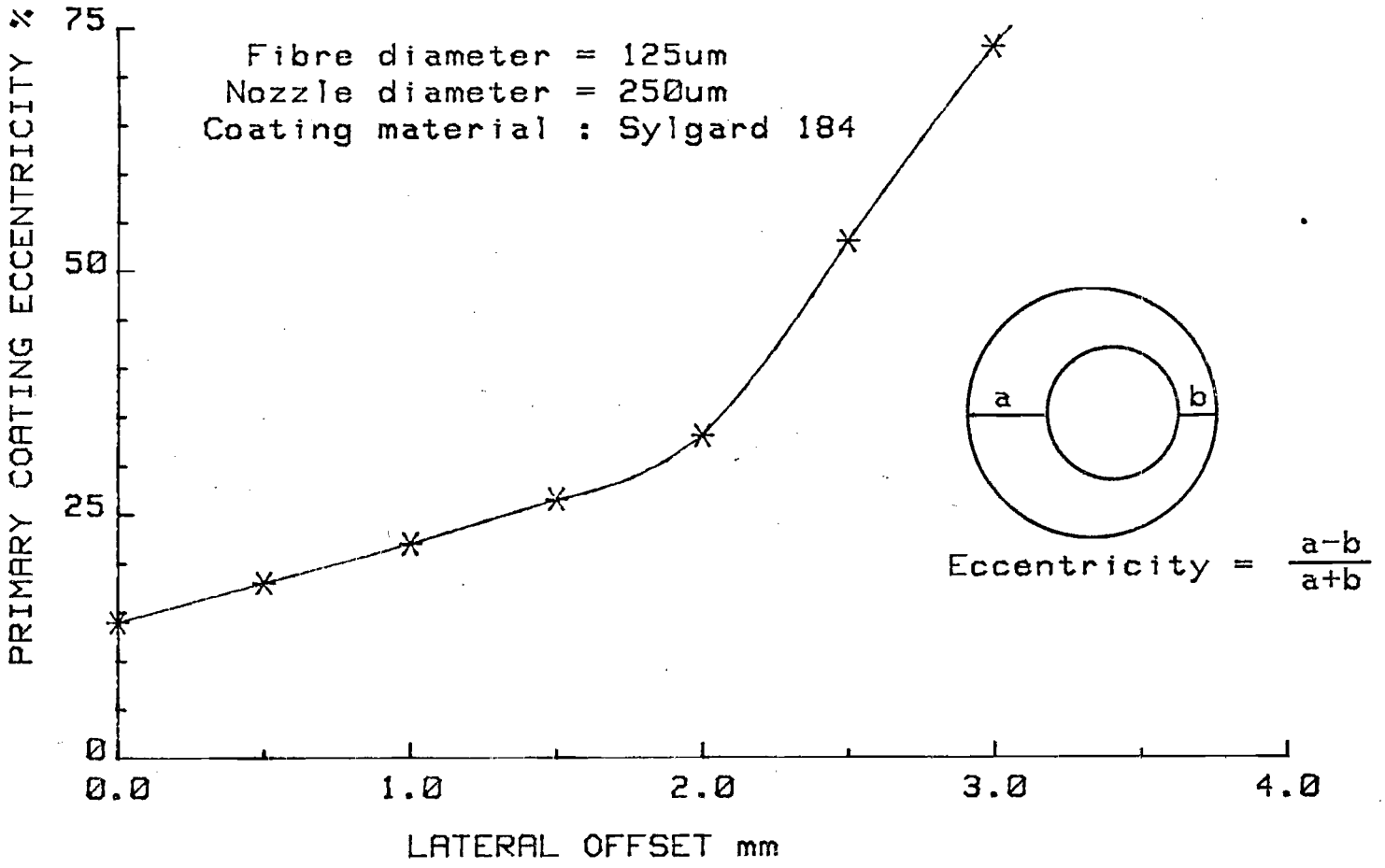

EFFECT OF LATERAL OFFSET BETWEEN TAPERED-NOZZLE COATING-TIP AND FIBRE UPON ECCENTRICITY OF PRIMARY COATING WITH FIBRE.

FIGURE 5.8

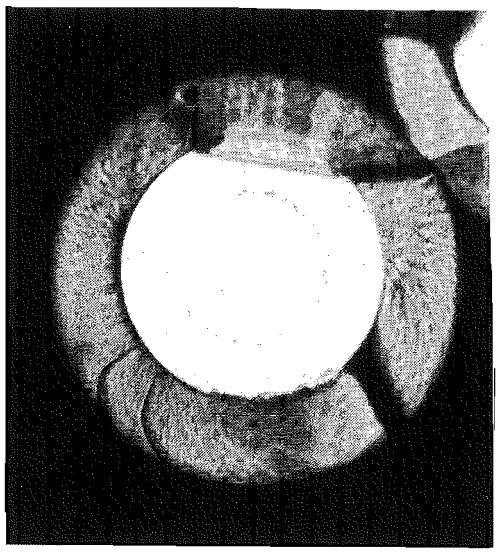

Well-centred silicone primary coating obtained using 200μm tapered-nozzle coating-tip.

FIGURE 5.9

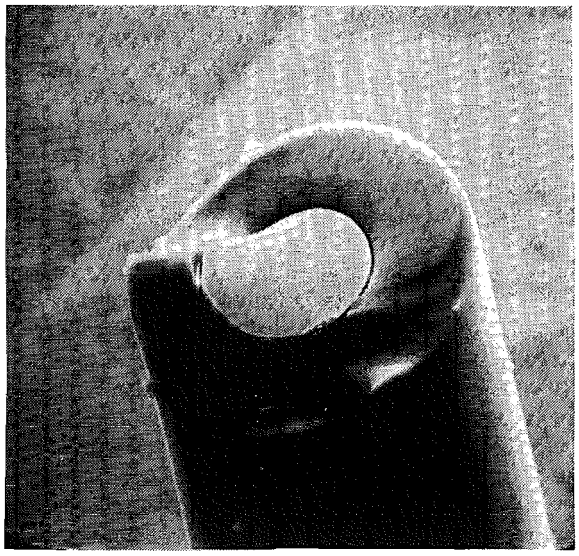

S.E.M. of silicone coating on 125μm fibre. Both fibre and coating were cleaved using the "score-and-break" technique.

FIGURE 5.10

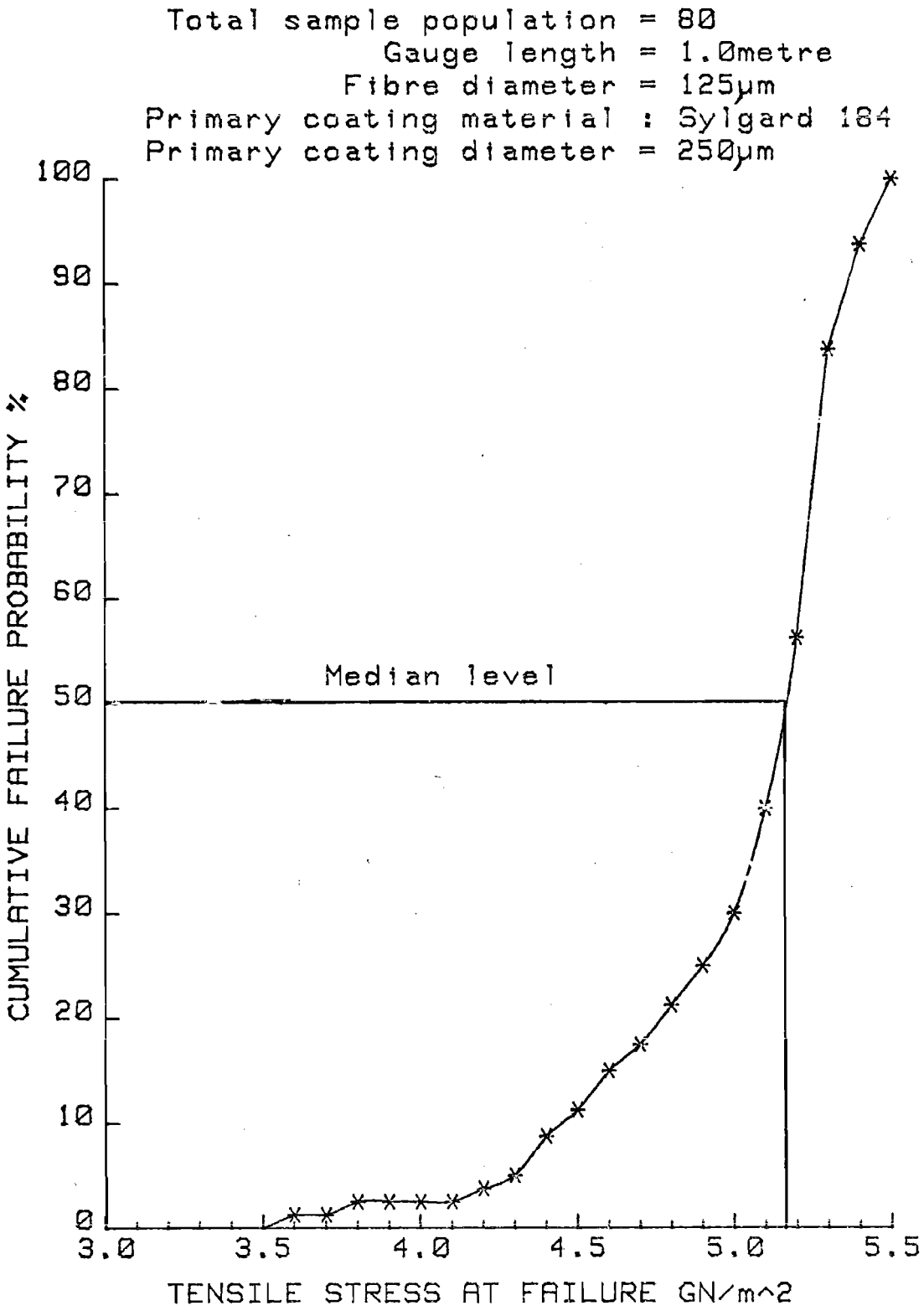

DISTRIBUTION OF TENSILE STRENGTHS IN RANDOM SAMPLES OF PRIMARY-COATED HCVD FIBRE

FIGURE 5.11

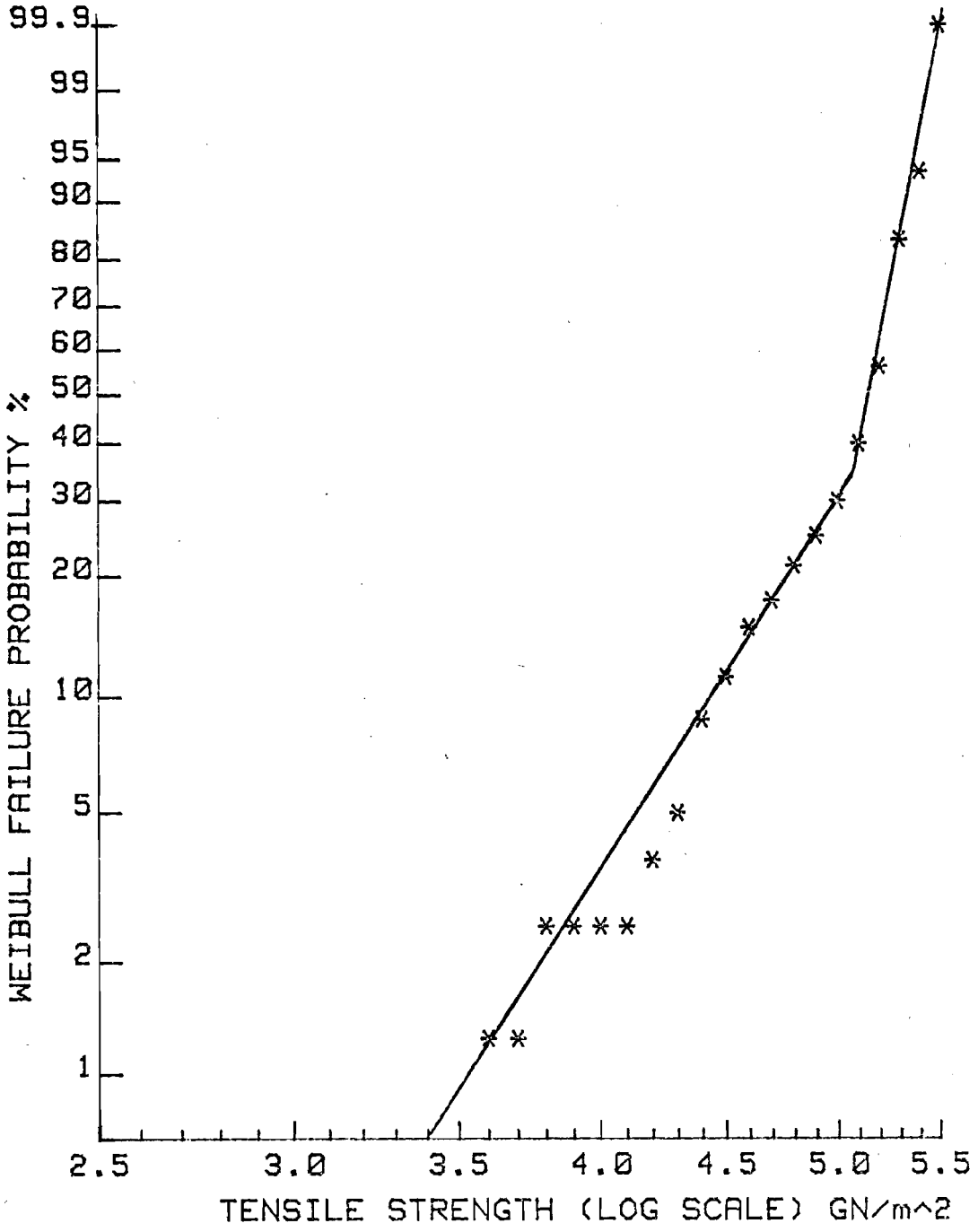

FIBRE STRENGTH DATA OF FIGURE 5.11 PLOTTED ON WEIBULL SCALES ($\ln\ln(1/(1-F))$ against $\ln(\sigma)$).

FIGURE 5.12

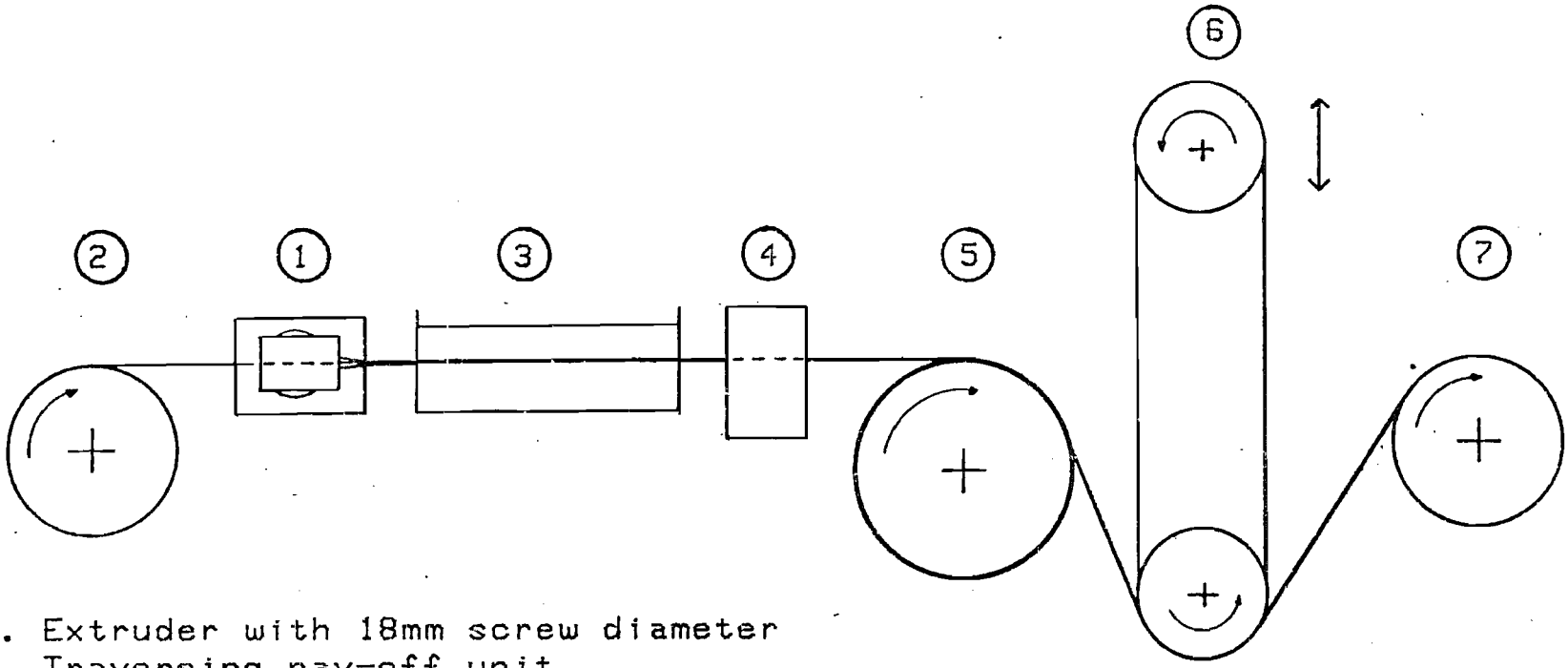

KEY:-

1. Extruder with 18mm screw diameter
2. Traversing pay-off unit
3. Cooling trough
4. Optical diameter monitor
5. Line capstan
6. "Dancing" accumulator
7. Take-up bobbin (speed controlled by position of accumulator dancer)

SCHEMATIC ILLUSTRATION OF EXTRUSION LINE FOR JACKETING OF OPTICAL FIBRES

FIGURE 5.13

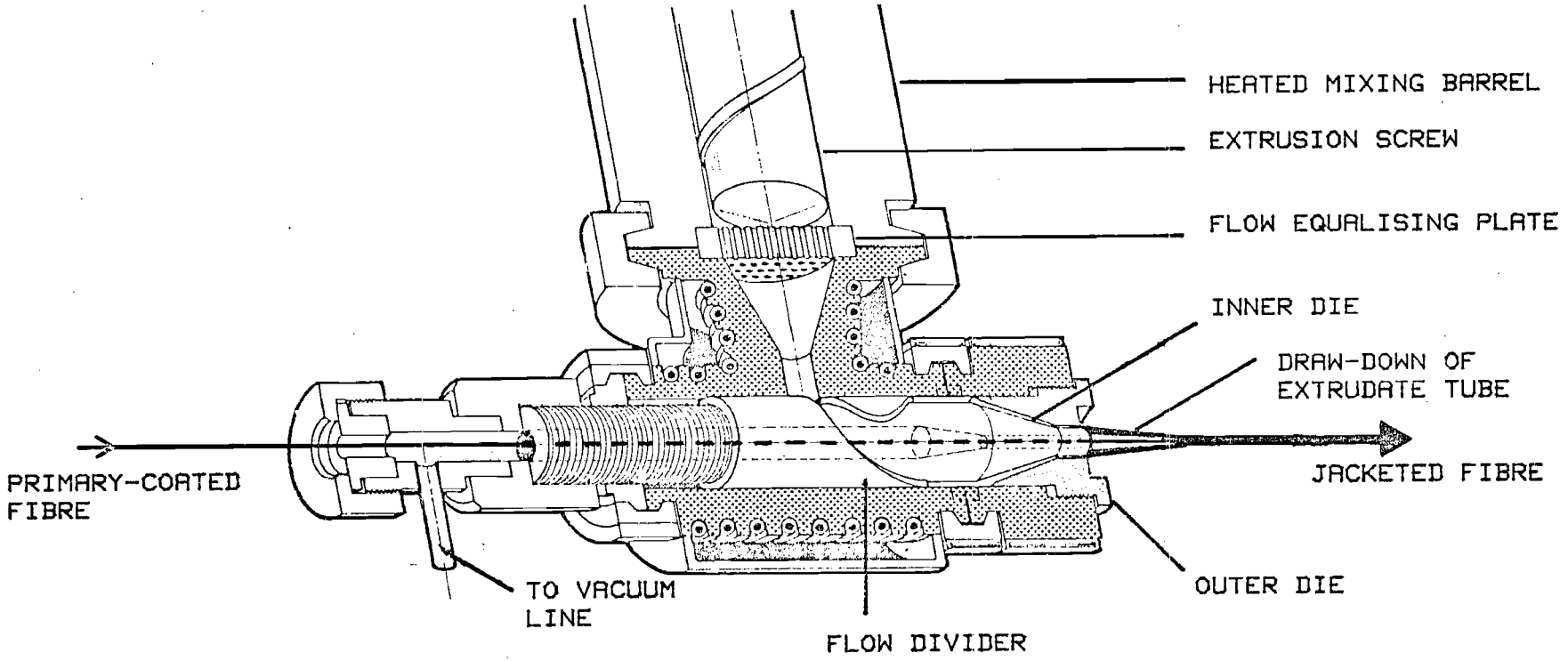

SECTIONAL VIEW THROUGH EXTRUDER CROSS-HEAD SHOWING TIGHT-JACKETING OF FIBRE USING THE FREE-TUBING AND DRAW-DOWN TECHNIQUES.

FIGURE 5.14

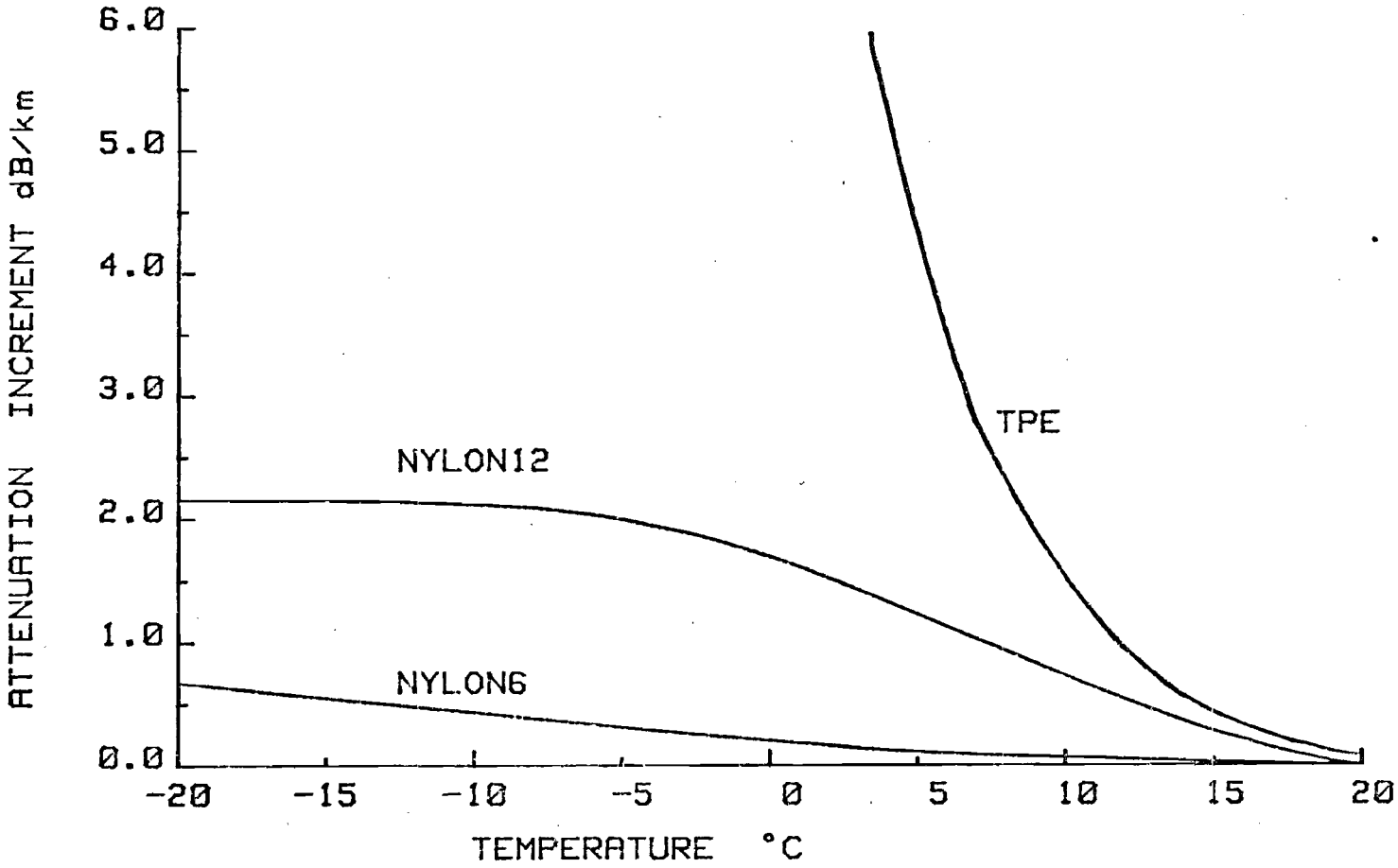

INCREASE OF ATTENUATION AS A FUNCTION OF TEMPERATURE AND COATING MATERIAL IN JACKETED FIBRES. (Overall jacket diameter = 500μm)

FIGURE 5.15

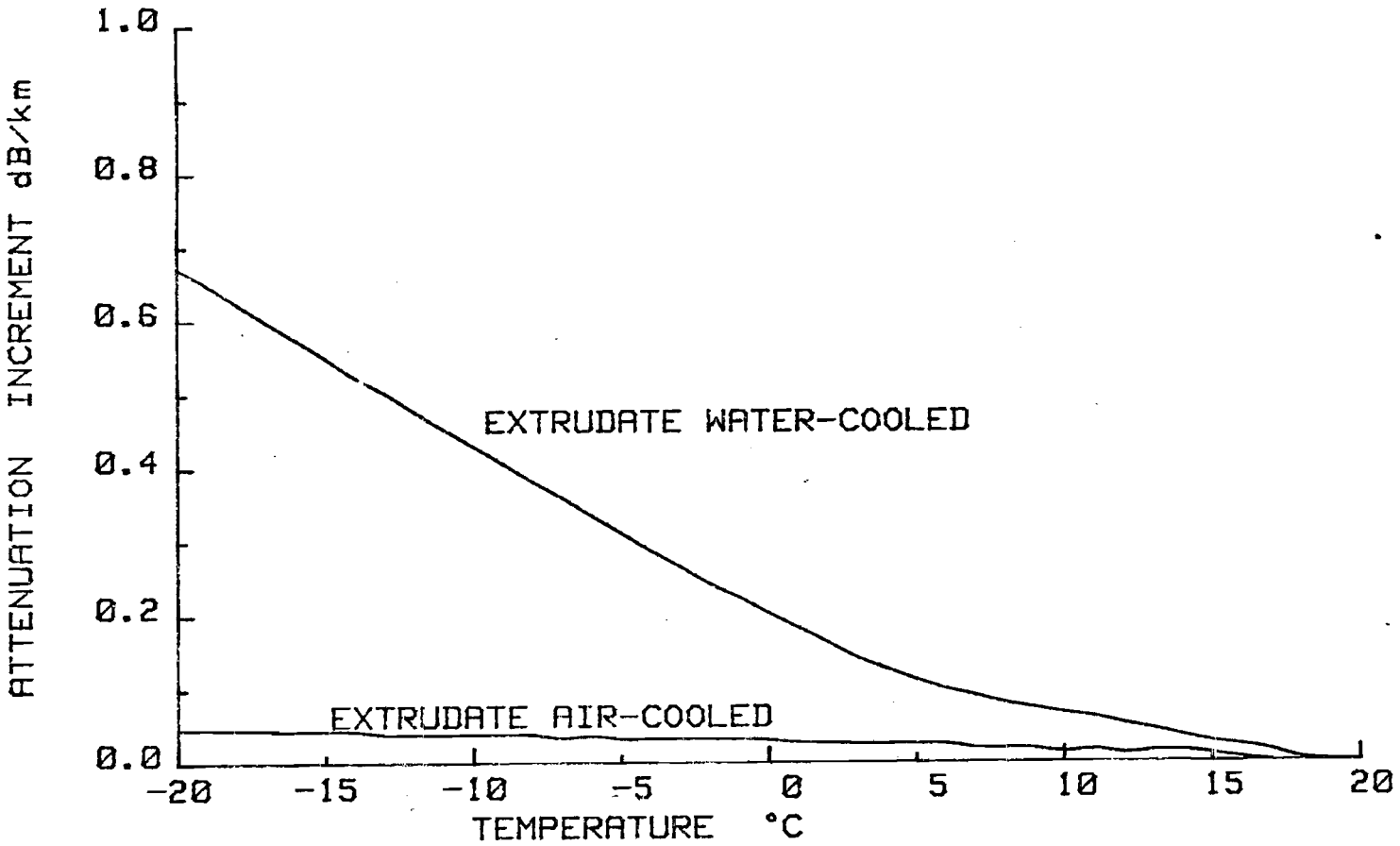

EFFECT OF EXTRUDATE COOLING CONDITIONS UPON ATTENUATION v. TEMPERATURE CHARACTERISTICS OF FIBRE JACKETED WITH NYLON6. (Jacket diameter = 500um)

FIGURE 5.16

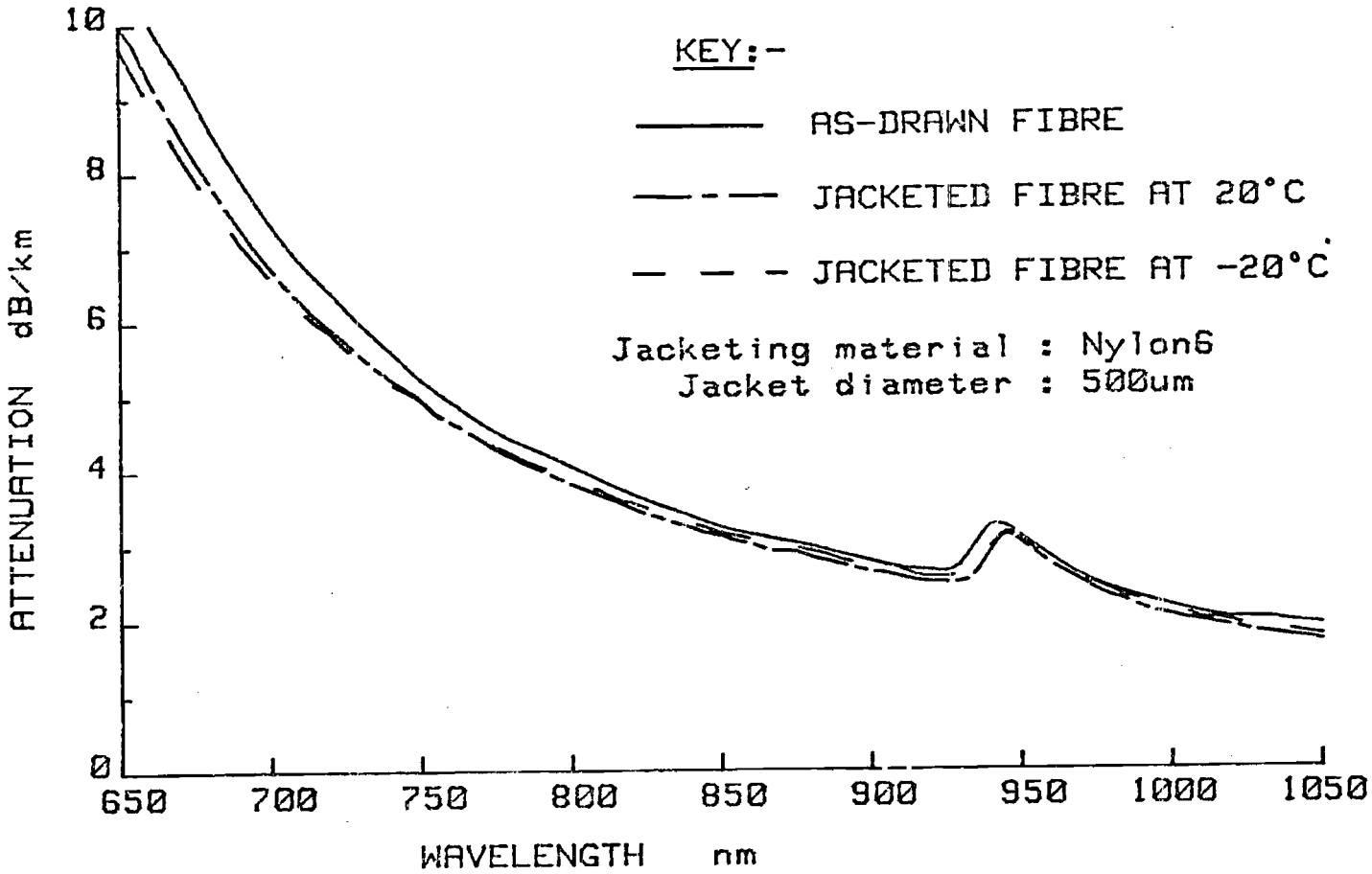

EFFECT OF JACKETING UPON SPECTRAL ATTENUATION CHARACTERISTICS OF GRADED-INDEX MULTIMODE FIBRE.

FIGURE 5.17

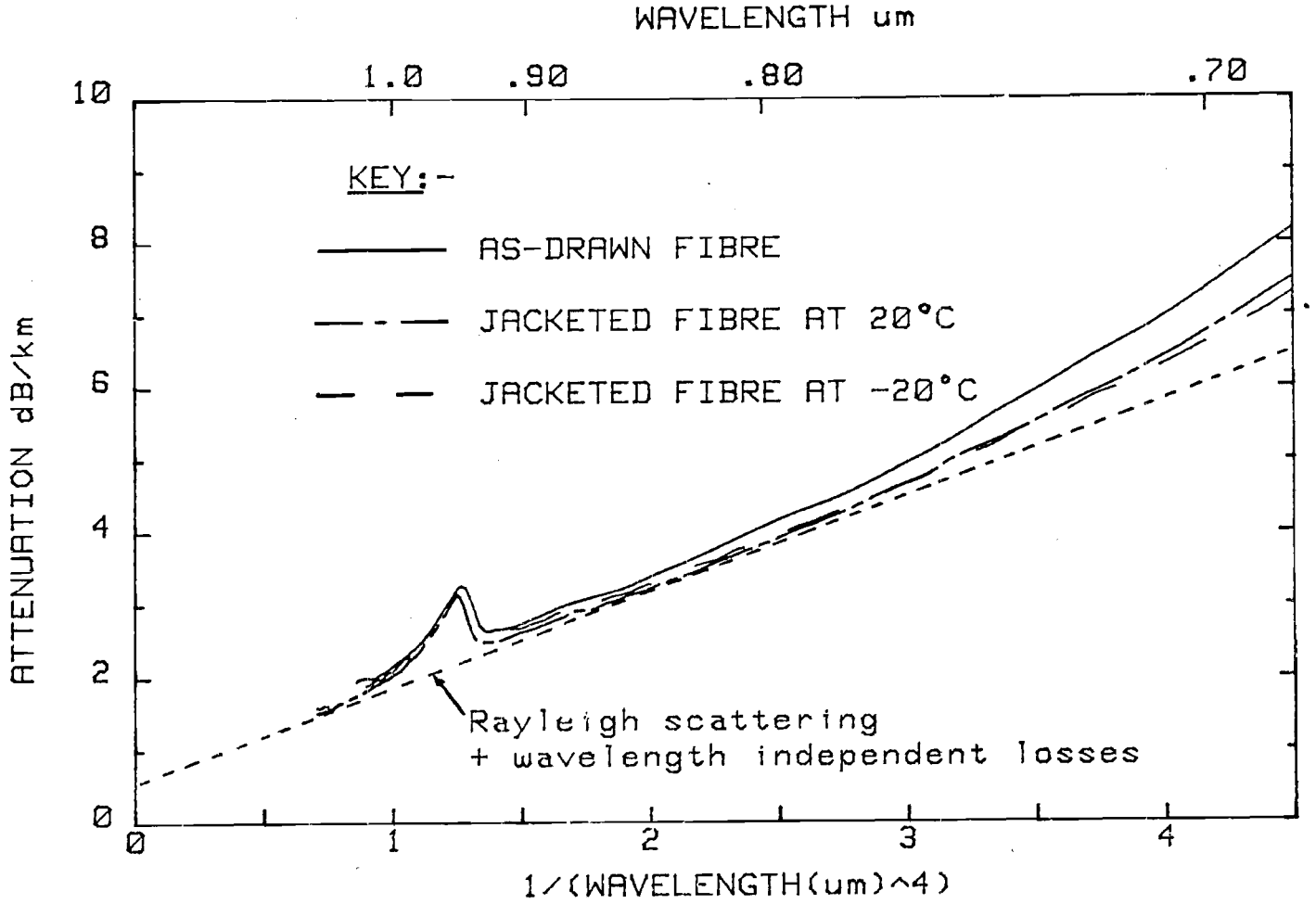

RESULTS OF FIGURE 5.17 PLOTTED ON ATTENUATION v. WAVLENGTH^{-4} SCALE.

FIGURE 5.18

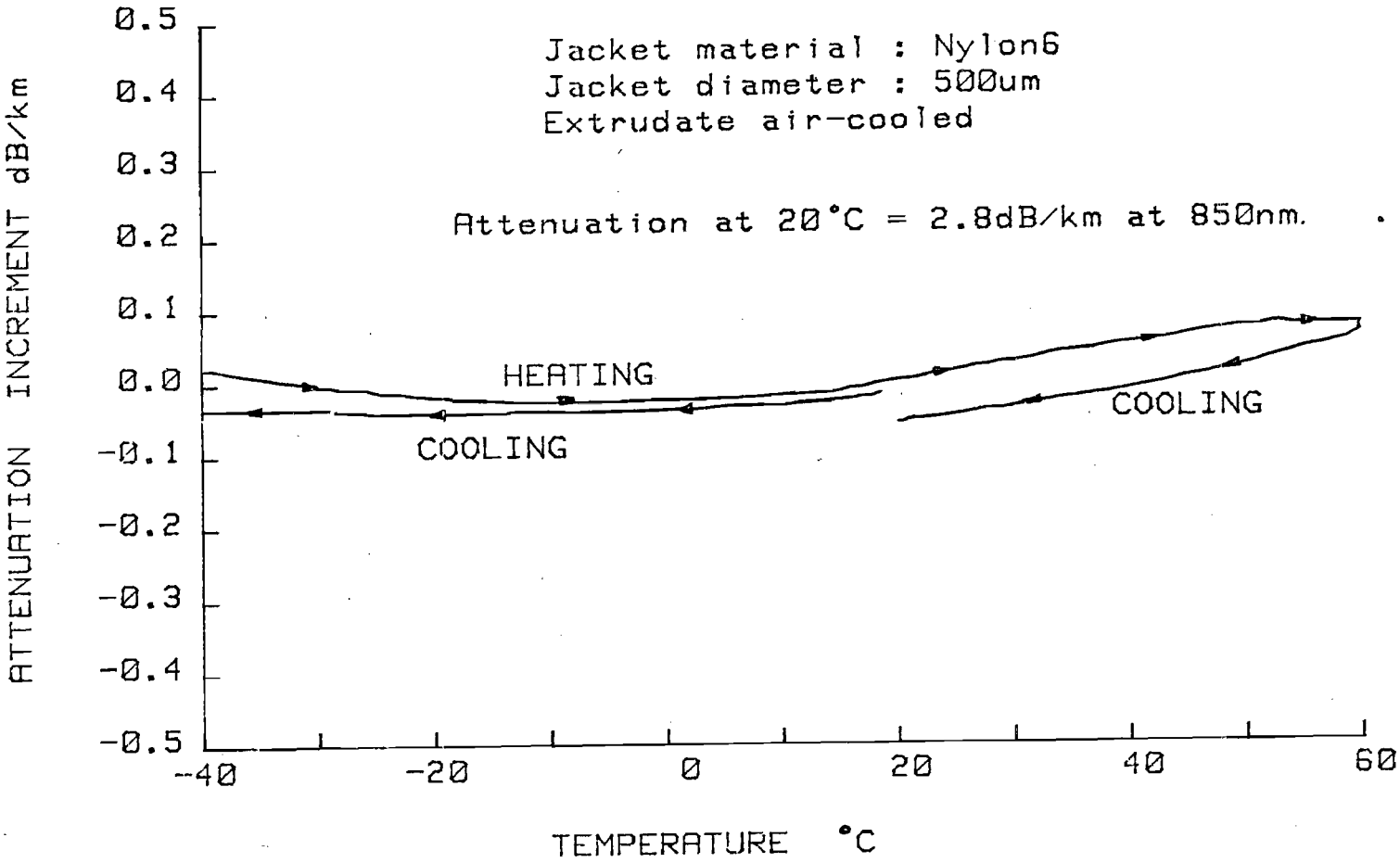

INCREASE OF ATTENUATION AS A FUNCTION OF TEMPERATURE IN GRADED-INDEX FIBRE JACKETED WITH NYLON6 TO 500μm DIAMETER.

FIGURE 5.19

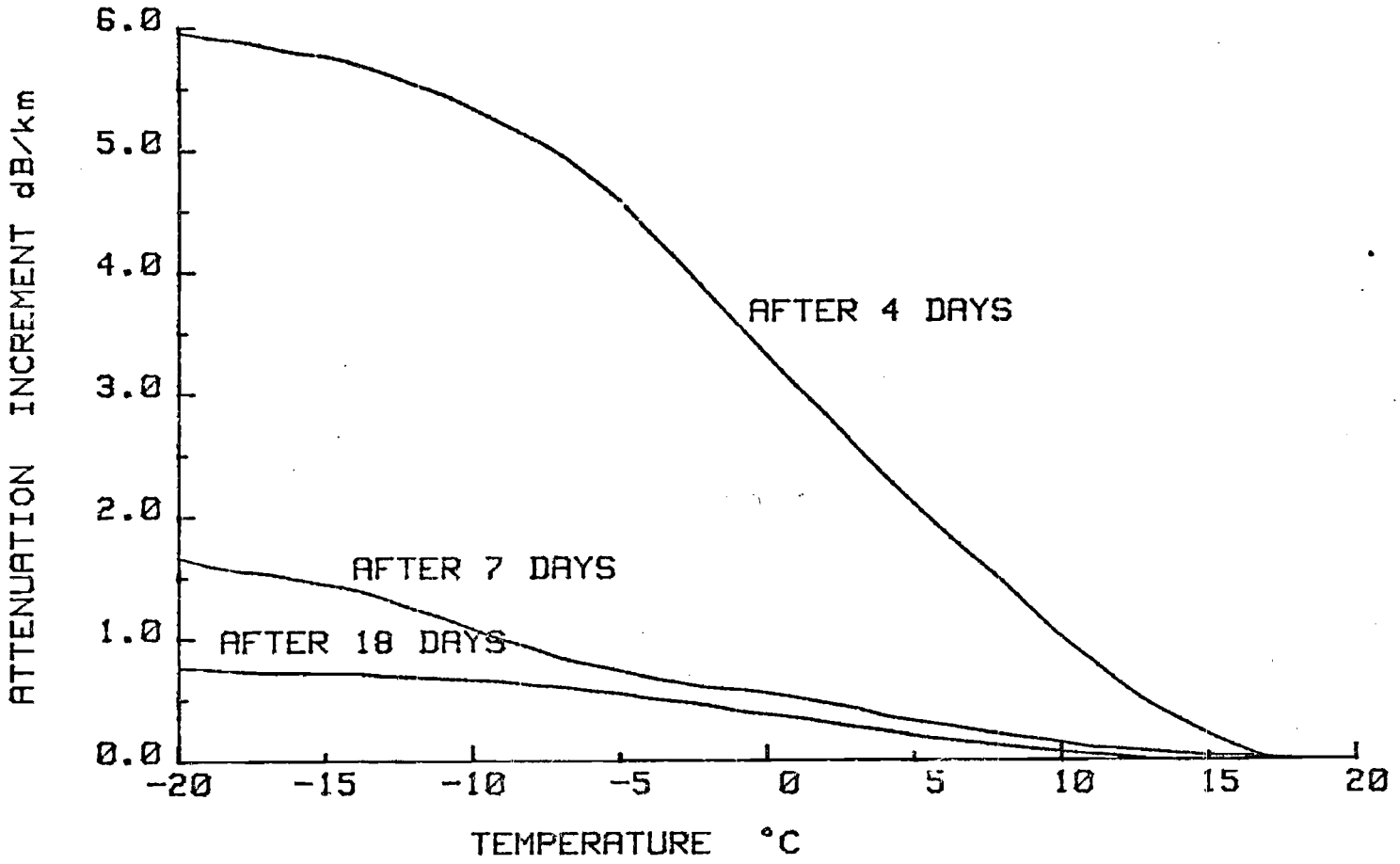

INCREASE OF ATTENUATION AS A FUNCTION OF TEMPERATURE AND TIME AFTER JACKETING IN FIBRE JACKETED WITH FULLY-PIGMENTED NYLON6

FIGURE 5.20

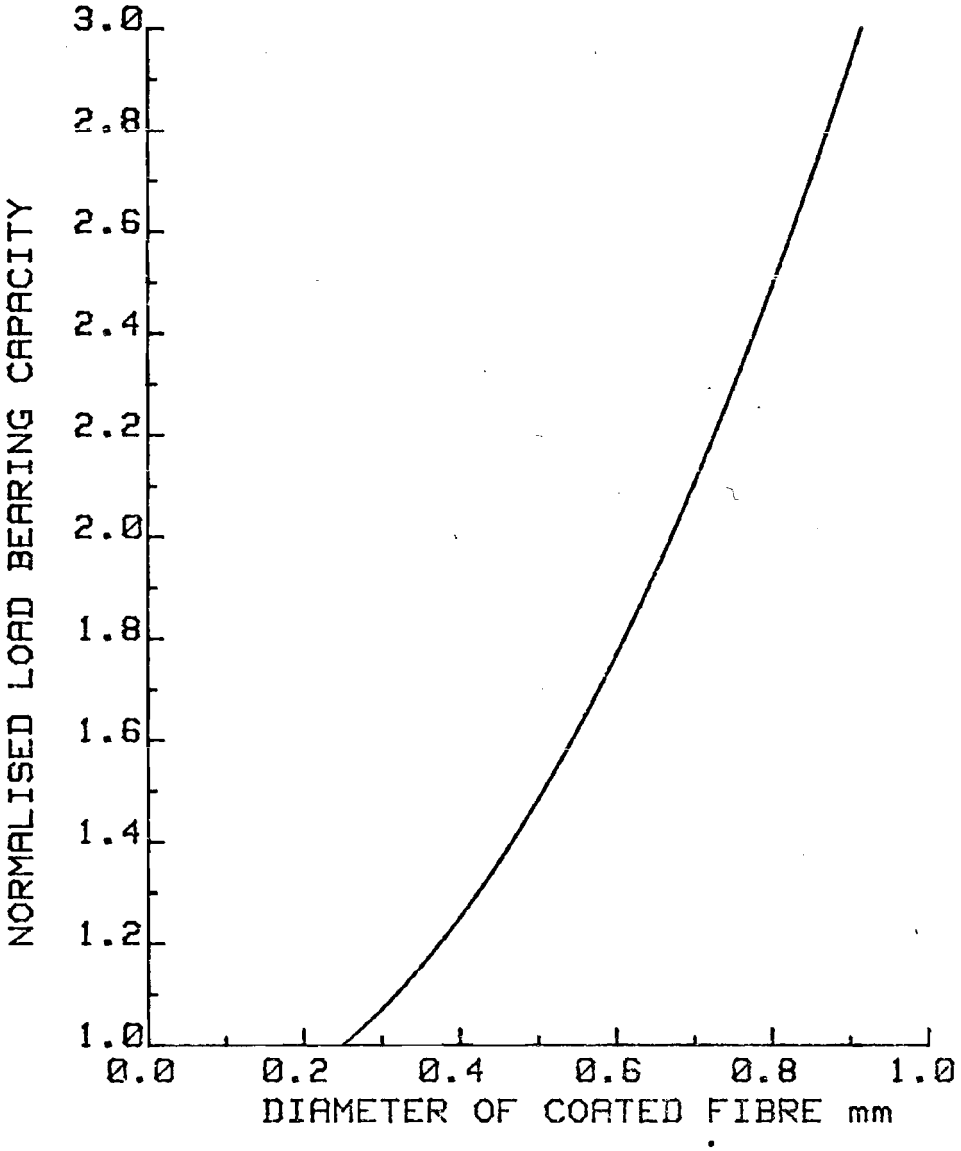

LOAD BEARING ABILITY OF 125μm FIBRE AS A FUNCTION OF NYLON6 JACKET DIAMETER
The fibre is assumed to have a low-modulus primary-coating of 250μm diameter. The Nylon6 jacket is assumed to be Hookean.

FIGURE 5.21

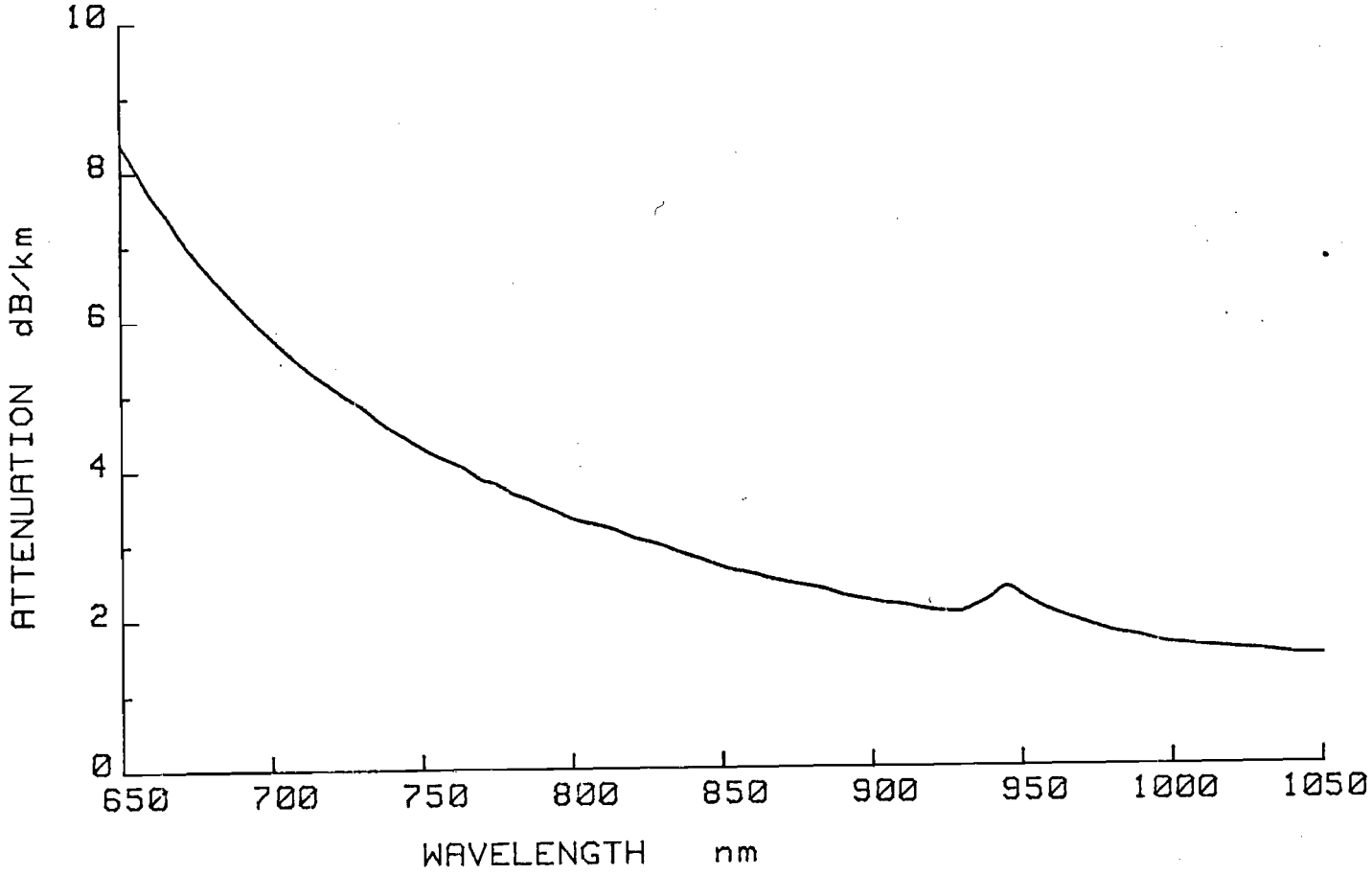

SPECTRAL ATTENUATION CHARACTERISTICS OF "STATE-OF-THE-ART" GRADED-INDEX FIBRE JACKETED TO 0.7mm DIAMETER WITH PIGMENTED NYLON-6

FIGURE 5.22